
# Chromatographic and Sensor-based Analysis of Skin Volatile Emissions

**Tasneem Shetewi, BSc.**

**Submitted for the award of MSc.**

**Primary Supervisor:**

Dr Aoife Morrin, Dublin City University

**Secondary Supervisors:**

Prof. Geraldine Boylan, University College Cork

Prof. Tomas Ward, Dublin City University

**School of Chemical Sciences** **September 2021**

**Declaration:**

*I hereby certify that this material, which I now submit for assessment on the programme of study leading to the award of MSc, is entirely my work, that I have exercised reasonable care to ensure that the work is original, and does not to the best of my knowledge breach any law of copyright, and has not been taken from the work of others save and to the extent that such work has been cited and acknowledged within the text of my work.*

Signed: 

ID NO: 14341976

Date: 06/09/2021

## Table of Contents

**List of Abbreviations**

| | |
|---|---|
| AA | Amino acid |
| AD | Atopic dermatitis |
| Cer | Ceramides |
| CI | Colour intensities |
| DCM | Dichloromethane |
| DMSO-$d_6$ | deuterated dimethyl sulfoxide |
| E.coli | Escherichia coli |
| ESI | Electron spray ionisation |
| FFA | Free fatty acid |
| FID | Flame ionisation detector |
| FLG | Filaggrin |
| FPCB | Flexible printed circuit board |
| GC-MS | Gas chromatography |
| HOMO | Highest occupied molecular orbital |
| HS-SPME | Headspace solid phase microextraction |
| IM | Ion mobility |
| IPA | Isopropyl alcohol |
| ISE | Ion selective electrode |
| LC | Liquid chromatography |
| LOD | Limit of detection |
| LUMO | Lowest unoccupied molecular orbital |
| MAF | Meldrum's activated furan |
| MAP | Meldrum's activated pyrrole |
| MEMS | Micro-electro-mechanical system |
| MMD | Moisture MeterD |
| MO | Metal oxide |
| MOGS | Metal oxide gas sensor |
| MS | Mass spectroscopy |
| MSD | Mass selective detector |
| NHE1 | Sodium-hydrogen exchanger 1 |
| NIST | National institute of standards and technology |
| NMF | Natural moisturising factor |
| NMR | Nuclear magnetic resonance |
| OH-Cer | N-ω-hydroxyceramides |
| PDMS | Polydimethylsiloxane |
| PEN | Polyethylene naphthalate |
| PL | Phospholipids |
| PMMA | Poly methyl methacrylate |
| PPM | Part per million |
| RH | Relative humidity |
| RT | Room temperature |

| | |
|---|---|
| Rt | Retention time |
| S. pyogenes | Streptococcus pyogenes |
| S.aureus | Staphylococcus aureus |
| S.epidermidis | Staphylococcus epidermidis |
| SC | Stratum corneum |
| SD | Standard deviation |
| SIFT | selected ion flow tube mass spectrometry |
| sPLA2 | Phospholipases A2 |
| SSL | Skin surface lipids |
| TEWL | Transepidermal water loss |
| TG | Triglycerides |
| th2 | Helper t |
| THF | Tetrahydrofuran |
| THF | Tetrahydrofuran |
| TLC | Thin layer chromatography |
| TS | Tape stripping |
| UCA | Urocanic acid |
| UV-Vis | Ultraviolet-visible spectroscopy |
| VFA | Volatile fatty acid |
| VOC | Volatile organic compounds |

**List of Figures**

technology. The change in the sensing material conductance due to the interaction with analytes is proportional to the concentration of the analytes in the sensor environment.

**Figure 2.1** Set up for skin VOC sampling using SPME fiber housed in a glass funnel serving to define the headspace (HS).

**Figure 2.2** Chromatograms for recovered volatiles from the female forehead (top), female forearm (middle) and male forearm (bottom). Asterix mark high abundant volatile compounds released from skin.

**Figure 2.3** Grouped bar chart showing normalised peak areas for compound classes recovered from skin volatile samples collected from the female forehead (n=10 participants), female forearm (n=10 participants) and male forearm (n=9 participants).

**Figure 2.4** Skin volatile emission abundances over time recovered from the volar forearm (n= 3 female participants). The x-axis represents (A) total peak area, (B) total acid peak area and (C) peak area of n-hexadecanoic acid. Different colours represent different participants.

**Figure 2.5** Overlayed chromatograms for a recovered volatile sample taken before (brown) and immediately after (blue) application of IPA on the volar forearm.

**Figure 2.6** Chromatographic peak areas for volatile emissions sampled from the volar forearm over time post application of IPA. (A) total peak area, (B) peak area of total identified acids, (C) peak area of n-hexadecanoic acid and (D) peak area of total identified aldehydes. One participant was sampled multiple times for this study where different colours represent different samples.

**Figure 2.7** Box plot showing normalised median peak areas of individual VFAs emitted from the female forehead (n=10 participants), female forearm (n=10 participants) and male forearm (n=9 participants).

**Figure 2.8** Box plot showing skin surface pH measurements collected using a flat glass pH probe for the female forehead, female forearm and male forearm (n=10 participants for female

**List of Tables**

## List of Publications and Presentations

### Publications

Shetewi T, Finnegan M, Fitzgerald S, Xu S, Duffy E, Morrin A. Investigation of the relationship between skin-emitted volatile fatty acids and skin surface acidity in healthy participants - a pilot study. *J Breath Res.* 2021 Mar 25. doi: 10.1088/1752-7163/abf20a. Epub ahead of print. PMID: 33765666.

### Poster Presentations

Shetewi T., Duffy E. and Morrin A., *Investigating the Relationship Between Acidic Skin Volatiles and Skin Surface pH,* Annual Conference on Chemical Sensors for wearable Device, Haifa, Israel (2020).

Shetewi T., Duffy E. and Morrin A., *Investigating the Relationship Between Skin Volatiles and pH*, IABR Breath summit, Leicestershire, United Kingdom (2019)

Gunnoo J., Shetewi T., Duffy E., and Morrin A., *Colorimetric Sensing of Human Volatiles from Skin*, Breathomics, Manchester, United Kingdom (2019)

**Acknowledgment**

I would like to praise and thank god, who has granted me with countless blessing, knowledge, and opportunity so that I have been finally able to complete the thesis.

I would like to show my greatest appreciation to my supervisor Dr Aoife Morrin for her continuous support, guidance and encouragement throughout my master's course. I am forever grateful and proud to be graduating with all the knowledge that you have shared with me.

I would like to thank the technical staff of the chemistry department in DCU with a special thank you to Marry Ross for her constant help with the gas chromatography instruments.

Thank you to all my postgraduate friends in DCU. Mathavan, Asmitha and Roberta. Thank you for all the support and good times.

Finally, I would like to acknowledge the guidance and support received from my parents and siblings.

Tasneem Shetewi, BSc.

Title: chromatographic and sensor-based analysis of skin volatiles

**Abstract**

Non-invasive techniques for skin analysis including wearable sensor are continuously being explored for their use in personalised healthcare to track movement, blood pressure and heart rate among many other parameters. Recently, focus has shifted towards the development of such wearable sensors for use in biochemical analysis. Accurately diagnosing or predicting the course of an epidermal disease in an individual is challenging due to the complex nature of the skin. Epidermal sensors are a subclass of wearable sensors that are designed to have intimate contact with the skin and are used to monitor physical changes in the skin barrier and detect skin disease biomarkers that can be related to human health. Challenges associated with epidermal sensors is the difficulty of sampling from the skin and also tuning the sensor for the selective detection of a target biomarker or set of biomarkers.

The overall aim of this thesis is to investigate the skin volatile emission profile as a potential matrix for analysis and to obtain bio-diagnostic information related to skin health. Chapter 1 of the thesis reviews the literature related to skin structure, function and the methods used for non-invasive skin surface assessment. Chapter 2 explore the potential of using skin volatile samples collected via solid phase micro extraction in a wearable format as a means to assess skin surface pH. Chapter 3 describes the synthesis of a novel dye and the development of dye into a wearable colorimetric skin sensor for the detection of skin emitted volatiles. Although, this sensor is at its early stages of development it has demonstrated selectivity towards skin volatile amines. The work done highlights the possibility of using skin volatiles as a means of assessing skin properties whereby, the measurement of skin surface pH based on the volatile emissions was demonstrated using a wearable colorimetric sensor. Since, skin pH is an important property to monitor for optimal skin barrier function and cutaneous antimicrobial defence, it is envisaged that this sensor could be deployed for health monitoring in the future.

# Chapter 1

# Towards Non-invasive and Wearable Devices for Skin Surface Diagnostics

## 1.1 Introduction

The skin is a complex organ covering the body's surface and accounting for 15% of the total body weight.[1] It performs multiple vital functions. These are made possible thanks to the skin's intricate structure consisting of various tissue types that are organised in three distinct layers; the epidermis (and associated appendages), dermis and hypodermis. These layers work together to maintain homeostasis and dictate the skin barrier function that serves to isolate the internal body from the external atmosphere.[1] Factors such as the skin's pH, lipid composition, water content, as well as microbial habitation, influence the quality of this barrier.[2]

The outer surface of the skin known as the stratum corneum SC, is the body's first line of defence against the extremal environment. Its compact structure, chemical composition and orientation make it a great physical protection against invading foreign bodies.[3] Skin appendages such as nail and hair also play a role in protecting the skin.[4] Appendages like the sebaceous and sweat gland contribute to the chemical barrier of the SC. Secretions by these glands are deposited on the surface of the SC and collectively are responsible for forming the chemical barrier associated with the SC.[4] Sweat released on the skin surface creates the hydrophilic characteristics associated with the SC.[5] When excreted in sufficient amounts, sweat ensures the proper hydration and thus proper function of the SC barrier. Similarly, sebaceous gland secretions called sebum create a hydrophobic film that prevents excess loss of water from the SC thus maintaining the hydration in this layer at an optimal.[6] Sebum also provides skin bacteria with nutritional components required for microbial growth.[7] To fight off pathogenic bacterial that can penetrate the skin barrier, an acidic environment allows for the selective growth of commensal bacteria while preventing the growth of pathogenic microorganisms that thrive in alkaline environments.[8] Moreover, the acidic environment of the SC is essential for key processes involved in the synthesis and maintenance of a competent skin barrier structure.[9] Certain enzymes of the skin also display an acidic pH optima. Only at the reduced pH of the SC can these enzymes function so as to maintain the structure and function of the SC barrier. Deficiencies in SC lipids, and/or their structural arrangement has been previously linked to skin disorders such as atopic dermatitis (AD).[2,10] AD patients also show increase skin surface pH which prevent proper stacking and organisation of the SC lipids thus disturbing the SC barrier function.[11] Thus, non-invasive monitoring of skin properties such as skin pH and hydration levels as well as sebum and skin micro floral composition offer a great means of understanding the skin barrier activity.

Along with fluidic; hydrophilic (sweat) and lipophilic (sebum) secretions, the skin glands are responsible for releasing volatile organic compounds (VOCs). Changes in the body's physiology- be it through acquiring an infectious disease or changing environmental conditions- can be reflected through a change in the VOC composition.[12,13] By characterising these VOCs it is possible to gain beneficial information about the metabolic state of an individual.[14,15] Microorganisms that reside on the skin also produce VOCs derived from interactions with skin gland secretions and also via their own metabolism. Skin surface pH is a significant factor in determining the type of microorganism that will reside on the skin; it sets the environment for commensal bacteria to grow while suppressing the growth of pathogenic bacteria to die.[13] The low concentration (0.55 to 4790 fmol $cm^{-2}$ $min^{-1}$) at which the volatiles are released means suitable and sensitive sampling procedures, pre-concentration steps and detection techniques need to be employed.[16] In terms of VOC sampling procedures, those that avoid direct contact with skin and are solvent-free are superior as they eliminate potential contaminants.[17] The high degree of sensitivity associated with mass spectrometry (MS) makes it an ideal candidate for separating and identifying such low amounts. Gas-chromatography mass spectrometry (GC-MS) is the gold standard for such trace level VOC investigation as it is equipped with sophisticated identification systems that can perform simultaneous analysis of hundreds of compounds.

As the skin is the body's first line of defence that is readily available for diagnostic purposes, demand is ongoing for devices and methods that are capable of performing continuous skin monitoring. Blood is the most utilised body fluid for diagnostics due to the high concentrations of biomarkers present. Invasive methods that use, needles have proven to be effective at the analytical measurement of skin surface composition.[18,19] Non-invasive devices offer potential for diagnostic approaches as they do not penetrate the skin avoiding the risk of tissue damage and infection while allowing for patient comfort.[20–22] Thus there is need to identify suitable biological matrices that can be collected without skin penetration - sweat, interstitial fluid, and skin VOCs. Furthermore there is a push toward devices that are capable of collecting such matrices to be fabricated as wearable sensor-based platforms that can produce continues and real-time information on biomarkers in these matrices. This review will discuss the different types of layer present on the skin in terms of composition morphology and function paying detailed attention analytical methods including wearable sensors that have been designed to assess skin surface a) lipids, b) pH, c) water content and d) microbial flora. The literature discussed here within demonstrate exciting opportunities for the non-invasive measuring of

physiological conditions simply by developing wearable sensing devices capable of selective and specific motoring of fluids and components expelled by the body during metabolism. Thus, future patient monitoring and clinical care will be based on affordable and user friendly wearable devices that enable remote and long-term patient motoring.

### 1.2 Layers of the skin

Human skin is composed of three distinct layers: subcutaneous layer (also known as the hypodermis) the dermis and the epidermis which vary in structure function and composition (**Figure 1A**).[23] The hypodermis layer, found deep within the skin acts as an adhesive layer that binds the skin to the to the skeletal frame. Directly above the hypodermis is the dermis layer responsible for protecting the skin against mechanical damage. The most superficial epidermis layer is composed of sublayers (**Figure 1B**) the deepest of which is called the stratum basale is biologically active and constantly generating new cells that develop as they travel through the layers until they reach the outermost sublayer known as the stratum corneum (SC).[24]

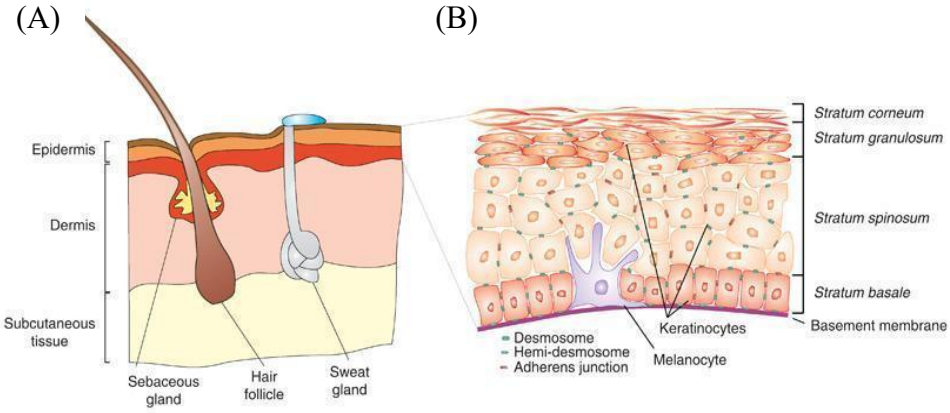


**Figure 1.1** Structure of the human skin. (A) The three main layers that comprise skin; subcutaneous layer, dermis and epidermis. Appendages including the sebaceous and sweat glands and hair follicles are found within the skin layers (B) Composition of the epidermis which is sub-divided into different layers. Figure adapted from Kern *et al*. [25]

The hypodermis layer located deep within the skin is comprised primarily of adipose tissue that is interconnected by collagen and fibres.[23] Rose *et al*. (1978) first showed that the tissue in the hypodermis layer is arranged vertically in a lattice orientation of varying geometric shapes. Adipose homeostasis is one of the important functions associated with this layer. It regulates lipolysis, adiponectin and leptin secretion.[26] Due to its rich fatty composition, it also acts as an insulator layer, shock absorber and energy storage unit.[27] Along with aiding the skin in binding

to the underlying skeletal and muscular frame the hypodermis also supplies vessels and nerves to the overlying skin layers known as the dermis.[23]

The dermis layer is a highly vascularised system that consists of collagen and connective tissues responsible for the elasticity and flexibility of the skin. [23,27] Different cells reside here, including fibroblasts that are responsible for synthesising components of the connective tissue, as well as macrophages and mast cells that are involved in immune and anti-inflammatory responses.[27] Besides protection against mechanical injury, the dermis plays a vital role in thermal regulation and water retention.[27] It also contains receptors of sensory stimuli. Appendages like hair follicles, sebaceous and sweat glands originate here.

The epidermis is a multi-layered region (**Figure 1B**) with varying total thickness levels depending on the body part: on the eyelid, for example, its thickness is approx. 0.06 mm, while on the feet and palms it is about 0.8 mm.[27] Development of keratinocytes - via differentiation, proliferation and keratinisation - leads to structural and compositional change in the sublayers of the epidermis as they migrate from the stratum basale through the stratum spinosum and stratum granulosum to reach the outermost SC.[27] Thus each epidermal layer is believed to represent a different maturation stage of keratinocytes. During this process, the keratinocytes produce lipids and proteins, but once they reach the SC, the cells become enucleated (corneocytes) and are referred to as nonviable cells unlike the cells of the lower epidermal layers (viable dermis).[23] Melanocytes, Merkel and Langerhans cells are other cells that populate the viable layers; however, unlike keratinocytes, they do not part take in keratinisation.[27] Melanocytes are dendritic cells that produce melanin; a pigmented material responsible for the colour of skin, hair and eyes. Melanin produced is packed into organelles called melanosomes that are sent to neighbouring basal keratinocytes.[27] These melanosomes absorb the potentially harmful ultra-violet radiation that penetrates the skin to prevent the release of free radicals in the basal layer.[23,27] Another type of dendritic cells specific to the epidermis are Langerhans cells. These cells comprise a subset of leukocytes that detect and counteract invasive foreign bodies. Binding of antigens to the surface of the body triggers an inflammatory signal. This initiates a series of changes to the Langerhans cells as they migrate from the epidermis to the dermis, and onto the lymph nodes where they synthesis T cells that generate an immune response.[27,28] Merkel cells are the mechanosensory receptors that are localised in touch-sensitive parts of the body such as fingertips and lips.[23]

The epidermis is 10-15 layers in-depth with low hydration levels (10-20% compared to 70% as found in the viable epidermis).[27,29] The SC is analogous to a brick wall structure, where the corneocytes represent the "bricks" that are embedded in a "mortar" represented by an intercellular matrix of lipids and desmosomes (adhesive protein complexes) as seen in **Figure 1.2**.[27] Corneocytes are flat elongated cells (thickness: 1.5 $\mu$m, length: 50 $\mu$m) composed primarily of keratin (70%-80%) and lipids (20%) surrounded by a cornified cell envelope (thickness 10 nm).[29] The cornified cell envelope is a polymeric protein/lipid envelope formed just below the cytoplasmic membrane found on the exterior of corneocytes. It consists of two parts; lipid envelope and a protein envelope.[29] The protein envelope dictates the biomechanical properties of the cells by crosslinked structural proteins (filaggrin, involucrin, loricrin, elafin, cystatin A, and desmosomal proteins) through amide and sulfide bonds.[29] The lipid envelope comprises N-ω-hydroxyceramides (OH-Cer) covalently bound to the protein envelope.[27] Other major lipid components of the SC include ceramides (CER), cholesterol, free fatty acids, cholesterol esters, and cholesterol sulfate. Behen *et al*. used mechanism-based inhibitions studies to identify the importance of OH-Cer for the formation of normal SC intercellular lipid lamellae that maintain the skin barrier structure.[30] Replacement of these specific CER with a fatty acid equivalent leads to uncontrolled loss of water and the release of the hygroscopic content from the corneocytes into the SC.[31]

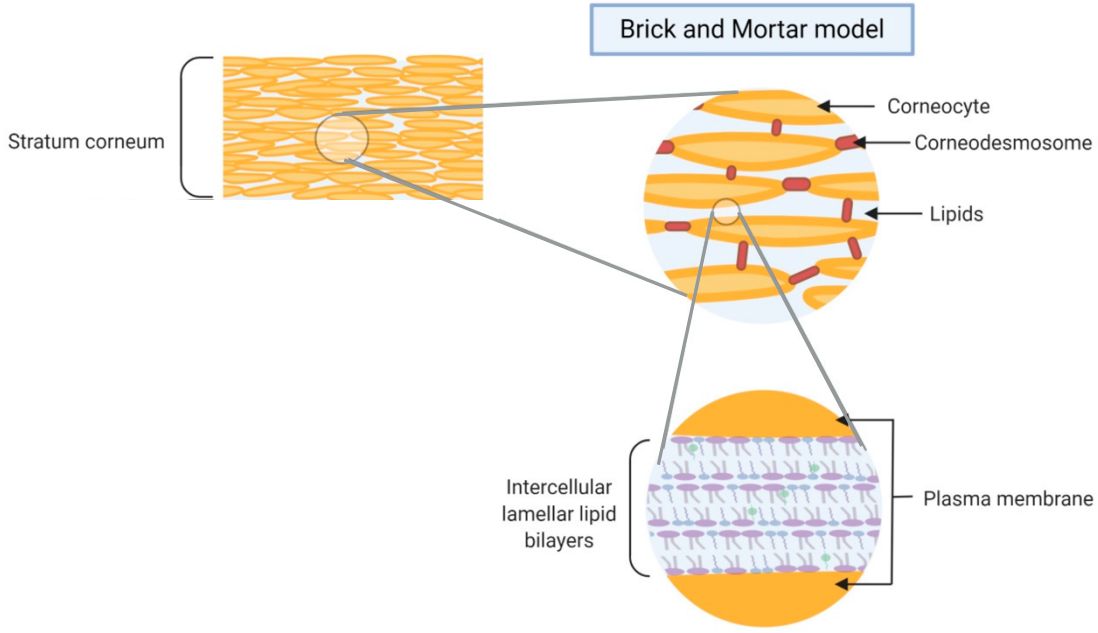


**Figure 1.2** Brick and mortar model of the SC figure adapted from Yang *et al*.[32]

### 1.3 Skin barrier and other functions

The skin outweighs any other organ in terms of function.[15] As the human integument, its primary role is to separate the internal bodily environment from the external environment. Once established, this interface not only prevents the penetration of microorganisms into the body but also plays a major role in homeostasis.[16] Four elements help maintain skin homeostasis: physical, chemical, microbial and immunologic barriers.

#### *1.3.1 Physical barrier*

The first layer of physical defence of the body is the tightly packed SC layer. The physical barrier of the skin is provided mainly by the composition and structure of this layer consisting of protein enriched cells (corneocytes with cornified cell envelops and corneodesomes) and lipid enriched intercellular space. The nucleated epidermis also contributes to the physical barrier through tight, gap and adherens junctions, as well as through desmosomes. The tough protein/lipid polymer structure of the cornified cell envelope protect the tissue against physical and chemical damage. Cross-linking of filaggrin (FLG) protein to the cornified envelope leads to aggregation of keratin filaments into microfibrils that supports the tightness of the SC. For substance exchange between the skin and the environment, the SC is the rate-limiting step.[16] Not only is it responsible for regulating the exchange of substance on the skin surface but also prevents excess loss of water from the skin through the secretion of sebum from glands. This lipid-rich substance creates an insulating layer that prevents skin dehydration. Thus, changes in epidermal structure and lipid composition can deteriorate the skin barrier allowing it to become susceptible to the entry of allergens, immunological reaction and inflammation in skin disorders.

#### *1.3.2 Chemical and microbial barrier*

The SC is referred to as the 'acidic mantle' represents the pH gradient of the skin. This provides the outermost SC layer with the necessary acidic environment (4-6 pH units). The physiological environment of the body is basic (pH 7.4) and thus pH at the viable epidermis is also maintained at his pH however, at the SC the environment is acidic. This implies a gradient of about 2 pH units over a short distance of 10$\mu$m, the thickness of the epidermis. This skin pH gradient shows the steepest change in the SC directly overlying the stratum granulosum, an area with high activity of pH-dependent enzymes. The acidic environment of the SC is essential for protecting the skin and it does so in two ways.[16] Firstly, it allows for selective on skin habitation of commensal bacteria that grow in acidic environments such as *Corynebacterium* bacteria

strains, while preventing the growth of pathogenic microorganisms such as *Staphylococcus aureus* (*S.aureus*) and *Streptococcus pyogenes* (*S.pyogenes*) that thrive in more alkaline environments.[17] Secondly, it helps maintain the integrity of the SC as many skin enzymes require an acidic environment to function. Formation of CER is facilitated via pH-dependent enzymes: aSMase and b-GlcCer'ase (S7) that show optimal activity at pH 5. Besides pH, SC water content is important for maintaining a functional barrier. The skin's chemical barrier is maintained when there is adequate moisture in the skin. Water-soluble substances called natural moisturising factor (NMF) are responsible for maintaining optimal sin hydration and thus barrier function. NMF is composed of small hydrophilic molecules generated from proteolysis of FLG including urea, lactic acid, urocanic acid, and various amino acids.[59,60] Optimal skin hydration is essential for the activity of enzymes that break down FLG to produce the NMF. Another aspect of the skin chemical barrier are the gland secretions. Glands are appendages located deep within the skin layers (discussed in more detail in Section *1.4.3*). While sweat glands participate in ion and nitrogenous waste excretion via sweat, sebaceous gland release a lipid-rich substance called sebum consisting of squalene, triglycerides, wax esters, free cholesterol and free fatty acids.[23] Sebum contributes to the physical barrier of the SC via preventing the evaporation of excess water from the skin, it also serves a chemical function as it is a nutrient rich medium that promotes the growth of skin bacteria.

### *1.3.3 Immunologic barrier*

A range of immune cells (Langerhans cells, dermal dendritic cells and macrophages) are found in the skin. These cells participate in immune surveillance. They contain antigen-presenting cells that initiate an immune response through priming naïve t lymphocytes which in turn elicit a response to newly encountered antigens.[16] The importance of such cells is significant, because a compromised skin barrier is the main route of pathogen entry into the body. Atopic dermatitis (AD) is a common skin disease believed to rise due to immune abnormalities.[55] Patients with AD show; impaired skin barrier, reduced epidermally derived antimicrobial products, defects in receptor functions, reduced diversity in the skin microflora and inflammation.[55] There is consensus that the leaky epithelial barrier in AD encourages allergen sensitisation, microbial colonisation and even infections.[55,56] The increased levels of Helper t cells (th2) cytokines found on AD skin significantly affect skin barrier protein expression and function, and this, in turn, increases the risk of *S.aureus* colonisation.[55] Several immune function genes are associated with the predisposition of AD; however, these gene mutations are not unique to AD, and some are associated with asthma and allergies. Genes found on chromosome 1q21

encoding epidermal cornification (build-up of dead corneocyte cells) and s100 proteins have been associated with skin barrier dysfunction.[57] Of these, the most widely studied is FLG protein for forms the structure of the cornified envelope and is critical for keratin alignment.[56,59] Experiments done on mice lacking FLG showed increased susceptibility to allergen sensitisation.[58] Mutations in genes that code FLG are highly associated with AD as well as ichthyosis Vulgaris and is identified as a major risk factor.[56,59,61] Skin models that lack FLG gene expression were synthesised in vitro and tested to reveal unaltered keratinocyte differentiation with abnormal lamellar body formation and impaired barrier function.[60] Furthermore, studies done on human AD patients suggest that FLG mutations play a role in barrier skin function. However, their contribution to impaired skin barrier as measured by transepidermal water loss (TEWL) remains uncertain.[60] Thus, absence of FLG does not seem to be the only reason for barrier function impairment in AD, and may also be dependent on chemical barrier and skin hydration levels

*1.3.4 Other functions*

Thermoregulation is another vital role of the skin. Thermoreceptors found on the skin detect heat and cold and provide temperature information to the hypothalamus, which in turn through thermoregulation mechanisms achieves temperature homeostasis.[16] Similarly, adipose tissue in the hypodermis insulates the skin from the cold and prevent excess heat loss. Hair on the skin provides extra insulation by trapping a thin layer of air that prevents heat loss during cold times.[16] Large volumes of sweat can be generated during periods of exercise or stress while reduced perspiration is observed in cold conditions. Perspiration released by the sweat glands on to the surface of the skin reduces body temperature by dissipating the heat required to evaporate the water in the sweat. Blood vessels also constrict or dilate to adjust the blood flow and hence the heat lost through the skin. Collectively, these thermoregulating mechanisms help maintain an optimal core body temperature of 37 ºC.[16]

Apart from temperature sensing, nerve endings on the dermis capable of detecting touch, vibration and pain are also necessary for locomotion and coordination. Furthermore, the skin carries out a variety of metabolic functions. Subcutaneous fat stored deep within the layers of the skin can be mobilised rapidly during energy deprivation. The skin is the primary site of vitamin D synthesis.[18] Exposure to sunlight and particularly ultraviolet irradiation produces a vitamin D precursor deep within the epidermis which is then converted to vitamin D by keratinocytes.[16,18]

## 1.4 Skin appendages

These are structures that connect to the epidermal surface of the skin but originate mainly from the dermis and hypodermis layers.[23]Major appendages include hair, nails and glands.[23,33] Collectively, they allow for the normal function of the skin when it comes to touch, temperature sensation, excretion, perspiration and thermoregulation.[33]

### *1.4.1 Hair*

Hair follicles are minuscule organs that produce hair and are distributed everywhere on the skin surface except for the palm, soles and portion of the genitalia.[23]They vary in size and morphology. Vellus and terminal hair follicles are the two types, vellus hair is short, fine and lightly coloured while hair from terminal follicles is thicker, longer and darker.[8] Beard, pubic and axillary hair are terminal hairs that are hormonally regulated, and only appears after puberty.[34] Hair grows in three cycles of uneven durations; the growth phase (anagen), the regressing phase (catagen) and the quiescent phase (telogen).[23,33]aThe growth cycle is controlled by chemical signals and growth factors that determine the length, thickness and colour of the hair. These different hairs have different functions associated with them. Terminal hair such as that found on the scalp protects against skin cancer, while terminal eyelash, eyebrows and nose hairs act as filters that protect the body from airborne particles.[33]

### *1.4.2 Nails*

Nails are structures that cover the upper tips of phalanges of the fingers and toes. They consist of nail matrix (area of nail growth), nail plate (hard plate consisting of densely packed keratin) nail bed (the skin beneath the nail plate) and periungual skin (thickened skin around the edges).[23] The nail plate is comprised of approximately 80% hard α-keratin and 20% soft α-keratin.[35] Keratin is a fibrous protein that is rich in sulfur and is composed of polypeptide chains. Directly under the nail plate is the nail matrix, an area of highly proliferating cells such as the Langerhans cells and melanocytes that determine the nail plate pigmentation.[35] The nail matrix produces the nail plate consisting of approx.200 cell layers distributed in a ratio of 3:5:2 among three tightly organised layers known as the dorsal, intermediate and ventral. The dorsal and intermediate plates have similar sulfur concentrations. The amino acid cysteine that forms disulfide bonds is found in a higher concentration in the intermediate plate. Thus there is a higher degree of crosslinking associated with the intermediate plate, which limits swelling and suggests it's importance in barrier properties. One-fourth of the total length of the nail is

covered with thickened SC skin known as the cuticle, which protects against penetration of water and chemical toxins.[35]

*1.4.3 Glands*

Sebaceous, eccrine and apocrine are the main glands of the skin. The latter two glands produce sweat and are known as sweat glands while the sebaceous gland releases an oily substance known as sebum whose composition is outlines in Section *1.5.2.2*. It forms an insulative layer that prevents excessive loss of moisture from the skin.[6] Eccrine sweat glands are present at birth and are found covering the entire surface of the body whereas apocrine sweat glands only develop following puberty.[36,37] The composition of sweat from these two gland types is different.[38] Eccrine sweat composition is governed by factors such as diet, metabolic rate and drug administration.[38] Water is the primary component of eccrine sweat that also contains small amounts of minerals (such as sodium, potassium calcium and magnesium) and metabolites (such as lactate, ammonia and urea).[38] In contrast apocrine glands release viscous lipid-rich sweat that contains proteins and steroids in terms of composition but also contains similar mineral and metabolite composition as eccrine sweat.[38,39]

Variations in the structure and function of these glands allow for their different distribution in the body. Sebaceous glands are found midway of the dermis layer, almost always adjacent to a hair follicle with a duct emptying into the follicular canal.[6,36] They are responsible for regulating certain sex hormones in the body; linking them to the skin condition acne vulgaris.[6] Full development and maximum secretion of sebum from these glands is achieved only after puberty.[6]

Apocrine glands are larger approximately 10-fold greater in diameter compared to eccrine glands.[36] They are split into two segments; the coiled secretory portion and the straight duct portion.[37] The coiled secretory portion is the gland itself and is found in the lower dermis of the skin.[36] It's walls are composed of cells known as granules. The small granules are round while the large granules are fine, electron-dense and rich in iron.[37]The duct region is the gland's terminus and leads directly into fair follicles. Sweat produced from the glands is directed into these hair follicles rather than being excreted directly onto the skin.

Eccrine glands are simple, coiled tube-like structures that can be split into two domains; the secretory portion and the ductal portion.[36,37] The duct consists of two layers of cells and is

covered internally with a material called the cuticle.[36] On the other hand, the secretory portion consists of a single layer of cells.[36] As a consequence, the duct has a slightly smaller diameter than the secretory portion. Unlike apocrine glands, eccrine glands directly open to the skin surface.[40] A key role of eccrine glands is thermoregulation; that converts the sweat into vapour; cooling down the body.[37] This process of homeostasis is crucial for maintaining a constant environment within the body.

## 1.5 Stratum corneum

The SC is a surface rich in bodily secretions that make up the hydrophobic and hydrophilic domains associated with the SC. These secretions encompass surface molecules like lipids, peptides, cytokines, and nucleic acids. It is also home for a variety of microorganisms that influence human health and disease, and which produce metabolites including toxins, antibiotics and VOCs. Altogether, this surface offers great potential as biomarkers for localised diseases like AD and cancer, and even systemic conditions like diabetes, cystic fibrosis and cardiovascular disease.[41,42]Thus, for the above mentioned reasons and due to ease of accessibility and possibility of performing non-invasive skin monitoring on the SC, this review will henceforth describe the chemical composition of this layer and discuss the analytical techniques and sensing approaches for monitoring changes in the SC that relate to health.

### *1.5.1 SC water content*

Vital functions of the SC is highly dependent on its water content that brings about the hydrophilic properties of the SC.[5] SC water content varies with varying thickness of the SC layers.[43] Both endogens and exogenous factors help maintain SC hydration. The epidermis produces an aqueous protective coating known as the NMF (endogenous) that also comprises sweat (exogenous) released by sweat glands, both of these factors help maintain SC water levels at an optimal. The amino acid (AA) components of NMF have been reported to play an important role in influencing the state of hydration in the SC.[44–46] Uchiwa *et al* show that the SC hydration significantly decrease after extraction of NMF with water treatment.[46] Furthermore, correlation between AA and SC hydration was demonstrated, however most reports that should such correlation examined the SC of patients with dry skin due to conditions such as AD.[44,47] Along with AA, lactate and potassium that are found in eccrine sweat gland metabolism contribute significantly to the hydration state of the SC.[48,49] Sweat composition and function will be discussed in more detail in Section *1.5.3*.

The outer SC layer is equilibrium with ambient water content while the deeper layers exchange water with the epidermis and is almost saturated. Warner *et al*. showed that water concentration increases from 25% at the outer SC to 70% at the stratum granulosum level.[50] Skin moisturising studies carried out using nuclear magnetic resonance (NMR) and Raman spectroscopy confirm the existence of such water gradients across the SC layers.[51,52]

In general, approx. 25-35% of the water present in the skin is bound to internal skin structures, while the remaining water is present as a free solvent.[53] Hansen and Yellin studied bound water using thermal and vibration based techniques to find that bound water interacts with two structural components; proteins and lipids.[54] Modification of water-lipid interactions affects the structure of the SC. Increases in overall water content decreases the force of attraction between aliphatic chains, thus increasing lipid fluidity of the SC.[50] Free water contains a mixture of AA and its derivatives as well as various salts. All together they play a role in maintaining SC chemical and mechanical properties.[55]

Three main factors maintain SC hydration levels at an optimal level; the formation and organisation of lipids into the intercellular lamellar lipid membrane; the crosslinking of corneocytes and the presence of NMF in the corneocytes of the SC.[12] Epidermal water content affects the permeability barrier and mechanical properties of the SC and is also responsible for regulating the hydrolytic enzymes involved in the corneocyte desquamation process.[56] According to Blank, flexibility of the SC is permitted when it contains 10-20% water. Once water content is lower than 10% skin barrier impairment is possible.[57]

In dry skin, the corneosomes responsible for the adhesion of corneocytes and the intercorneocyte lipid bilayer are disturbed. Unlike what is observed in moisturised skin, the corneosomes in dry skin undergo less enzymatic degradation and so build up in superficial SC layers.[50] Low SC hydration levels are linked with skin barrier abnormalities. Failure of the SC to retain water leads to dryness and reduced barrier functions. AD is one of the most prevalent skin disease associated with dry skin whereby AD patients show increased water loss from skin that leads to reduced SC water content.[10]

*1.5.1.1 Methods for SC water content analysis*

When assessing skin hydration levels, bioelectrical methods are commonly used. Here an alternating current (AC) is applied to a section of the skin and the resistance faced by the current

is measured. Changes in the hydration of the skin is known to correlate with this resistance and so the skin electrical properties such as conductance, capacitance and impedance are often used to measure water content in skin.[55,56,58] Since 25-35% of water in the body is bound to internal skin structures, understand how changes in hydration levels of the skin can affect the structural composition is important.[53] Leveque *et al*. showed that in dry skin, the keratin chains of the SC are tightly bound to each other, and so the skin behaves as a weak conducting material.[59] Application of water creates space between these chains as water-binding sites on the keratin become fully occupied.[60] Thus, the water content and water capacity of SC keratinised tissue, as governed by electrical measurements, can be exploited to aid in further understanding the skin barrier function. Skin impedance measurement are useful for obtaining skin hydration levels. Commercially available probes like Corneometer® and the Moisture MeterD (MMD) measure skin impedance to give a quantitative measure of skin water content. These probes have been employed in clinical research to evaluate various quantitative skin barrier parameters.[61,62] Another interesting probe is the GPSkin Barrier® that uses also uses impedance to measure SC hydration levels as well as TEWL.[63] Taken together, these measurements are useful for assessing systematic and cutaneous skin conditions. The GPSkin Barrier® are also superior to the other probes in terms of data processing, as results are transmitted to an internet server via a smartphone to be recorded.

To go further, and replace the probe-based approach for skin hydration assessment, focus has been directed towards wearable devices for skin hydration monitoring. For example, Yao *et al*. developed a wearable and fully stretchable hydration sensor based on an impedance measurement.[62] The sensor consisted of two silver nanowire electrodes inlaid into a polydimethylsiloxane (PDMS) matrix. The electrodes were embedded just below the PDMS surface and the stretchable nature of the silver/PDMS electrode allowed for conformal contact of the sensor to the skin. Using a commercial skin hydration impedance probe, the sensor was calibrated and integrated into a wearable wristband together with the necessary electrical components (analyser chip, battery and Bluetooth chip) for data acquisition and wireless communication. Also, in 2017, Kabri *et al*. described a tattoo sensor using graphene electrodes to measure skin hydration.[61] The electrodes were laminated on the skin just like a temporary tattoo. Skin hydration was obtained by measuring the impedance of the skin between the electrodes. Values obtained were comparable to those measured by the Corneometer® hand held probe. Again in 2017, our research group developed a screen-printed silver electrode tattoo sensor for assessing skin barrier integrity.[64] The tattoo sensor comprised of two

concentric circle silver electrodes used to measure SC impedance spectroscopy on the SC. The obtained impedimetric measurements were compared against measurements obtained by the Delfin MostureMeterD probe. The tattoo sensor was demonstrated to be capable of detecting changes in skin hydration/dehydration and was proposed as a wearable tool for skin barrier monitoring.[64,65] Wang *et al*. developed a thin, 'tape-free' tattoo sensor for evaluating skin hydration (among other parameters) via impedimetric measurement.[66] It consisted of gold electrodes arranged in a hexagonal configuration and covered with conductive hydrogel for better skin contact. The multi-sensor, cut-and-paste tattoo was fabricated on polyethylene naphthalate (PEN) material in an open mesh structure for increased breathability and negligible stiffness. The mesh design prevented the accumulation of sweat at the tattoo-skin interface, minimising sweat artefacts.

The development of wearable devices for diagnostic purposes has gained much attention due to their practicality, ease of use and their potential for continuous monitoring. Swisher *et al*. demonstrated the integration of impedance on a flexible device that can be used for the early detection of pressure ulcers via the mapping of pressure-induced damage via changes in tissue water content.[67] The flexible sensor array comprised gold inkjet printed electrodes deposited on PEN material. A hydrogel layer was incorporated  improve contact with skin. To test performance, the sensor array was mounted onto a rat model, and by using impedance spectroscopy across the array of electrodes, the study showed that pressure damaged tissue had lower impedance relative to healthy tissue. The variation in impedance was attributed to reduced membrane integrity possible brought about due reduced tissue water content. Although the study lacks in-vivo measurements on human skin, the results obtained demonstrated the feasibility of using impedance as a non-invasive method for early detection of pressure ulcers.

### 1.5.2 *SC lipid content*

Along with the aqueous portion of the SC, the lipid components of the SC give rise to the hydrophobic properties associated with this layer. These lipids can be categorised into epidermal (endogenous) and sebaceous (exogenous) lipids. Epidermal lipids are present within the cornified layer of the SC while sebaceous  lipids come from sebum secreted by sebaceous glands on to the surface of the SC. Together these lipids form a hydrophobic film known as the skin surface lipid (SSL) fraction and is responsible for regulating the SC barrier function.

*1.5.2.1 Epidermal lipids*

The SC comprises three major classes of epidermal lipids; CER (50%) cholesterol (25%) and free fatty acids (FAA) (15%). In the human SC, FFA consist of a single carbon chain with variation in number of carbons that make up the chain as well as the degree of saturation and mono and poly-unsaturation (**Figure 1.3**).[68] The composition of CER is more complex. Each Cer consists of an acyl chain and a sphingoid base that are linked via an amide bond. Both chain can vary in their carbon composition. The acyl chain can be a non-hydroxy fatty acid, an $\alpha$ -hydroxy fatty acid or an esterified $\omega$ -hydroxy fatty acid. The sphingoid can have optional double bonds or hydroxy groups leading to 5 different structures.[68] Thus the huge variation in the structure of these lipids means that hundreds of uniquely structure CER are possible.

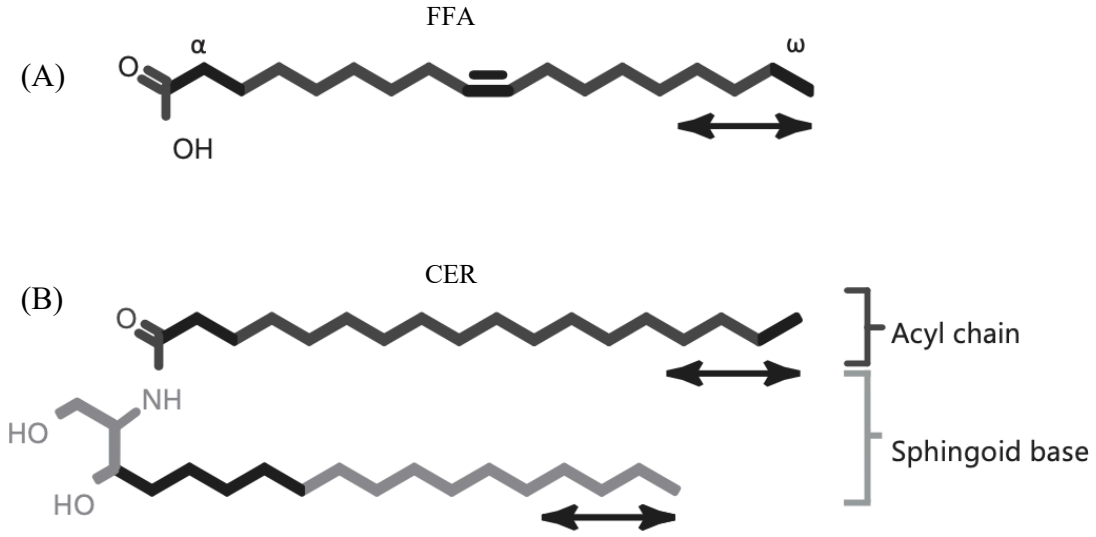


**Figure 1.3** General structure of the two most abundant SC lipid classes. Changes in the chemical structure are likely to occur at the position marked in black. The carbon chain length my vary as indicated by the double headed arrows. (A**)** Molecular structure of FFA where position $\alpha$ and $\omega$ can contain one or more double bonds to give an unsaturated fatty acid. (B**)** Molecular structure of CER consists of an acyl chain connected to sphingoid base via an amide bond.[68]

These epidermal lipids are generated from precursors (phospholipids, glucoceramides sphingomyelin and free sterols) that are delivered to the SC by lamellar bodies.[55] The lamellar bodies possess the enzymes (lipid hydrolases and proteases) required for this lipid processing

step.[55] Changes in surface acidity and calcium gradient can alter the activity of these enzymes, which disrupts the barrier function.[55]Furthermore, deficiencies in any of these classes of lipids and/or their structural arrangement can also affect the integrity of this barrier. The structural organisation of these lipids has been investigated extensively using methods such as x-ray diffraction, infrared spectroscopy and electron microscopy.[55]Early studies revealed the presence of continuous lipid sheets in the extracellular space of the SC. With further advancement in technology, it became evident that a lipid membrane bilayer exists.[55] However, the packing of the lipids in the SC membrane bilayer is different from that in other phospholipid membranes. Various models have been postulated; these include the 'sandwich model" proposed by Bouwstra *et al.*, in which a long periodicity phase, consisting of three regions (a central liquid crystalline layer surrounded by two crystalline gel phases in an orthorhombic arrangement on both sides) was identified and the "single gel phase" model that represents a single coherent lipid phase with no boundaries as suggested by Norlén.[27]CER1 is essential for the formation of the periodic phase. Cholesterol content in the SC is believed to increase the fluidity of the membrane, facilitating the elastic properties of skin.[27,55] Acids also play a role in regulating the skin barrier by shifting the physical equilibrium of the skin bilayer to a noncrystalline state.[69] A wide distribution of long chain saturated FFA, mono and polyunsaturated fatty acids and hydroxyl FFAs have been observed on the SC.[70] These classes of compounds were first reported in 1970 by H.C FU *et al*. who scraped cells from skin, and exposed them to trypsin. They then performed an extraction to isolate the lipids and thin layer chromatography (TLC) to identifying them.[71] The most abundant of these were C22, C24 and C26, with trace amounts of long-chain (C32-C36) saturated and monounsaturated FFAs.[29,69,70] Furthermore, there is evidence that these FFAs, generated from phospholipids (PL) help to regulate SC acidity and integrity.[72] The structural organisation of the lipid bilayer membrane provides the optimal ratio between permeability and fragility of the epidermal barrier.

*1.5.2.2 Sebaceous lipids*

Sebaceous lipids are another lipid type present on the SC. They are secreted by sebaceous glands in the form of a lipophilic mixture called sebum which consists of squalene, TGs, wax esters, free cholesterol and FFAs.[73]The most significant of these are triglycerides (TGs) and FA making up 57% of sebum content followed by wax esters (26%) squalene (12%) and the least abundant cholesterol and its esters that account for 4.5% of the mixture.[73]

Dominant FFAs in secreted sebum are chain lengths comprised between 14 and 18 carbon atoms.[74] The FFA content of sebum is known to be at least partially attributed to the hydrolysis

of sebum-derived TGs by lipases of resident bacteria whose activity is known to be modulated by pH.[75] While sebum derived FFAs play a role in dictating SC pH, the most characteristic sebum derived lipids are squalene and wax esters. Squalene is an unsaturated triterpene with strong moisturising and antioxidant effects.[73] It is a precursor in the biosynthesis of cholesterol; however, in the sebaceous glands, incomplete conversion to cholesterol leads to accumulation of squalene. The build-up of squalene in the sebaceous glands is not clearly understood. However, it can be linked to increased expression of squalene synthase or to decrease in expression or activity of the enzyme that converts squalene to cholesterol.[73] Squalene is unique to the sebaceous glands and is not found anywhere else in the body and is thus a useful marker to distinguish between sebaceous and extracellular lipids.[73]

*1.5.2.3 Methods for SC lipid analysis*

As mentioned previously, thin layer chromatography is one of the earlier methods used to study SC lipids.[71,76] Chromatography separates mixtures liquids or gases based on their affinity to the stationary phase. Both, good separation, as well as sensitive detection techniques, are essential when studying SC lipids. Today mass spectroscopic (MS) techniques are heavily relied on for its superior identification ability. MS conditions are suitable for detecting FFAs, squalene, cholesterol as well as wax esters and sterol oxidation products which are all known components of SC lipids.[77] Liquid chromatography (LC) is well-established for lipid separations and is usually coupled with MS for lipid identification. Maskukawa *et al*. developed the first comprehensive method for quantification of CER in the human SC.[78] They used tape stripping (TS) to sample the SC lipids followed by extraction and analysis using normal phase LC coupled with electrospray ionisation-MS (NPLC-ESI-MS). To validate the method, the group showed that results obtained by this method were comparable to those obtained by TLC. In this work, two new subclasses of CER were identified, bringing the total to 11 known subclasses.[78] Similarly, using TS to isolate SC from the skin, Smeden *et al*. were also able to identify the 11 previously detected CER classes along with an additional subclass of CER using LC tandem MS (LC-MS-MS).[79]Also using tandem MS, Shin *et al*. were able to establish a platform that can structurally identify the most abundant type of CER on the human SC known as the n-type CER.[80] They used TS followed by solvent extraction to collect the SC lipids and a chip-based direct infusion nanoelectrospray-ion trap MS was used to analyse the samples. Direct infusion into a tandem MS is 10-fold faster than traditional methods as no chromatographic separation is required. Gas chromatography (GC) is another technique that is widely used for separation of complex mixtures like SSL. Derivatisation step is required for

fatty acid analysis especially for long chain fatty acids associated with skin lipids.[81] Guffroy *et al*. use high-temperature GC-MS to separate SSL, high temperature allows for better separation of long chain high molecular weight lipids.[82] For sampling the group tapped lipid-free adsorbent papers to the skin for 30 min, after which the paper was transferred to vial and lipid extracted. Extracted solution was diluted before sample separation via GC-MS. Using this method the group were able to identify more than 200 compounds associated with SSL and quantitatively compare their presence at different body parts.[83,84] Also using GC, Sears *et al*. investigate the variation in lipid composition of fingerprints.[85] Participants were asked to rub their hands together to evenly distribute skin surface residues and fingerprint samples were imprinted on a polyester material. The polyester was extracted and the solution was analysed via GC-MS for FFA and GC-flame ionisation detector (FID) for squalene analysis. Results should variation in skin lipid between participants when factors such as gender, age and diet were accounted for. GC-FID has also been used to study variation of sebum content in males with and without acne.[83] In this study, TS was used to sample the skin and liquid extraction was performed to isolate the lipids. Participant with acne should increase secretion of sebum that contained higher levels of squalene but lower FFA content relative to participant without acne. While the majority of reports used TS for SC sampling, Thomas *et al*. used a PDMS skin patch coupled with thermal desorption secondary electrospray ionisation-MS (TD-SESI-MS) to collect and analyse skin FAs.[86] This technique was validated against TD-GC-MS and showed more than 95% analytical agreement. TD-SESI-MS proved to be more advantageous as the analysis time was reduced by 79% compared to GC-MS. This platforms show promising potential for high throughput screening of skin volatile biomarkers including lipids. One of the characteristics linked to AD is the impaired immune system, specifically the dysregulation and overactivation of type 2 immune response. Using TS and LC-MS-MS Leung *et al*. investigated the effect of type 2 immune hyperactivation on skin surface lipids.[87] Chromatographic results showed that lipids TS from the SC of AD subjects showed a reduction in long chain FFAs. Furthermore, RNA sequencing revealed the decreased expression of elongase enzyme that is responsible for forming long-chain FFAs.

Sadowski *et al*. developed a method capable of simultaneously analysing epidermal and sebaceous lipids for the first time recently.[88] The comparative study used high-throughput shotgun MS to analyse CER classes, TGs and cholesterol esters in TS SC and compared SC lipid composition based on anatomical site, gender and age. Selective analysis of lipid material originating from the epidermal rather than sebaceous glands was also possible by setting the

electrospray ionisation (ESI) in the negative mode ((-)ESI). Cemera *et al*. demonstrate how this modality allows for the preferable detection of lipid species that form deprotonated ions which originated predominantly from the epidermis. Sebum derived lipids are neutral and so are unfavourable for this detection.[74] Analysis of FFAs and cholesterol was performed using HPLC/(-)ESI-TOF-MS. Although (-)ESI is unable to differentiate between sebum and SC derived FFA, knowledge of the different chain lengths and unsaturation pattern of FFA present in each compartment allowed for discrimination.[74]

### *1.5.3 Sweat*

As well as exogenous sebaceous lipids on the surface of the skin, an exogenous aqueous emission from glands is sweat. This aqueous fraction is derived from eccrine and apocrine sweat gland secretion. As discussed previously in Section *1.5.2* the composition of sweat originating from each of these gland types is different. Sweat is complex aqueous matrix that contains various micronutrients like magnesium, calcium and iron, however water and NaCl are most abundant in the mixture.[89,90] Blood sampling although is the gold standard for diagnostics, is invasive and requires processing for plasma protein removal. Due to the presence of very nominal impurities in sweat, very little sample preparation is required relative to blood and indeed other body fluids.[91] In addition sweat is released naturally and thus can be sampled without irritating the skin and in a non-invasive manner.[91] Sweat is also more chemically stable meaning it can be stored for longer periods of time unlike other biofluids. Thus, sweat is a great bodily-fluid for non-invasive skin sampling. Biomarkers that can be measured in sweat include lactate, amino acids, sodium and potassium ions all of play an important role in skin hydration and proper SC function.

#### *1.5.3.1 Methods of sweat analysis*

An ideal sweat sampler is one that is easy to use and is capable of collecting sweat reproducibly and in sufficient volumes for subsequent analysis. Various sampler designs have been proposed but the most simple technique uses an occlusive patch containing filter paper or gauze to collect skin sweat samples.[91] A major drawback of this approach is that occlusion of the skin can lead to variation in sample pH and skin irritation.[91] A nonocclusive approach was investigated using filter paper mounted on a surgical dressing film and lined with an adhesive layer for skin contact.[91] The semipermeable film allowed for selective transfer of water, oxygen and carbon dioxide from the skin surface underneath while hindering penetration of non-volatile substances. However, these patched are not useful for quantitative sweat analysis as

evaporation of water from the sweat leaves behind metabolites ($Na^+$ and $Cl^-$) in a concentrated form without knowledge of the total volume of excreted sweat.[92] Another drawback of the patch approach is that sample collection is done over a long period of time (hours to days) whereby sweat composition is likely variable.[92] Methods such as the Macroduct® that collect sweat directly from the skin surface into a coil of plastic tubing that can either be analysed immediately for ionic composition or directed (via pressure from an empty syringe) to the conductivity cell for conductivity analysis.[93,94] This device although expensive offers fast and quantitative collection of sweat for a variety of studies since sample collection is rapid (30 minute) and thus changes in sweat composition can be related to a certain time frame or an intervention occurring.[92] Since liquid sweat is collected, it is possible to measure its volume and thus normalise the amounts of analytes detected. The small size of the device is particularly desirable to targeted site studies.

Recently, sweat collection techniques have been tailored towards wearable devices that can collect sweat via on-board analysis of sweat for diagnostic purposes.[95] Gao *et al* have revolutionised the sweat biosensing field with a flexible wearable sensor array that use microfluids to collect sweat directly from the body and simultaneously measure multiple analytes (**Figure 1.4**).[96] The sensor is driven by a flexible printed circuit board (FPCB). Silver electrodes printed on polyethylene terephthalate PET substrate can electrochemically measure sweat metabolites (glucose and lactate) and electrolytes (sodium and potassium). A water-adsorbent pad was placed between the skin and the sensor to collect sweat for stable and reliable sensor readings and to prevent. Generation of sweat was performed by increasing sweating rate via exercise.

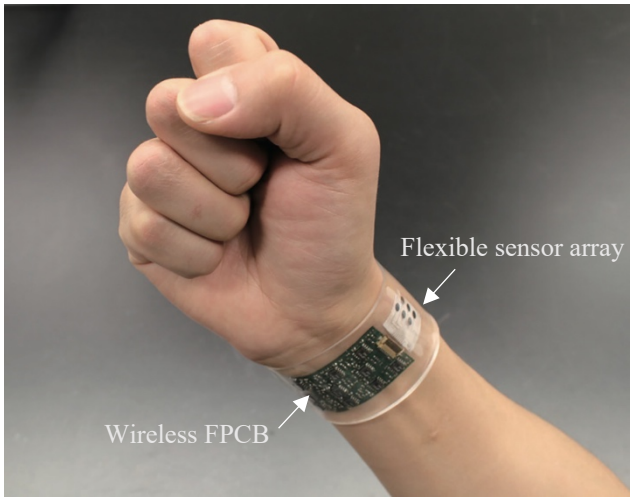


**Figure 1.4** Photograph of the wearable sensor on a subjects wrist showing the flexible sensor array and wireless FPCB developed by Gao *et al*.[96]

Besides exercise, it is possible stimulate sweat release from the body through chemical means. Emaminejad *et al*. explored the use of iontophoresis to deliver sweat inducing agonists (pilocarpine or acetylcholine) to the sweat glands. Kim at al. developed a wearable temporary-tattoo biosensing system capable of real-time non-invasive alcohol monitoring through the use of flexible iontophoretic-sensing electrodes with wireless electronics.[97] This tattoo based sensor employs an alcohol-oxidase enzyme and a Prussian Blue electrode transducer that can detect sweat alcohol levels when tattooed onto the skin. Participants had ethanol concentrations measured before and after consumption of alcohol, with higher ethanol levels being detected following alcohol consumption with this tattoo platform. The wearable device showed more reliable results compared to the tradition breathalyser method which is associated with inaccuracies caused by temperature, humidity and consumer products such as mouthwash. It also proved to be a faster method of measuring blood alcohol concentration relative to other transdermal devices taking only 10 min.

In addition to alcohol sensing in sweat, caffeine and levodopa have also been explored as potential analytes for detection in sweat. A wearable sensor consisting of a carbon working electrode modified with carbon nanotube/Nafion film was used for oxidative detection of caffeine.[98] To extract the sweat, participant were asked to cycle on stationary bike while wearing the sensing platform packaged in a PDMS wristband. Strong correlation was found between ingested levels of caffeine and caffeine in sweat as measured by the sensing devise. The study highlights an alternative method to urine testing for illicit drug use in athletic

competition. For levodopa sensing, a wearable sweat sensor similar in design to that of the caffeine sensor was used but a silver/chromium electrode with immobilised tyrosinase enzyme was employed.[99] The device from this study showed promising potential for optimising levodopa dosages for patients with Parkinson's disease, as opposed to the traditional way of assessing dosage via the subjects' motor function.

pH is another parameter that can be assessed by measuring the hydrogen ion concertation found in sweat. Section *1.5.4* will review such devices for non-invasive sweat pH measurement.

*1.5.4 Skin surface pH*

Originally the acidic nature of the skin was thought to be a defence mechanism against invading organisms. Recently, it was demonstrated that an acidic environment is essential for key processes involved in the synthesis and maintenance of a competent skin barrier structure.[13,100] Formation of CER is dependent on aSMase and b-GlcCer'ase (S7) enzymes that displays pH optima of 5. Only at this reduced pH of the SC can the enzymes generate enough CER to form the lamellar bilayers.[101] The importance of the acidic nature of skin is demonstrated in skin diseases such as AD where the ammonia induced alkylation in neonates' skin causes irritation and further perturbation of the skin barrier.[55] Recovery is delayed with neutral pH as it interferes with SC lipid processing. Emollients with low pH have been used to speed up barrier recovery.[102] Thus, the acidic mantle of the skin plays a significant role in SC homeostasis, the restoration of the disrupted barrier and the maintenance of the skin microbial flora.[55]

Acidification of the SC is achieved and maintained via various endogenous and exogenous. mechanisms as seen in **Figure 1.5**. The acidic nature of the SC is for permeability barrier function and cutaneous antimicrobial defence. One endogenous mechanism proposed involves the secretory phospholipases A2 (sPLA2) that generate FFAs from the hydrolysis of epidermal PL and other complex lipids.[72] In general, medium and long chain FFAs have $PK_a$ values of approx. 4-5-5.0 suggesting their preferable existence on the SC that has pH values of 4.1-5.8.[103] Inhibitory studies targeting the family of enzymes responsible for converting PL to FFA showed that blocking this process affected SC acidity which resulted in abnormalities in the skin's barrier function and thus highlighting, the importance of these family of enzyme in maintaining FFA composition of the SC.[72] Insufficient levels of FFA on the SC can lead to improper function of the SC barrier. AD, is characterised by a decrease in FFA chain length and an increase in unsaturated FFA.[11] This disruption in FFA composition affects the lipid organisation in the SC and thus the skin barrier function.[11] Another endogenous contributor to

the acidification of the SC is the sodium-hydrogen exchanger 1 (NHE1) which actively pumps protons into the lower layer of the SC.[25] The activation of this pump is regulated by a gene, $BRAF^{V600E}$,that codes a protein responsible for directing cell growth. $BRAF^{V600E}$, is the most frequent mutation in melanoma. Indeed, patients with this type of skin cancer suffer from pH dysregulation depicting high extracellular pH values.[104] High pH increases permeability of eh SC making it easier for foreign bodies to penetrate the skin.[105] furthermore, the uncontrolled pH fluctuation promotes malignant transformation of melanocytes.[104]

Exogenous mechanism include FFA generation by sebaceous glands as discussed in Section *1.5.2.2* Eccrine gland-derived sweat products such as lactic acid (generated via glycolysis) is another exogenous mechanism that contributes to the acidity of the SC.[103,106] However, the lower pKa of 3.9 lactic acid outside the range of physiological skin surface pH, likely accounts for a less significant buffering role than that of FFAs. Trans-urocanic acid (UCA) generated from the proteolysis of FLG is also proposed as a source of SC acidity (urocanic acid has a pKa of 4.7).[103] It was Krien *et al*. who first proposed that the pathway of FLG degradation to histidine (His) to UCA alone could explain the acidic pH of the SC.[107] FLG is rich in basic amino acids such as, His, arginine and glutamine. Deimination of histidine via histidase releases UCA. Not only is it important for maintaining the acidic skin surface pH required for enzymatic activity within the SC, but UCA also effects habitation of SC by *S.aureus* at physiological concentrations.[108]

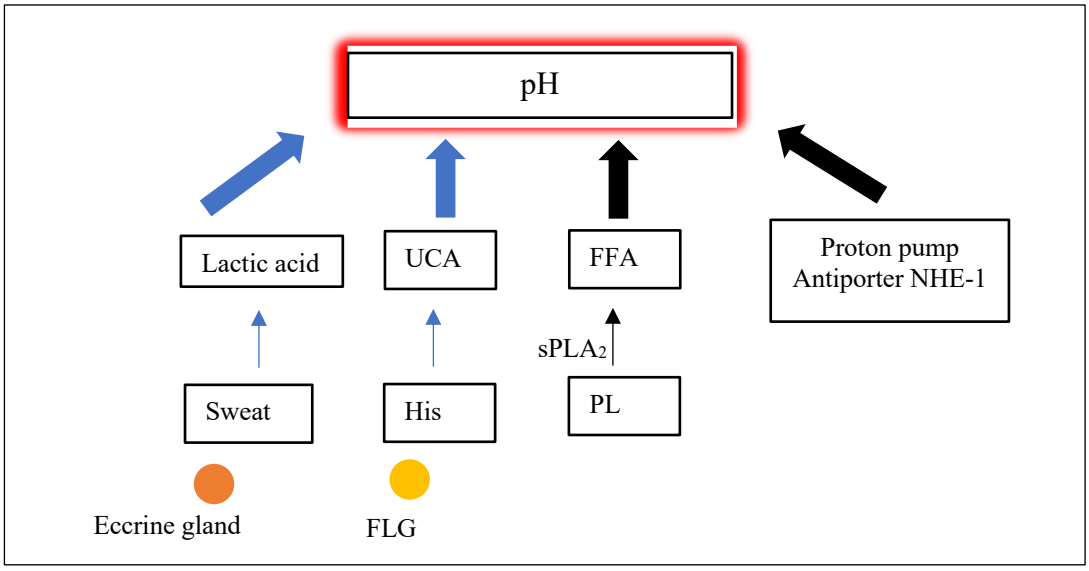


**Figure 1.5** Contributors to skin surface pH. Endogenous pH sources are depicted as black arrows, and exogenous pH sources as blue arrows.[109]

*1.5.4.1 Methods of skin surface pH analysis*

By definition, pH is a measure of the -log[$H^+$] concentration in an aqueous solution. This measurement is typically performed using a pH probes comprising an ion selective electrode (ISE) that measure the activity of a target analyte (hydrogen ion) and convert it into a measurable electric signal.[110] An ISE comprises an indictor electrode and a reference electrode. The indicator electrode has a perm-selective membrane that allows for the hydrogen ion to partition freely in and out of the membrane material. When the probe comes in contact with a solution containing hydrogen ions, the diffusion of the ions towards the membrane creates a voltage at the sample-membrane phase boundary. The difference in voltage between the reference and the indicator electrodes is the measured potential signal and is a measure of the solution's pH.[111] Skin surface pH measurements reflect an 'apparent pH reading' because the skin is not an aqueous medium. Instead, the skin has lipids that release hydrogen ions into the water layer applied on the skin by the pre-wetted electrode.[56,112] Skin surface pH is most commonly measured using a glass (or flat) electrode interface as opposed to the more common bulb-shaped probe **Figure 1.6**.[113]

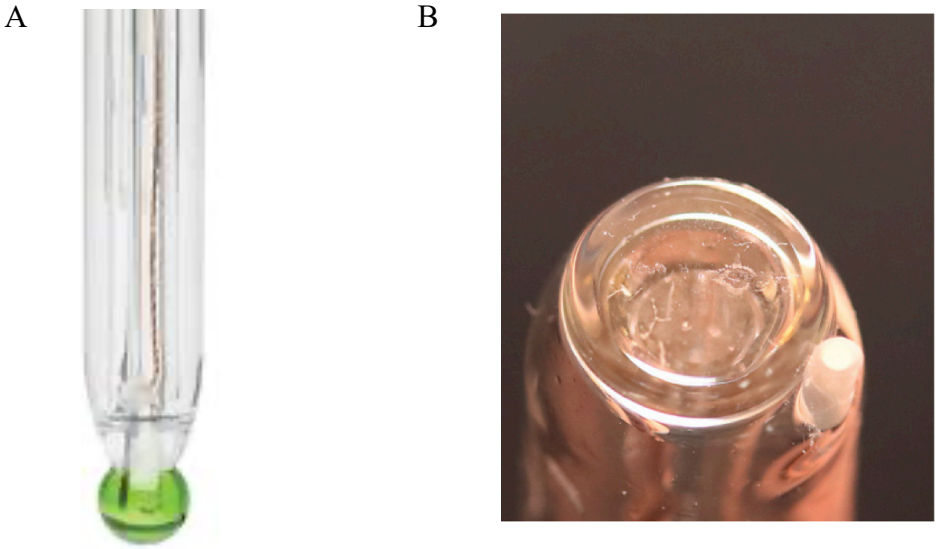


**Figure 1.6** (A) Bulb glass pH electrode for conventional solution pH measurements and (B) adapted planar glass electrode for skin surface pH measurements.

As well as taking measurements directly from the SC surface, sweat pH measurements have been used as a measure of the skin surface pH. However, one of the major barriers to

performing this measurement in sweat lies in the sampling step. One approach to sampling involves the use of gauze pads to collect sweat that was then analysed off-line in a tedious and time consuming way that is subject to error like the introduction of contaminants from the sampling material.[91] Sensing devices that have intimate contact with skin for sampling in-situ monitoring have emerged as a more attractive option.[114–116] Wang *et al*. described a platform capable of potentiometric real-time monitoring of pH via collected sweat samples. The device incorporates a solid-contact ISE coated with a polyaniline membrane, fabricated into a pH sensitive tattoo via conventional screen printing. pH sensitivity of the polyaniline lies in its reversible transition between salt and base emeraldine.[114] Performance of this sensor was tested in the pH range of 3-7, which covers the pH range of human sweat. However, on-body monitoring revealed that the sensor generated a response only after a high sweat flow was generated (participant cycling for 10 mins. Nyelin *et al*. also explore the use of sweat for the simultaneous measurement of pH together with calcium.[115] To generate sweat, subjects cycled on a bike for 30 min at a constant workload. To generate volumes of sweat was generated for the epidermal sensor to detect pH and calcium. The multiplexed system was essential as biological calcium measurements depend on pH. While the pH sensing electrode detected hydrogen ions ($H^+$) via the deprotonated layer of polyaniline on its surface, a calcium ($Ca^{2+}$) ionophore electrode was used for $Ca^{2+}$ sensing. When applied to skin, the wearable device showed that an increased $Ca^{2+}$ potential was detected and an increase in potential was detected by the pH electrode as pH decreased. Reading accuracy of this device was comparable to those obtained using inductively coupled plasma-MS (ICP-MS). These results highlight the possible use of this device for detecting and diagnosing diseases and conditions such as myeloma, cirrhosis, primary hyperparathyroidism and kidney stones via non-invasive skin analysis. Although sweat is accessible, the requirement to produce sweat in large volumes for diagnostic analysis is a limitation. To overcome this, Yang *et al*. explored the use of paper microfluidics to develop a microneedle-based sensor that requires only micro volumes of sweat for analysis.[116] As well as electrochemical methods, colorimetric sensors are another interesting sensing approach to measuring sweat pH. Choi *et al*. report the use of a colorimetric array in which universal pH dye solution along with other cocktail dye assays was integrated into a Polymethylmethacrylate (PMMA) patch for measurement of pH, sweat rate and sweat composition.[117] When worn on the skin device used an adsorbent pad with microfluids channels to collect the sweat into a reservoir and direct it to multiple test regions to record sweat pH among other parameters. Typical of colourimetric sensors; the fabricated patch did not require electrical wiring and analysis was performed using a smartphone camera. Zhang *et*

*al*. explored a wearable colourimetric sensor for in situ sweat sampling and quantitative sweat analysis for pH other sweat metabolites.[118] The colorimetric band consisted of organic and inorganic dyes drop cast on a PET substrate. Litmus solution, mercuric thiocyanate, potassium iodide-glucose oxidase system and o-cresolphthalein complexone made up the colorimetric assay for the respective detection of chlorine, glucose and calcium. A subject was required to exercise for several min until a visible amount of sweat was generated. Although quantitative, the approach was not entirely satisfactory due to the low sensitivity and high error in analyte estimation. To eliminate these drawbacks, the group of Rogers have recently developed a state of the art sweat sampling and sensing system capable of sensitive analysis of sweat.[119,120] The device was fabricated using lithography techniques along with PDMS to develop analysis system that only require micro volumes of sweat. The group demonstrated in-situ monitoring of pH along with sweat loss rate and concentration measurements for lactate, glucose and chloride. on-body sampling device is done via microfluids channels that collect sweat from the skin and direct it to the various dye chamber of the device. The initial design contained pH sensitive dyes such as methyl red for pH detection.[119] The colour change was compared to reference markers such as lightness as well as the red green and blue (RGB) values for estimating sweat pH. This device was limited to a single use. In a recent iteration, the group eliminated this limitation by developing a platform with a disposable microfluidic system. A magnet facilitated the attachment/detachment of the microfluidic system to the electronic sensor body. This wearable sensor that uses a combination of electronics for electrochemical detection and colourimetry for visual readout to monitor multiple parameters simultaneously is highly advantageous. Furthermore, the research has culminated in a commercially available pH sensor, My Skin Track pH launched in 2019 by L'Oreal.[121] A smartphone camera is used for imaging the colorimetric dye, and an algorithm is used for processing the colour difference before and after exposure to sweat, thus giving an estimated skin pH value.[119]

### *1.5.5 Skin volatile emission*

The characteristic human odour can be divided into three classes.[122] The "primary odour" consists of compounds whose concentrations are static over time regardless of diet and environmental factors.[122] The "secondary odours" are also endogenous compound, but their abundances are influenced by diet and environment.[122] Other exogenous compounds coming from topically applied ointments such as creams lotions soaps or perfumes are classified as tertiary odour.[122] The production of VOCs responsible for the human odour is governed by secretions from the three glands eccrine, apocrine and sebaceous as mentioned previously.[123,124]

The different distributions of these glands reflect distinct odour emitted from different body parts.[36,37] In general, eccrine and sebaceous glands are omnipresent on the skin.[40] Eccrine glands are localised mainly in the palms and soles whereas sebaceous glands are primally located on the scalp and face but not in the palms and soles.[40] In contrast, apocrine glands are only found in specific locations of the body: the axillae, areola, and nipples of the breast, ear canal, eyelids, wings of the nostril, perianal region, and some parts of the external genitalia.[36] Initially, sweat is an odourless substance consisting mainly of water and salt, but bacterial activity on apocrine sweat secretions cause odour. Thus the skin releases a variety of volatile metabolites with different biological origins that are subject to bacterial action.[124] The most frequently present microorganisms on the SC belong to families like *Corynebacterium*, *Staphylococcus*, *Propionibacterium, Streptococcus, Micrococcus*, *Kocuria*, *Malassezia*, *Brevibacterium*, *Dermabacter*, *Acinetobacter*, and *Methylobacterium*.[125] Many factors contribute to their successful growth on human skin, mainly; their ability to grow aerobically and anaerobically over wide ranges of temperatures (15-40°C) and pH (4.5-8), their halotolerance and their ability to breakdown host polymers cell and utilise them for energy.[126] The different characteristics associated with each microbe dictates what part of the body it will grow on. *Propionibacterium acnes* accounts for approximately half of the total microbiota of the skin.[126] Due to their anaerobic nature, they predominantly inhabit regions of the body with a high density of hair follicles like the face and the scalp.[126] Microbial metabolites, especially those linked to the activity of *S.aureus, Staphylococcus epidermidis (S.epidermadis)* and *Propionibacterium play a role in* cutaneous skin disorders such as psoriasis, AD and rosacea.[127] However, the majority of bacteria residing on the skin are non-pathogenic and symbiotic. They can help regulate the host's immune system and eliminate competition from other pathogenic bacteria by producing toxic compounds like bacteriocins or antibiotics.[128] As part of their natural metabolism microorganisms produce VOCs and microbial VOCS that include a variety of compounds such as fatty acids and their derivatives, nitrogen and sulfur-containing compounds, terpenes and aromatic compounds. Studies carried out on the headspace composition of bacterial cultures grown in vials revealed differential production of volatile depending on bacterial strains and growth conditions.[129,130] For example, volatile profiles produced by *Pseudomonas aeruginosa* varied as incubation temperature was raised from 30 °C to 37 °C.[129] While 1-undecene was dominant in both profiles, an increase in long chain methyl ketones (*e.g.* 2-undecanone) was observed at the higher temperature.[129] Strains of *S.epidermidis* also produced long chain methyl ketones, but fewer alcohols, aldehydes and alkenes were present. However, only 1 strain produced 3-methyl butanal suggesting that differences in the

breakdown of VOCs between strains occur. Among the strains grown in vials no identifiable VOCs were obtained from *Rerythopolis* cultures, and very low levels of VOCs were recovered from *B. epidermidis* and *C. xerosis*.[129]

The volatile human fingerprint is a lot more complicated and prone to changes with varying microbial inhibitions. Not only do these skin florae produce their own metabolic VOCs, but they also degrade secretions from our skin glands to produce other VOCs that contribute to the skin's overall VOC profile.[131] Skin VOC emissions are derived from gland secretions and the metabolism of skin microbiota.[131] Many of these VOCs are responsible for body odour. Any changes in the body's physiology - be it through acquiring an infectious disease or changing environmental conditions- may be reflected through a change in the body's VOC profile.[23,27] By understanding these VOCs, it is possible to gain beneficial information about the metabolic state of an individual.[23] Certain abnormal conditions such as cancer, metabolic disorders and infectious diseases can affect the daily VOC profile of an individual.[131,132] The detection of unusual VOC or disease specific VOC allows for potential use as diagnostic biomarkers. The low concentration, at which the VOC are emitted means suitable and sensitive sampling procedures, pre-concentration steps and detection techniques need to be employed.[131]

*1.5.5.1 Methods for skin volatile analysis*

The most commonly employed technique for skin VOC analysis is GC-MS due to its advanced identification capacity and ability to analyse hundreds of species simultaneously.[133] Mass spectroscopy is a sensitive method for VOC detection, identification and characterisation. Prior to the analysis of collected VOCs, a sampling method needs to be implemented.

There is no standardised method for collecting skin VOC samples. The literature describes many different ways of skin sampling.[134–136] In their review, Dormont *et al*. for example investigate four sampling methods for VOC collection followed by GCMS analysis. Solvent extraction was done by slightly scraping the sampling area with a razor then placing it in an organic solvent (diethyl ether or dichloromethane). Diethyl ether extracted more compounds of the ester chemical class relative to dichloromethane. Possible contamination of the sample with compounds that are non-volatile at body temperature is an issue associated with set sampling method.[134] Non-contact headspace solid phase microextraction (HS-SPME) was also performed.[134] Here the sampling site was enclosed in a non-reactive plastic bag and following equilibration (15 min), a SPME fibre was introduced into the bag. This solvent-free method is

advantageous as the collection fibres are thermally desorbed directly onto GC injector without need for sample pre-treatment.[134] The latter two methods investigated by Dormont *et al*. contact SPME and dynamic headspace were novel and tailored towards on field collection of human VOCs.[134] Compound identification was done via GC-MS, and subsequent retention index matching was performed. Their results show that dynamic headspace trapped the greatest number of VOCs. As expected and unlike the other sampling methods, solvent extraction picked up some molecules with high relative molecular weight, possibly ones that are non-volatile at body temperature.[134]

To avoid contamination of skin volatiles with non-volatile skin secretions, there is increased interest in developing wearable non-contact sampling methods for skin VOC collection. Jiang *et al*. described a wearable HS sampling method using PDMS membrane sandwiched between two layers of stainless steel mesh (**Figure 1.7).**[137] When placed on the skin, the mesh prevents contact of PDMS with the skin, and an aluminium foil was used to cover the sampler and secure it in place using surgical tape**.** The sampler was left on the skin for 60 min to collect VOCs after which desorption onto GC-MS was performed, and a custom library was used to characterise recovered compounds. The sampler was used to track the metabolism of alcohol in participants after drinking a single shot of whiskey. The maximum peak for ethanol was observed 50 min after alcohol consumption, and this was in agreement with blood alcohol concentration. However, this sampling method was inefficient at quantitatively detecting semi and low volatile compounds such as 1-octadecanol. To overcome this, it was proposed that increasing the sampling time or introducing activity to elevate body temperature may help in solving this issue.

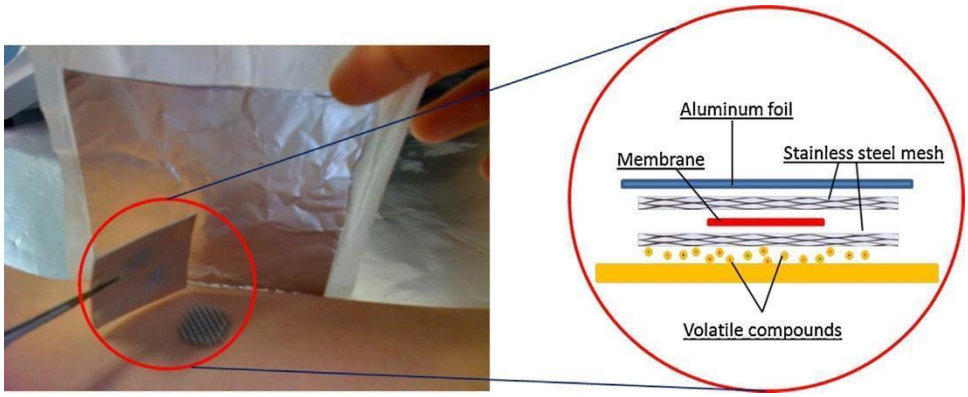


**Figure 1.7** Schematic diagram of membrane sandwich set up used for skin volatile collection. The Zoomed in portion shows the PDMS collection membrane sandwiched between two stainless mesh. [137]

Our group utilise a HS-SPME sampling method in a wearable sampling format (**Figure 1.8**).[138–140] The wearable sampling platform consists of a glass funnel with a septa-sealed narrow inlet that holds the SPME fibre in place during sample collection. The glass HS is taped to the forearm. The SPME fibre is exposed to the volatiles entrapped in this glass headspace for 15 min which ensured equilibrium (between HS and SPME fibre) was reached Using this method, our group have assessed skin volatile composition following skin barrier disruption via TS.[139] For this, VOC samples were collected before and after TS and GC-MS was used for compound identification. Results showed quantitative differences in some sebum derived components before and after TS of the skin was performed.. Although this wearable device is not currently soft or conformable with skin , it is a convenient sampling method that can be used to study variations in skin volatiles in individuals with a compromised skin barrier.[139,140]

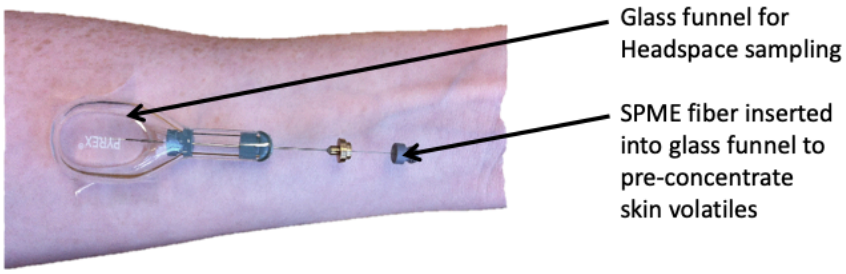


**Figure 1.8** HS-SPME wearable sampler using a glass funnel with septa seal to define HS during skin volatile sample collection.

SPME is one of the more advantageous sampling method in which equilibrium is reached in a non-exhaustive manner where the amount of compounds extracted depends on the distribution constant between the gases and coating phase on the fibre.[141] Once a suitable coating polymer is identified equilibrium can be reached within minutes.[139] SPME is a two-step process that requires sorption of analyte onto the fiber then direct desorption is possible when SPME-GC-MS is used. Other frequently used direct MS techniques for skin volatile analyses include selected ion flow tube mass spectrometry (SIFT-MS), proton transfer reaction mass spectrometry (PTR-MS) and ion mobility mass spectrometry (IM-MS).[142,143] Direct methods of VOC analyses are superior as no preconcentration-step required which reduces sample handling thus eliminating possible route of sample contamination. GC coupled with ion mobility spectrometry GC-IMS has also been applied to the monitoring of skin VOCs, but since

IMS does not have a commercially available library of compounds, parallel GC-MS analysis is required.[142] Thus, GC is the superior method for sample separation.

The low cost, short response time, and stability of metal oxide gas sensors (MOGS) make them a popular choice as a portable approach for the detection of VOCs. In fact, metal oxide semiconductors are among the preferred candidates for the detection of the trace amounts of gases (<ppm level).[144]

The basic operation of a MOGS is based on the change in conductivity of the sensor in the presence of oxidising or reducing gases.[144] The sensing material is deposited on electrodes and an insulator layer, such as a micro-electro-mechanical system (MEMS) is used to achieve thermal isolation of the heating unit **(Figure 1.9).** The top layer of this sensor is exposed to the target analytes. Exchange of charged species between the target gas and the metal oxide (MO) sensing surface can be done via catalytic reaction. The adsorption/desorption of analyte gases at elevated temperatures (provided by microheater) causes a change in charge carrier concentration. This affects the physical and electrical properties of the sensing material leading to changes in the conductivity of the device. Thus an electrical signal is used to represent the type and concentration of a gas present.

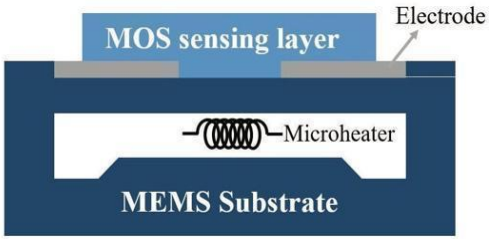


**Figure 1.9** Cross sectional view of a MOS sensor comprising of a set of electrodes, micro-heater, and sensing layer fabricated on a thin suspended membrane using MEMS fabrication technology. The change in the sensing material conductance due to the interaction with analytes is proportional to the concentration of the analytes in the sensor environment.[144]

Carmona *et al*. present an innovative way of volatile sweat assessment.[145] Here they describe a method for characterising bacteria present in sweat. For that, they prepared two SnO2-based gas sensors via a) thin film using the retroaxial growth and thermal oxidation methods and b) nanowires using direct evaporation-condensation techniques. The synthesised sensors were then integrated into a commercially available electronic nose coupled with an auto-sampler headspace system. Different microorganisms blends were grown in artificial sweat. Results

from the developed sensor were compared to conventional GC-MS. Although the device did discriminate between microbiota species, It would be interesting to investigate the effectiveness of the system for analysing real human sweat samples which are more complex in composition.

In a recent publication, Güntner *et al*. demonstrated the use of metal oxides array to accelerate urban search and rescue of entrapped humans via detection of volatile human signature.[146] The fabricated portable device consists of three nanostructured metal oxide sensors: Si-doped tungsten oxide, Si-doped molybdenum oxide and Ti-doped zinc oxide for sensitive and selective detection of trace acetone, ammonia and isoprene, respectively. The array also contained commercial sensors for relative humidity (RH) and $CO_2$ detection. The sensing device showed high discriminatory power for detecting the human signature from the background at a signal/noise ratio of 3. When tested on humans entrapped in a plethysmography chamber, the results obtained by the sensor array were in agreement with benchtop selective reagent ionisation time-of-flight mass spectrometry.

The MO devices discussed above are examples of non-wearable sensors. More recently, the first wearable metal oxide sensor that can non-invasively monitor alcohol emissions from the skin was reported.[147] Three MO sensors were sputter coated with tin dioxide using RF reactive magnetron and fabricated into a wearable electronic bracelet. Along with the metal oxide sensors, the wristband had a humidity and temperature sensor and a printed circuit board for data collection. The bracelet was strapped to the wrist. A constant current was passed through the sensor as conductivity was being measured. In-vivo analyses were conducted, and the performance of the wrist band was validated using a mobile benchmark test (analysis of blood and breath samples). Participants were asked to consume different alcohol concentrations. The results showed that the sensor was effective at discriminating between different concentrations of ethanol vapour emitted from the skin. The sensor displayed a greater response to ethanol and better power consumption than commercial sensors

## 1.6 Conclusion

Skin is the body's largest organ, whose primary purpose is protection. Potentially the skin can offer insight into a person's health. Exploring skin properties such as sweat and skin volatile profile compositions has proven beneficial approaches for the non-invasive assessment of skin for diagnostic applications. Epidermal sensors are replacing the use of expensive probes and other invasive methods for skin assessments. These sensors are less intrusive as they assess the readily accessible skin matrix. Although progression in this field is evident, there still exists room for research opportunities, especially around biomarker sampling (eg from sweat, SC, VOC emission) and sensor deployment as wearables on the skin. The thesis will introduce a new hypothesis as well as further explore exciting results in the field of skin surface measurements and skin volatile emission.

## 1.8 Thesis outline

The purpose of this work is to develop an epidermal platform approach for monitoring physiological activity relating to skin barrier function through the non-invasive assessment of skin properties such as skin pH and volatile organic composition. The thesis investigates the relationship between acidic skin volatile emissions and skin surface pH to determine the possibility of measuring skin pH via volatile composition. A wearable colorimetric sensor comprising a novel dye for the selective detection of amine emissions from the skin is describe.

Chapter 2- reports on the assessment of skin surface pH via the assessment of skin volatile emissions using headspace approach. The volatile emissions from different body sites (forearm and forehead) for males and females were characterised. pH was also collected and a linear regression trend line was conducted to investigate the relationship between acidic volatile emissions and skin surface pH. The effect of alcohol on skin surface pH and volatile emissions was also investigated.

Chapter 3- reports the synthesis of a colorimetric dye and its fabrication into a wearable sensor for the detection of amines emitted from skin. Response of the dye was tested in both liquid and solid state. Sensors were applied to the skin of participants at different body sites and the corresponding response was evaluated.

Chapter 4- discusses conclusions and recommendations for future work arising from this thesis.

## 1.8 References


1. Kolarsick, P. A. J., Kolarsick, M. A. & Goodwin, C. Anatomy and Physiology of the Skin. *J. Dermatol. Nurses Assoc.* **3**, 203–213 (2011).
2. Sahle, F. F., Gebre-Mariam, T., Dobner, B., Wohlrab, J. & Neubert, R. H. H. Skin Diseases Associated with the Depletion of Stratum Corneum Lipids and Stratum Corneum Lipid Substitution Therapy. *Skin Pharmacol. Physiol.* **28**, 42–55 (2015).
3. Proksch, E., Brandner, J. M. & Jensen, J.-M. The skin: an indispensable barrier. *Exp. Dermatol.* **17**, 1063–1072 (2008).
4. Kanitakis, J. Anatomy, histology and immunohistochemistry of normal human skin. *Eur. J. Dermatol. EJD* **12**, 390–399; quiz 400–401 (2002).
5. Takahashi, M., Kawasaki, K., Tanaka, M., Ohta, S. & Tsuda, Y. The mechanism of stratum corneum plasticization with water. in *Bioengineering and the Skin: Based on the Proceedings of the European Society for Dermatological Research Symposium, held at the Welsh National School of Medicine, Cardiff, 19–21 July 1979* (eds. Marks, R. & Payne, P. A.) 67–73 (Springer Netherlands, 1981). doi:10.1007/978-94-009-7310-7_8.
6. Hoover, E. & Krishnamurthy, K. Physiology, Sebaceous Glands. in *StatPearls* (StatPearls Publishing, 2020).
7. Hodge, B. D. & Brodell, R. T. Anatomy, Skin Sweat Glands. in *StatPearls* (StatPearls Publishing, 2020).
8. Rippke, F., Berardesca, E. & Weber, T. M. pH and Microbial Infections. *Curr. Probl. Dermatol.* **54**, 87–94 (2018).
9. Drislane, C. & Irvine, A. D. The role of filaggrin in atopic dermatitis and allergic disease. *Ann. Allergy Asthma Immunol. Off. Publ. Am. Coll. Allergy Asthma Immunol.* **124**, 36–43 (2020).

10. Kubo, A., Nagao, K. & Amagai, M. Epidermal barrier dysfunction and cutaneous sensitization in atopic diseases. *J. Clin. Invest.* **122**, 440–447 (2012).

11. Smeden, J. van *et al.* The importance of free fatty acid chain length for the skin barrier function in atopic eczema patients. *Exp. Dermatol.* **23**, 45–52 (2014).

12. Del Rosso, J. Q. & Levin, J. The Clinical Relevance of Maintaining the Functional Integrity of the Stratum Corneum in both Healthy and Disease-affected Skin. *J. Clin. Aesthetic Dermatol.* **4**, 22–42 (2011).

13. Schmid-Wendtner, M.-H. & Korting, H. C. The pH of the Skin Surface and Its Impact on the Barrier Function. *Skin Pharmacol. Physiol.* **19**, 296–302 (2006).

14. Shirasu, M. & Touhara, K. The scent of disease: volatile organic compounds of the human body related to disease and disorder. *J. Biochem. (Tokyo)* **150**, 257–266 (2011).

15. Rondanelli, M. *et al.* Volatile Organic Compounds as Biomarkers of Gastrointestinal Diseases and Nutritional Status. *J. Anal. Methods Chem.* **2019**, e7247802 (2019).

16. Mochalski, P., King, J., Unterkofler, K., Hinterhuber, H. & Amann, A. Emission rates of selected volatile organic compounds from skin of healthy volunteers. *J. Chromatogr. B Analyt. Technol. Biomed. Life. Sci.* **959**, 62–70 (2014).

17. Kataoka, H., Saito, K., Kato, H. & Masuda, K. Noninvasive analysis of volatile biomarkers in human emanations for health and early disease diagnosis. *Bioanalysis* **5**, 1443–1459 (2013).

18. Samant, P. P. & Prausnitz, M. R. Mechanisms of sampling interstitial fluid from skin using a microneedle patch. *Proc. Natl. Acad. Sci. U. S. A.* **115**, 4583–4588 (2018).

19. Samant, P. P. *et al.* Sampling interstitial fluid from human skin using a microneedle patch. *Sci. Transl. Med.* **12**, (2020).

20. Liu, Y., Pharr, M. & Salvatore, G. A. Lab-on-Skin: A Review of Flexible and Stretchable Electronics for Wearable Health Monitoring. *ACS Nano* **11**, 9614–9635 (2017).

21. Jayathilaka, W. A. D. M. *et al.* Significance of Nanomaterials in Wearables: A Review on Wearable Actuators and Sensors. *Adv. Mater.* **31**, 1805921 (2019).

22. Jin, H., Abu-Raya, Y. S. & Haick, H. Advanced Materials for Health Monitoring with Skin-Based Wearable Devices. *Adv. Healthc. Mater.* (2017) doi:10.1002/adhm.201700024.

23. Maibach, H. & Honari, G. *Applied Dermatotoxicology: Clinical Aspects*. (Academic Press, 2014).

24. Wong, R., Geyer, S., Weninger, W., Guimberteau, J.-C. & Wong, J. K. The dynamic anatomy and patterning of skin. *Exp. Dermatol.* **25**, 92–98 (2016).

25. Kern, F., Niault, T. & Baccarini, M. Ras and Raf pathways in epidermis development and carcinogenesis. *Br. J. Cancer* **104**, 229–234 (2011).

26. Amisten, S. *et al.* An atlas of G-protein coupled receptor expression and function in human subcutaneous adipose tissue. *Pharmacol. Ther.* **146**, 61–93 (2015).

27. Vitorino, C., Sousa, J. & Pais, A. Overcoming the skin permeation barrier: challenges and opportunities. *Curr. Pharm. Des.* **21**, 2698–2712 (2015).

28. Kubo, A., Nagao, K. & Amagai, M. 3D Visualization of Epidermal Langerhans Cells. in *Molecular Dermatology* (eds. Has, C. & Sitaru, C.) vol. 961 119–127 (Humana Press, 2013).

29. Benson, H. A. E. Skin Structure, Function, and Permeation. in *Topical and Transdermal Drug Delivery* 1–22 (John Wiley & Sons, Ltd, 2012). doi:10.1002/9781118140505.ch1.

30. Behne, M. *et al.* Omega-hydroxyceramides are required for corneocyte lipid envelope (CLE) formation and normal epidermal permeability barrier function. *J. Invest. Dermatol.* **114**, 185–192 (2000).

31. Elias, P. M. *et al.* Formation and Functions of the Corneocyte Lipid Envelope (CLE). *Biochim. Biophys. Acta* **1841**, 314–318 (2014).

32. Yang, G. *et al.* Skin Barrier Abnormalities and Immune Dysfunction in Atopic Dermatitis. *Int. J. Mol. Sci.* **21**, 2867 (2020).

33. Zhang, B. *et al.* Chapter 52 - Bioengineering Skin Constructs. in *Stem Cell Biology and Tissue Engineering in Dental Sciences* (eds. Vishwakarma, A., Sharpe, P., Shi, S. & Ramalingam, M.) 703–719 (Academic Press, 2015). doi:10.1016/B978-0-12-397157-9.00056-4.

34. Skin Tissue Engineering and Regenerative Medicine - 1st Edition. https://www.elsevier.com/books/skin-tissue-engineering-and-regenerative-medicine/albanna/978-0-12-801654-1.

35. Baswan, S. *et al.* Understanding the Formidable Nail Barrier: A Review of the Nail Microstructure, Composition and Diseases. *Mycoses* **60**, 284–295 (2017).

36. Murphrey, M. B. & Vaidya, T. Histology, Apocrine Gland. in *StatPearls* (StatPearls Publishing, 2020).

37. Saga, K. Structure and function of human sweat gland studied with histochemistry an cytochemistry. *Prog. Histochem. Cytochem.* **37**, 323–86 (2002).

38. Chen, Y.-L., Kuan, W.-H. & Liu, C.-L. Comparative Study of the Composition of Sweat from Eccrine and Apocrine Sweat Glands during Exercise and in Heat. *Int. J. Environ. Res. Public. Health* **17**, (2020).

39. Baker, L. B. Physiology of sweat gland function: The roles of sweating and sweat composition in human health. *Temp. Multidiscip. Biomed. J.* **6**, 211–259 (2019).

40. Cui, C.-Y. & Schlessinger, D. Eccrine sweat gland development and sweat secretion. *Exp. Dermatol.* **24**, 644–650 (2015).

41. Esteves, C. Z. *et al.* Skin Biomarkers for Cystic Fibrosis: A Potential Non-Invasive Approach for Patient Screening. *Front. Pediatr.* **5**, (2018).

42. Rigopoulos, D., Larios, G. & Katsambas, A. Skin signs of systemic diseases. *Clin. Dermatol.* **29**, 531–540 (2011).

43. Crowther, J. M. *et al.* Measuring the effects of topical moisturizers on changes in stratum corneum thickness, water gradients and hydration in vivo. *Br. J. Dermatol.* **159**, 567–577 (2008).

44. Horii, I., Nakayama, Y., Obata, M. & Tagami, H. Stratum corneum hydration and amino acid content in xerotic skin. *Br. J. Dermatol.* **121**, 587–592 (1989).

45. Hoste, E. *et al.* Caspase-14 Is Required for Filaggrin Degradation to Natural Moisturizing Factors in the Skin. *J. Invest. Dermatol.* **131**, 2233–2241 (2011).

46. Nakagawa, N. *et al.* Relationship Between NMF (Lactate and Potassium) Content and the Physical Properties of the Stratum Corneum in Healthy Subjects. *J. Invest. Dermatol.* **122**, 755–763 (2004).

47. Watanabe, M., Tagami, H., Horii, I., Takahashi, M. & Kligman, A. M. Functional Analyses of the Superficial Stratum Corneum in Atopic Xerosis. *Arch. Dermatol.* **127**, 1689–1692 (1991).

48. Taylor, N. A. & Machado-Moreira, C. A. Regional variations in transepidermal water loss, eccrine sweat gland density, sweat secretion rates and electrolyte composition in resting and exercising humans. *Extreme Physiol. Med.* **2**, 4 (2013).

49. Watabe, A. *et al.* Sweat constitutes several natural moisturizing factors, lactate, urea, sodium, and potassium. *J. Dermatol. Sci.* **72**, 177–182 (2013).

50. Bernengo, J. & de Rigal, J. Physical Methods to Measure Stratum Corneum Water Content In Vivo. in *Agache's Measuring the Skin: Non-invasive Investigations, Physiology, Normal Constants* (eds. Humbert, P., Fanian, F., Maibach, H. I. & Agache, P.) 299–340 (Springer International Publishing, 2017). doi:10.1007/978-3-319-32383-1_29.

51. Querleux, B. *et al.* In vivo Hydration Profile in Skin Layers by High-Resolution Magnetic Resonance Imaging. *Skin Pharmacol. Physiol.* **7**, 210–216 (1994).

52. Caspers, P. J., Bruining, H. A., Puppels, G. J., Lucassen, G. W. & Carter, E. A. In Vivo Confocal Raman Microspectroscopy of the Skin: Noninvasive Determination of Molecular Concentration Profiles. *J. Invest. Dermatol.* **116**, 434–442 (2001).

53. Narasimha Murthy, S. & Shivakumar, H. N. CHAPTER 1 - Topical and Transdermal Drug Delivery. in *Handbook of Non-Invasive Drug Delivery Systems* (ed. Kulkarni, V. S.) 1–36 (William Andrew Publishing, 2010). doi:10.1016/B978-0-8155-2025-2.10001-0.

54. Hansen, J. R. & Yellin, W. NMR and Intrared Spectroscopic Studies of Stratum Corneum Hydration. in *Water Structure at the Water-Polymer Interface* (ed. Jellinek, H. H. G.) 19–28 (Springer US, 1972). doi:10.1007/978-1-4615-8681-4_4.

55. Darlenski, R., Sassning, S., Tsankov, N. & Fluhr, J. W. Non-invasive in vivo methods for investigation of the skin barrier physical properties. *Eur. J. Pharm. Biopharm. Off. J. Arbeitsgemeinschaft Pharm. Verfahrenstechnik EV* **72**, 295–303 (2009).

56. Plessis, J. du *et al.* International guidelines for the in vivo assessment of skin properties in non-clinical settings: Part 2. transepidermal water loss and skin hydration. *Skin Res. Technol.* **19**, 265–278 (2013).

57. Blank, I. H. Further observations on factors which influence the water content of the stratum corneum. *J. Invest. Dermatol.* **21**, 259–271 (1953).

58. Lu, F. *et al.* Review of Stratum Corneum Impedance Measurement in Non-Invasive Penetration Application. *Biosensors* **8**, 31 (2018).

59. Kohli, R., Archer, W. I., Roberts, J. M. C., Cochran, A. J. & Li Wan Po, A. Impedance measurements for the non-invasive monitoring of skin hydration: a reassessment. *Int. J. Pharm.* **26**, 275–287 (1985).

60. Björklund, S. *et al.* Skin Membrane Electrical Impedance Properties under the Influence of a Varying Water Gradient. *Biophys. J.* **104**, 2639–2650 (2013).

61. Kabiri Ameri, S. *et al.* Graphene Electronic Tattoo Sensors. *ACS Nano* **11**, 7634–7641 (2017).

62. Yao, S. *et al.* A Wearable Hydration Sensor with Conformal Nanowire Electrodes. *Adv. Healthc. Mater.* **6**, 1601159 (2017).

63. Ye, L., Wang, Z., Li, Z., Lv, C. & Man, M.-Q. Validation of GPSkin Barrier® for assessing epidermal permeability barrier function and stratum corneum hydration in humans. *Skin Res. Technol. Off. J. Int. Soc. Bioeng. Skin ISBS Int. Soc. Digit. Imaging Skin ISDIS Int. Soc. Skin Imaging ISSI* **25**, 25–29 (2019).

64. De Guzman, K. & Morrin, A. Screen-printed Tattoo Sensor towards the Non-invasive Assessment of the Skin Barrier. *Electroanalysis* **29**, 188–196 (2017).

65. Guzman, K. D., Al-Kharusi, G., Levingstone, T. & Morrin, A. Robust epidermal tattoo electrode platform for skin physiology monitoring. *Anal. Methods* **11**, 1460–1468 (2019).

66. Wang, Y. *et al.* Low-cost, μm-thick, tape-free electronic tattoo sensors with minimized motion and sweat artifacts. *Npj Flex. Electron.* **2**, 1–7 (2018).

67. Swisher, S. L. *et al.* Impedance sensing device enables early detection of pressure ulcers in vivo. *Nat. Commun.* **6**, 6575 (2015).

68. van Smeden, J. & Bouwstra, J. A. Stratum Corneum Lipids: Their Role for the Skin Barrier Function in Healthy Subjects and Atopic Dermatitis Patients. *Curr. Probl. Dermatol.* **49**, 8–26 (2016).

69. Norlén, L., Nicander, I., Lundsjö, A., Cronholm, T. & Forslind, B. A new HPLC-based method for the quantitative analysis of inner stratum corneum lipids with special reference to the free fatty acid fraction. *Arch. Dermatol. Res.* **290**, 508–516 (1998).

70. Cui, L. *et al.* Advancements in the maintenance of skin barrier/skin lipid composition and the involvement of metabolic enzymes. *J. Cosmet. Dermatol.* **15**, 549–558 (2016).

71. Ansari, M. N., Nicolaides, N. & Fu, H. C. Fatty acid composition of the living layer and stratum corneum lipids of human sole skin epidermis. *Lipids* **5**, 838–845 (1970).

72. Fluhr, J. W. *et al.* Generation of Free Fatty Acids from Phospholipids Regulates Stratum Corneum Acidification and Integrity. *J. Invest. Dermatol.* **117**, 44–51 (2001).

73. Picardo, M., Ottaviani, M., Camera, E. & Mastrofrancesco, A. Sebaceous gland lipids. *Dermatoendocrinol.* **1**, 68–71 (2009).

74. Ludovici, M. *et al.* Influence of the sebaceous gland density on the stratum corneum lipidome. *Sci. Rep.* **8**, 11500 (2018).

75. Freinkel, R. K. & Shen, Y. The origin of free fatty acids in sebum. II. Assay of the lipases of the cutaneous bacteria and effects of pH. *J. Invest. Dermatol.* **53**, 422–427 (1969).

76. Gray, G. M. & White, R. J. Glycosphingolipids and ceramides in human and pig epidermis. *J. Invest. Dermatol.* **70**, 336–341 (1978).

77. Camera, E. *et al.* Use of lipidomics to investigate sebum dysfunction in juvenile acne. *J. Lipid Res.* **57**, 1051–1058 (2016).

78. Masukawa, Y. *et al.* Comprehensive quantification of ceramide species in human stratum corneum. *J. Lipid Res.* **50**, 1708–1719 (2009).

79. van Smeden, J. *et al.* LC/MS analysis of stratum corneum lipids: ceramide profiling and discovery. *J. Lipid Res.* **52**, 1211–1221 (2011).

80. Shin, J.-H. *et al.* A lipidomic platform establishment for structural identification of skin ceramides with non-hydroxyacyl chains. *Anal. Bioanal. Chem.* **406**, 1917–1932 (2014).

81. Chiu, H.-H. & Kuo, C.-H. Gas chromatography-mass spectrometry-based analytical strategies for fatty acid analysis in biological samples. *J. Food Drug Anal.* **28**, 60–73 (2020).

82. Michael-Jubeli, R., Bleton, J. & Baillet-Guffroy, A. High-temperature gas chromatography-mass spectrometry for skin surface lipids profiling. *J. Lipid Res.* **52**, 143–151 (2011).

83. Pappas, A., Johnsen, S., Liu, J.-C. & Eisinger, M. Sebum analysis of individuals with and without acne. *Dermatoendocrinol.* **1**, 157–161 (2009).

84. Smith, R. N., Braue, A., Varigos, G. A. & Mann, N. J. The effect of a low glycemic load diet on acne vulgaris and the fatty acid composition of skin surface triglycerides. *J. Dermatol. Sci.* **50**, 41–52 (2008).

85. Croxton, R. S., Baron, M. G., Butler, D., Kent, T. & Sears, V. G. Variation in amino acid and lipid composition of latent fingerprints. *Forensic Sci. Int.* **199**, 93–102 (2010).

86. Martin, H. J., Reynolds, J. C., Riazanskaia, S. & Thomas, C. L. P. High throughput volatile fatty acid skin metabolite profiling by thermal desorption secondary electrospray ionisation mass spectrometry. *The Analyst* **139**, 4279–4286 (2014).

87. Berdyshev, E. *et al.* Lipid abnormalities in atopic skin are driven by type 2 cytokines. *JCI Insight* **3**, (2018).

88. Sadowski, T. *et al.* Large-scale human skin lipidomics by quantitative, high-throughput shotgun mass spectrometry. *Sci. Rep.* **7**, 43761 (2017).

89. Souza, S. L., Graça, G. & Oliva, A. Characterization of sweat induced with pilocarpine, physical exercise, and collected passively by metabolomic analysis. *Skin Res.*

*Technol. Off. J. Int. Soc. Bioeng. Skin ISBS Int. Soc. Digit. Imaging Skin ISDIS Int. Soc. Skin Imaging ISSI* **24**, 187–195 (2018).

90. Delgado-Povedano, M. M., Calderón-Santiago, M., Luque de Castro, M. D. & Priego-Capote, F. Metabolomics analysis of human sweat collected after moderate exercise. *Talanta* **177**, 47–65 (2018).

91. Jadoon, S. *et al.* Recent Developments in Sweat Analysis and Its Applications. *Int. J. Anal. Chem.* **2015**, e164974 (2015).

92. Agrawal, K., Sivamani, R. K. & Newman, J. W. Noninvasive profiling of sweat-derived lipid mediators for cutaneous research. *Skin Res. Technol.* **25**, 3–11 (2019).

93. Mastella, G., Cesare, G., Borruso, A., Menin, L. & Zanolla, L. Reliability of sweat-testing by the Macroduct® collection method combined with conductivity analysis in comparison with the classic Gibson and Cooke technique. *Acta Paediatr. Oslo Nor. 1992* **89**, 933–7 (2000).

94. Hammond, K. B., Turcios, N. L. & Gibson, L. E. Clinical evaluation of the macroduct sweat collection system and conductivity analyzer in the diagnosis of cystic fibrosis. *J. Pediatr.* **124**, 255–260 (1994).

95. Chung, M., Fortunato, G. & Radacsi, N. Wearable flexible sweat sensors for healthcare monitoring: a review. *J. R. Soc. Interface* **16**, 20190217 (2019).

96. Gao, W. *et al.* Fully integrated wearable sensor arrays for multiplexed in situ perspiration analysis. *Nature* **529**, 509–514 (2016).

97. Kim, J. *et al.* Noninvasive Alcohol Monitoring Using a Wearable Tattoo-Based Iontophoretic-Biosensing System. *ACS Sens.* **1**, 1011–1019 (2016).

98. Tai, L.-C. *et al.* Methylxanthine Drug Monitoring with Wearable Sweat Sensors. *Adv. Mater.* **30**, 1707442 (2018).

99. Tai, L.-C. *et al.* Wearable Sweat Band for Noninvasive Levodopa Monitoring. *Nano Lett.* **19**, 6346–6351 (2019).

100. Proksch, E. Lowering skin pH: improved barrier function, anti-ageing and beyond. *Br. J. Dermatol.* **179**, 254–255 (2018).

101. Elias, P. M. Stratum corneum acidification: how and why? *Exp. Dermatol.* **24**, 179–180 (2015).

102. Yosipovitch, G. & Papoiu, A. D. P. What causes itch in atopic dermatitis? *Curr. Allergy Asthma Rep.* **8**, 306–311 (2008).

103. Proksch, E. pH in nature, humans and skin. *J. Dermatol.* **45**, 1044–1052 (2018).

104. Koch, A. & Schwab, A. Cutaneous pH landscape as a facilitator of melanoma initiation and progression. *Acta Physiol.* **225**, e13105 (2019).

105. Hachem, J.-P. *et al.* pH directly regulates epidermal permeability barrier homeostasis, and stratum corneum integrity/cohesion. *J. Invest. Dermatol.* **121**, 345–353 (2003).

106. Prakash, C., Bhargava, P., Tiwari, S., Majumdar, B. & Bhargava, R. K. Skin Surface pH in Acne Vulgaris: Insights from an Observational Study and Review of the Literature. *J. Clin. Aesthetic Dermatol.* **10**, 33–39 (2017).

107. Krien, P. M. & Kermici, M. Evidence for the Existence of a Self-Regulated Enzymatic Process Within the Human Stratum Corneum –An Unexpected Role for Urocanic Acid. *J. Invest. Dermatol.* **115**, 414–420 (2000).

108. Kezic, S. *et al.* Levels of filaggrin degradation products are influenced by both filaggrin genotype and atopic dermatitis severity. *Allergy* **66**, 934–940 (2011).

109. Cabanillas, B. & Novak, N. Atopic dermatitis and filaggrin. *Curr. Opin. Immunol.* **42**, 1–8 (2016).

110. Hu, J., Stein, A. & Bühlmann, P. Rational design of all-solid-state ion-selective electrodes and reference electrodes. *TrAC Trends Anal. Chem.* **76**, 102–114 (2016).

111. Allen, J. R. pH Electrodes, Ion-Selective Electrodes, and Oxygen Sensors: Electrochemical Sensors Used in the Medical Field. *Lab. Med.* **34**, 544–547 (2003).

112. Antonov, D., Schliemann, S. & Elsner, P. Methods for the Assessment of Barrier Function. *Skin Barrier Funct.* **49**, 61–70 (2016).

113. du Plessis, J. L., Stefaniak, A. B. & Wilhelm, K.-P. Measurement of Skin Surface pH. *Curr. Probl. Dermatol.* **54**, 19–25 (2018).

114. Lindfors, T., Ervelä, S. & Ivaska, A. Polyaniline as pH-sensitive component in plasticized PVC membranes. *J. Electroanal. Chem.* **560**, 69–78 (2003).

115. Nyein, H. Y. Y. *et al.* A Wearable Electrochemical Platform for Noninvasive Simultaneous Monitoring of Ca(2+) and pH. *ACS Nano* **10**, 7216–7224 (2016).

116. Anastasova, S. *et al.* A wearable multisensing patch for continuous sweat monitoring. *Biosens. Bioelectron.* **93**, 139–145 (2017).

117. Choi, J. *et al.* Soft, Skin-Integrated Multifunctional Microfluidic Systems for Accurate Colorimetric Analysis of Sweat Biomarkers and Temperature. *ACS Sens.* **4**, 379–388 (2019).

118. He, X. *et al.* Flexible and Superwettable Bands as a Platform toward Sweat Sampling and Sensing. *Anal. Chem.* **91**, 4296–4300 (2019).

119. Koh, A. *et al.* A soft, wearable microfluidic device for the capture, storage, and colorimetric sensing of sweat. *Sci. Transl. Med.* **8**, 366ra165 (2016).

120. Bandodkar, A. J. *et al.* Battery-free, skin-interfaced microfluidic/electronic systems for simultaneous electrochemical, colorimetric, and volumetric analysis of sweat. *Sci. Adv.* **5**, eaav3294 (2019).

121. USA, L. L'Oréal Unveils Prototype Of First-Ever Wearable Microfluidic Sensor To Measure Skin pH Levels. https://www.prnewswire.com/news-releases/loreal-unveils-

prototype-of-first-ever-wearable-microfluidic-sensor-to-measure-skin-ph-levels-300773342.html.

122. Pojmanová, P., Ladislavová, N., Škeříková, V., Kania, P. & Urban, Š. Human scent samples for chemical analysis. *Chem. Pap.* **74**, 1383–1393 (2020).

123. Jha, S. K. Characterization of human body odor and identification of aldehydes using chemical sensor. *Rev. Anal. Chem.* **36**, (2017).

124. Cuzuel, V. *et al.* Origin, Analytical Characterization, and Use of Human Odor in Forensics. *J. Forensic Sci.* **62**, 330–350 (2017).

125. Parlet, C. P., Brown, M. M. & Horswill, A. R. Commensal Staphylococci Influence Staphylococcus aureus Skin Colonization and Disease. *Trends Microbiol.* **27**, 497–507 (2019).

126. Bacteriology of Humans: An Ecological Perspective | Wiley. *Wiley.com* https://www.wiley.com/en-us/Bacteriology+of+Humans%3A+An+Ecological+Perspective-p-9781405161657.

127. Ellis, S. R. *et al.* The Skin and Gut Microbiome and Its Role in Common Dermatologic Conditions. *Microorganisms* **7**, 550 (2019).

128. Yamazaki, Y., Nakamura, Y. & Núñez, G. Role of the microbiota in skin immunity and atopic dermatitis. *Allergol. Int.* **66**, 539–544 (2017).

129. Timm, C. M., Lloyd, E. P., Egan, A., Mariner, R. & Karig, D. Direct Growth of Bacteria in Headspace Vials Allows for Screening of Volatiles by Gas Chromatography Mass Spectrometry. *Front. Microbiol.* **9**, 491 (2018).

130. Fitzgerald, S., Duffy, E., Holland, L. & Morrin, A. Multi-strain volatile profiling of pathogenic and commensal cutaneous bacteria. *Sci. Rep.* **10**, 17971 (2020).

131. Duffy, E. & Morrin, A. Endogenous and microbial volatile organic compounds in cutaneous health and disease. *Trends Anal. Chem.* **111**, 163–172 (2018).

132. Sethi, S., Nanda, R. & Chakraborty, T. Clinical Application of Volatile Organic Compound Analysis for Detecting Infectious Diseases. *Clin. Microbiol. Rev.* **26**, 462–475 (2013).

133. Duffy, E. & Morrin, A. Endogenous and microbial volatile organic compounds in cutaneous health and disease. *TrAC Trends Anal. Chem.* **111**, 163–172 (2019).

134. Dormont, L., Bessière, J.-M. & Cohuet, A. Human skin volatiles: a review. *J. Chem. Ecol.* **39**, 569–578 (2013).

135. Dormont, L., Bessière, J.-M., McKey, D. & Cohuet, A. New methods for field collection of human skin volatiles and perspectives for their application in the chemical ecology of human–pathogen–vector interactions. *J. Exp. Biol.* **216**, 2783–2788 (2013).

136. Grabowska-Polanowska, B. *et al.* Development of sampling method and chromatographic analysis of volatile organic compounds emitted from human skin. *Bioanalysis* **9**, 1465–1475 (2017).

137. Jiang, R., Cudjoe, E., Bojko, B., Abaffy, T. & Pawliszyn, J. A non-invasive method for in vivo skin volatile compounds sampling. *Anal. Chim. Acta* **804**, 111–119 (2013).

138. Duffy, E., Guzman, K. D., Wallace, R., Murphy, R. & Morrin, A. Non-Invasive Assessment of Skin Barrier Properties: Investigating Emerging Tools for In Vitro and In Vivo Applications. *Cosmetics* **4**, 44 (2017).

139. Duffy, E., Jacobs, M. R., Kirby, B. & Morrin, A. Probing skin physiology through the volatile footprint: Discriminating volatile emissions before and after acute barrier disruption. *Exp. Dermatol.* **26**, 919–925 (2017).

140. Duffy, E., Albero, G. & Morrin, A. Headspace Solid-Phase Microextraction Gas Chromatography-Mass Spectrometry Analysis of Scent Profiles from Human Skin. *Cosmetics* **5**, 62 (2018).

141. Schmidt, K. & Podmore, I. Current Challenges in Volatile Organic Compounds Analysis as Potential Biomarkers of Cancer. *J. Biomark.* **2015**, (2015).

142. Mochalski, P. *et al.* Monitoring of selected skin- and breath-borne volatile organic compounds emitted from the human body using gas chromatography ion mobility spectrometry (GC-IMS). *J. Chromatogr. B* **1076**, 29–34 (2018).

143. Reynolds, J. C. *et al.* Detection of volatile organic compounds in breath using thermal desorption electrospray ionization-ion mobility-mass spectrometry. *Anal. Chem.* **82**, 2139–2144 (2010).

144. Nazemi, H., Joseph, A., Park, J. & Emadi, A. Advanced Micro- and Nano-Gas Sensor Technology: A Review. *Sensors* **19**, (2019).

145. Núñez Carmona, E. *et al.* Detection of food and skin pathogen microbiota by means of an electronic nose based on metal oxide chemiresistors. *Sens. Actuators B Chem.* **238**, 1224–1230 (2017).

146. Güntner, A. T. *et al.* Sniffing Entrapped Humans with Sensor Arrays. *Anal. Chem.* **90**, 4940–4945 (2018).

147. Lawson, B. *et al.* Skin alcohol perspiration measurements using MOX sensors. *Sens. Actuators B Chem.* **280**, 306–312 (2019).

148. Dormont, L., Bessière, J.-M. & Cohuet, A. Human Skin Volatiles: A Review. *J. Chem. Ecol.* **39**, 569–578 (2013).

149. Stevens, D. *et al.* Spatial variations in the microbial community structure and diversity of the human foot is associated with the production of odorous volatiles. *FEMS Microbiol. Ecol.* (2015) doi:10.1093/femsec/fiu018.

150. Verhulst, N. O., Weldegergis, B. T., Menger, D. & Takken, W. Attractiveness of volatiles from different body parts to the malaria mosquito Anopheles coluzzii is affected by deodorant compounds. *Sci. Rep.* **6**, 27141 (2016).

151. Penn, D. J. *et al.* Individual and gender fingerprints in human body odour. *J. R. Soc. Interface* **4**, 331–340 (2007).

152. Elias, P. M. Primary role of barrier dysfunction in the pathogenesis of atopic dermatitis. *Exp. Dermatol.* **27**, 847–851 (2018).

153. Rippke, F., Schreiner, V., Doering, T. & Maibach, H. I. Stratum corneum pH in atopic dermatitis: impact on skin barrier function and colonization with Staphylococcus Aureus. *Am. J. Clin. Dermatol.* **5**, 217–223 (2004).

154. Piérard-Franchimont, C., Quatresooz, P. & Piérard, G. E. Sebum Production. in *Textbook of Aging Skin* (eds. Farage, M. A., Miller, K. W. & Maibach, H. I.) 343–352 (Springer, 2010). doi:10.1007/978-3-540-89656-2_33.

155. Bernier, U. R., Kline, D. L., Barnard, D. R., Schreck, C. E. & Yost, R. A. Analysis of human skin emanations by gas chromatography/mass spectrometry. 2. Identification of volatile compounds that are candidate attractants for the yellow fever mosquito (Aedes aegypti). *Anal. Chem.* **72**, 747–756 (2000).

156. Gallagher, M. *et al.* Analyses of volatile organic compounds from human skin. *Br. J. Dermatol.* **159**, 780–791 (2008).

157. Curran, A. M., Prada, P. A. & Furton, K. G. The differentiation of the volatile organic signatures of individuals through SPME-GC/MS of characteristic human scent compounds. *J. Forensic Sci.* **55**, 50–57 (2010).

158. Prada-Tiedemann, P. & Furton, K. Human Scent Detection: A Review of its Developments and Forensic Applications. *Rev. Cienc. Forenses* **1**, 81–87 (2008).

159. Bommannan, D., Potts, R. O. & Guy, R. H. Examination of the effect of ethanol on human stratum corneum in vivo using infrared spectroscopy. *J. Controlled Release* **16**, 299–304 (1991).

160. Gupta, R., Badhe, Y., Rai, B. & Mitragotri, S. Molecular mechanism of the skin permeation enhancing effect of ethanol: a molecular dynamics study. *RSC Adv.* **10**, 12234–12248 (2020).

161. Horita, D. *et al.* Molecular mechanisms of action of different concentrations of ethanol in water on ordered structures of intercellular lipids and soft keratin in the stratum corneum. *Biochim. Biophys. Acta BBA - Biomembr.* **1848**, 1196–1202 (2015).

162. Cartner, T. *et al.* Effect of different alcohols on stratum corneum kallikrein 5 and phospholipase A2 together with epidermal keratinocytes and skin irritation. *Int. J. Cosmet. Sci.* **39**, 188–196 (2017).

163. Filipiak, W. *et al.* A Compendium of Volatile Organic Compounds (VOCs) Released By Human Cell Lines. *Curr. Med. Chem.* **23**, 2112–2131 (2016).

164. James, A., Casey, J., Hyliands, D. & Mycock, G. Fatty acid metabolism by cutaneous bacteria and its role in axillary malodour. *World J. Microbiol. Biotechnol.* **20**, 787–793 (2004).

165. Kleesz, P., Darlenski, R. & Fluhr, J. W. Full-Body Skin Mapping for Six Biophysical Parameters: Baseline Values at 16 Anatomical Sites in 125 Human Subjects. *Skin Pharmacol. Physiol.* **25**, 25–33 (2012).

166. Farage, M. A., Hood, W., Berardesca, E. & Maibach, H. Intrinsic and Extrinsic Factors Affecting Skin Surface pH. *PH Skin Issues Chall.* **54**, 33–47 (2018).

167. Man, M. Q. *et al.* Variation of Skin Surface pH, Sebum Content and Stratum Corneum Hydration with Age and Gender in a Large Chinese Population. *Skin Pharmacol. Physiol.* **22**, 190–199 (2009).

168. Choi, S.-J. *et al.* Comparison of transepidermal water loss, capacitance and pH values in the skin between intrinsic and extrinsic atopic dermatitis patients. *J. Korean Med. Sci.* **18**, 93–96 (2003).

169. Jacobi, U., Gautier, J., Sterry, W. & Lademann, J. Gender-related differences in the physiology of the stratum corneum. *Dermatol. Basel Switz.* **211**, 312–317 (2005).

170. Lambers, H., Piessens, S., Bloem, A., Pronk, H. & Finkel, P. Natural skin surface pH is on average below 5, which is beneficial for its resident flora. *Int. J. Cosmet. Sci.* **28**, 359–370 (2006).

171. Bicchi, C., Cordero, C., Liberto, E., Sgorbini, B. & Rubiolo, P. Reliability of fibres in solid-phase microextraction for routine analysis of the headspace of aromatic and medicinal plants. *J. Chromatogr. A* **1152**, 138–149 (2007).

172. Spietelun, A., Pilarczyk, M., Kloskowski, A. & Namieśnik, J. Current trends in solid-phase microextraction (SPME) fibre coatings. *Chem. Soc. Rev.* **39**, 4524–4537 (2010).

173. Jiang, J. *et al.* Volatile fatty acids production from food waste: effects of pH, temperature, and organic loading rate. *Bioresour. Technol.* **143**, 525–530 (2013).

174. Lukitawesa, null, Patinvoh, R. J., Millati, R., Sárvári-Horváth, I. & Taherzadeh, M. J. Factors influencing volatile fatty acids production from food wastes via anaerobic digestion. *Bioengineered* **11**, 39–52 (2020).

175. Münch, E. v. & Greenfield, P. F. Estimating VFA concentrations in prefermenters by measuring pH. *Water Res.* **32**, 2431–2441 (1998).

176. Tang, Z., Yang, J., Yu, J. & Cui, B. A colorimetric sensor for qualitative discrimination and quantitative detection of volatile amines. *Sensors* **10**, 6463–6476 (2010).

177. Mazumder, S., Ahamed, R. A., McGahee, E., Wang, L. & Seyler, T. H. A New Automated Method for the Analysis of Aromatic Amines in Human Urine by GC–MS/MS. *J. Anal. Toxicol.* **43**, 25–35 (2019).

178. Ng, T. W., Chan, P. Y., Chan, T. T., Wu, H. & Lai, K. M. Skin squames contribute to ammonia and volatile fatty acid production from bacteria colonizing in air-cooling units with odor complaints. *Indoor Air* **28**, 258–265 (2018).

179. Visciano, P., Schirone, M. & Paparella, A. An Overview of Histamine and Other Biogenic Amines in Fish and Fish Products. *Foods Basel Switz.* **9**, (2020).

180. Doeun, D., Davaatseren, M. & Chung, M.-S. Biogenic amines in foods. *Food Sci. Biotechnol.* **26**, 1463–1474 (2017).

181. Lucaire, V., Schwartz, J.-J., Delhomme, O., Ocampo-Torres, R. & Millet, M. A sensitive method using SPME pre-concentration for the quantification of aromatic amines in indoor air. *Anal. Bioanal. Chem.* **410**, 1955–1963 (2018).

182. Sandlers, Y. Amino Acids Profiling for the Diagnosis of Metabolic Disorders. *Biochem. Test. - Clin. Correl. Diagn.* (2019) doi:10.5772/intechopen.84672.

183. Claes, L., Janssen, M. & De Vos, D. E. Organocatalytic Decarboxylation of Amino Acids as a Route to Bio-based Amines and Amides. *ChemCatChem* **11**, 4297–4306 (2019).

184. Thorn, R. M. S. & Greenman, J. Microbial volatile compounds in health and disease conditions. *J. Breath Res.* **6**, (2012).

185. Mohiuddin, S. S. & Khattar, D. Biochemistry, Ammonia. in *StatPearls* (StatPearls Publishing, 2021).

186. Li, M. *et al.* Human Ammonia Emission Rates under Various Indoor Environmental Conditions. *Environ. Sci. Technol.* **54**, 5419–5428 (2020).

187. Smallegange, R. C., Verhulst, N. O. & Takken, W. Sweaty skin: an invitation to bite? *Trends Parasitol.* **27**, 143–148 (2011).

188. Keller, R. W., Bailey, J. L., Wang, Y., Klein, J. D. & Sands, J. M. Urea transporters and sweat response to uremia. *Physiol. Rep.* **4**, (2016).

189. Nose, K. *et al.* Identification of Ammonia in Gas Emanated from Human Skin and Its Correlation with That in Blood. *Anal. Sci. Int. J. Jpn. Soc. Anal. Chem.* **21**, 1471–4 (2006).

190. Ferrer, F. M., Hobart, K. & Bailey, J. V. Detection of urease and carbonic anhydrase activity using a rapid and economical field test to assess microbially-induced carbonate precipitation. *bioRxiv* 2020.01.10.902379 (2020) doi:10.1101/2020.01.10.902379.

191. Neofotistos, A.-D. G., Tsagkaris, A. S. & Proestos, G. P. D. and C. Emerging Trends in Biogenic Amines Analysis. *Biog. Amines* (2019) doi:10.5772/intechopen.81274.

192. Jamalabadi, H., Mani-Varnosfaderani, A. & Alizadeh, N. PPy-Metal Oxide Hybrid Nanocomposite Sensor Array for Simultaneous Determination of Volatile Organic Amines in High Humid Atmosphere. *IEEE Sens. J.* **17**, 8282–8289 (2017).

193. Xiao-wei, H., Xiao-bo, Z., Ji-yong, S., Zhi-hua, L. & Jie-wen, Z. Colorimetric sensor arrays based on chemo-responsive dyes for food odor visualization. *Trends Food Sci. Technol.* **81**, 90–107 (2018).

194. Rakow, N. A., Sen, A., Janzen, M. C., Ponder, J. B. & Suslick, K. S. Molecular Recognition and Discrimination of Amines with a Colorimetric Array. *Angew. Chem. Int. Ed.* **44**, 4528–4532 (2005).

195. Oh, H. J. *et al.* Washable Colorimetric Nanofiber Nonwoven for Ammonia Gas Detection. *Polymers* **12**, 1585 (2020).

196. Helmy, S. *et al.* Photoswitching Using Visible Light: A New Class of Organic Photochromic Molecules. *J. Am. Chem. Soc.* **136**, 8169–8172 (2014).

197. Helmy, S., Oh, S., Leibfarth, F. A., Hawker, C. J. & Read de Alaniz, J. Design and Synthesis of Donor–Acceptor Stenhouse Adducts: A Visible Light Photoswitch Derived from Furfural. *J. Org. Chem.* **79**, 11316–11329 (2014).

198. Diaz, Y. J. *et al.* A Versatile and Highly Selective Colorimetric Sensor for the Detection of Amines. *Chem. – Eur. J.* **23**, 3562–3566 (2017).

199. Schmidt, F. M. *et al.* Ammonia in breath and emitted from skin. *J. Breath Res.* **7**, 017109 (2013).

200. Martínez-Lozano, P. Mass spectrometric study of cutaneous volatiles by secondary electrospray ionization. *Int. J. Mass Spectrom.* **282**, 128–132 (2009).

201. Furukawa, S. *et al.* Simultaneous and multi-point measurement of ammonia emanating from human skin surface for the estimation of whole body dermal emission rate. *J. Chromatogr. B Analyt. Technol. Biomed. Life. Sci.* **1053**, 60–64 (2017).

202. Bigi, F. *et al.* Clean synthesis in water. Part 2: Uncatalysed condensation reaction of Meldrum's acid and aldehydes. *Tetrahedron Lett.* **42**, 5203–5205 (2001).

203. Palmer, L. I. & Alaniz, J. R. de. Lewis Acid Catalyzed Rearrangement of Furylcarbinols: The Aza- and Oxa-Piancatelli Cascade Reaction. *Synlett* **25**, 08–11 (2014).

204. Piutti, C. & Quartieri, F. The Piancatelli Rearrangement: New Applications for an Intriguing Reaction. *Molecules* **18**, 12290–12312 (2013).

205. Šafář, P. *et al.* Dichotomy in the Ring Opening Reaction of 5-[(2-Furyl)methylidene]-2,2-dimethyl-1,3-dioxane-4,6-dione with Cyclic Secondary Amines. *Collect. Czechoslov. Chem. Commun.* **65**, 1911–1938 (2000).

206. Sidman, J. W. Electronic Transitions Due To Nonbonding Electrons Carbonyl, Aza-Aromatic, And Other Compounds. https://pubs.acs.org/doi/pdf/10.1021/cr50022a004 (2002) doi:10.1021/cr50022a004.

207. Bailey, D. C. Not Normal: the uncertainties of scientific measurements. *R. Soc. Open Sci.* **4**, (2017).

208. Sahu, P. K. & Lee, S.-L. Hydrogen-bond interaction in 1:1 complexes of tetrahydrofuran with water, hydrogen fluoride, and ammonia: A theoretical study. *J. Chem. Phys.* **123**, 044308 (2005).

209. Lam, T. H. *et al.* Understanding the microbial basis of body odor in pre-pubescent children and teenagers. *Microbiome* **6**, (2018).

210. Dekaboruah, E., Suryavanshi, M. V., Chettri, D. & Verma, A. K. Human microbiome: an academic update on human body site specific surveillance and its possible role. *Arch. Microbiol.* **202**, 2147–2167 (2020).

211. Luqman, A. *et al.* Trace amines produced by skin bacteria accelerate wound healing in mice. *Commun. Biol.* **3**, 1–10 (2020).

212. Luqman, A., Nega, M., Nguyen, M.-T., Ebner, P. & Götz, F. SadA-Expressing Staphylococci in the Human Gut Show Increased Cell Adherence and Internalization. *Cell Rep.* **22**, 535–545 (2018).

213. Shetewi, T. *et al.* Investigation of the relationship between skin-emitted volatile fatty acids and skin surface acidity in healthy participants - a pilot study. *J. Breath Res.* (2021) doi:10.1088/1752-7163/abf20a.

214. Lang, W., Blöck, T. M. & Zander, R. Solubility of NH3 and apparent pK of NH4+ in human plasma, isotonic salt solutions and water at 37 degrees C. *Clin. Chim. Acta Int. J. Clin. Chem.* **273**, 43–58 (1998).

# Chapter 2

# Investigating the Relationship Between Skin Volatiles and Skin Surface pH

## 2.1 Introduction

The surface of healthy skin is characterised by an acidic pH between 4.0 and 6.0.[9] The acidic nature of the SC is important both for permeability barrier formation and cutaneous antimicrobial defence.[13] Both passive and active mechanisms have been proposed to maintain the acidic pH of the skin surface.[72] Passive exogenous mechanisms proposed include FFA generation by sebaceous glands in the hydrolipid film as discussed above. Both sebaceous and eccrine secretions contain many substrates such as sebum and amino acids (found in eccrine sweat) that enable microbial biosynthesis of fatty acids. Eccrine gland-derived sweat products such as lactic acid also contribute as an exogenous mechanism to the acidity of skin.[103] An endogenous mechanism proposed resulting in FFA generation is phospholipid hydrolysis catalysed by secretory sPLA2 in the SC.[72] Active proton pump endogenous mechanisms are also proposed and take place in the lower layers of the SC.[103] Thus while several mechanisms involving a range of acidic species are responsible for maintaining the skin surface acidity, it is clear from the literature that FFA generation from numerous pathways are a significant contributor.

The skin surface also emits volatile compounds that are derived from glandular secretions and volatile that are released by the action of microbial bacterial on these glandular volatiles. [133] These volatiles can offer insight into a person's cutaneous physiology. These VOC emissions have the potential to offer insights into cutaneous physiology.[133,148] Volatile emissions related to other pathologies such as melanoma, malaria and wound infection have also been studied.[130,149,150] Skin volatile profiles of healthy individuals have been shown to be influenced by gender and other genetic traits.[86,151] However, little consistency has been seen across these studies with regards to the compounds observed, likely due to the wide variety of sampling and analysis approaches being used but also the highly variable nature of the skin matrix itself. More research is required to further identify and quantify compounds in the healthy skin volatile profile before associations with disease states can be more certain.

Given that changes in skin pH play an important role in the pathogenesis of many skin diseases and conditions, the approach of monitoring skin surface pH via the skin VOC emission represents an exciting approach for personalised monitoring from early diagnosis to treatment response. A pH sensing technology based on this principal may hold particular relevance in atopic dermatitis (AD) as elevated skin surface pH occurs in active AD.[152] AD is a common

chronic inflammatory skin disease often presenting in infancy and childhood where impaired skin barrier function leads to pruritus, inflammation, and reduced quality of life. Currently, the diagnosis of AD and response to treatment is based on physician evaluation and patient history. Thus, there is a significant need for non-invasive, on-body sensor systems capable of detecting small, but clinically meaningful changes in skin barrier function to inform clinical decision making. Skin surface pH is closely linked with skin barrier function whereby for example, elevated skin pH exacerbates barrier function by affecting the colonization of *S.aureus*.[153] Thus, the assessment of skin surface pH via the assessment of the VOC emission may offer earlier and more sensitive measurements of AD disease progression.

This research aims to understand the link between the skin VFA emission and skin acidity. We identify and profile VFAs recovered at several skin sites in a participant study where VOCs were sampled from above the skin using solid phase microextraction (SPME) and analysed using GC-MS. The recovered VFAs in this study (C9-C16) are discussed in the context of gland type and densities at the different skin sites investigated and are largely attributed to glandular secretions and hydrolysis of triglycerides by resident skin bacteria. Skin acidity via skin surface pH were also measured in the study and the link between it and the VFA emission was explored. Regression modelling of the participant data at each site investigated showed strong linear correlations of normalised VFA emissions with hydrogen ion concentration. Reasons proposed to explain this correlation relate to the FFA content in the various sebaceous secretions, the pH-dependent hydrolysis of triglycerides in sebum by surface bacteria lipases, as well as the governing role of pH (and acid dissociation constants) on the equilibrium vapour pressures of VFAs above skin. This is the first time a direct link between VFA emission and surface pH has been demonstrated in skin to our knowledge, which represents a potentially useful finding for personalised monitoring of inflammatory skin disease where changes in skin surface pH are closely linked with disease flare-ups.

## 2.2 Materials methods

### *2.2.1 Participant study for GC-MS analysis of skin volatiles*

Healthy volunteers aged 20-30 were recruited (n=20 female (F) participants, n=9 male (M) participants) to study the association of VFA emissions to skin surface pH at the forehead and forearm. The same sampling procedure (described in Section *2.2.3*) was performed to collect samples from the forehead (F; n=10 participants) and forearm (F; n=10 participants and M; n=9 participants). No special dietary regimes were applied; however, participants were instructed not to apply perfumes or cosmetics on their arms on the days of sample collection. Participants were informed on the aim and purpose of the study and asked to provide written informed consent. The local ethics committee (Dublin City University Research Ethics Committee) approved the study on skin volatiles prior to commencement of the work, and the study was performed according to the Declaration of Helsinki.

### *2.2.2 Skin pre-treatment method*

Wipes (Cutisoft wipes, 70% isopropyl alcohol) were employed for cleaning the skin. A sampling region (5 x 5 $cm^2$) on the volar forearm was marked. Wipes were used to clean the skin within the marked boundary by gently rubbing the wipes across the skin three times in one direction. Skin volatile emissions were then collected using the SPME approach (**Figure 2.1**).

### *2.2.3 Sampling of the skin volatile emissions*

Solid phase microextraction (SPME) fibres were used for sampling skin volatiles and comprised of 50/30/20 μm divinylbenzene/carboxen/polydimethylsiloxane Stableflex (2 cm) assemblies (Supelco Corp., Bellefonte, PA, USA). The SPME fibre was housed within a wearable sampling platform that was affixed to the volar forearm, or forehead as specified using Leukosilk surgical tape (BSN Medical GmbH, Hamburg, Germany). This wearable sampling platform consisted of a glass funnel (3 mL volume, Pyrex®) and a septa (Supelco Thermogreen LB-2 Septa plug, Sigma Aldrich, Arklow, Ireland) which served to hold the SPME fibre in an enclosed headspace (HS) above the skin.[139] Sampling time was 15 min. Once a sample was collected, the SPME fibre was removed from the glass housing and analysed using GC-MS.

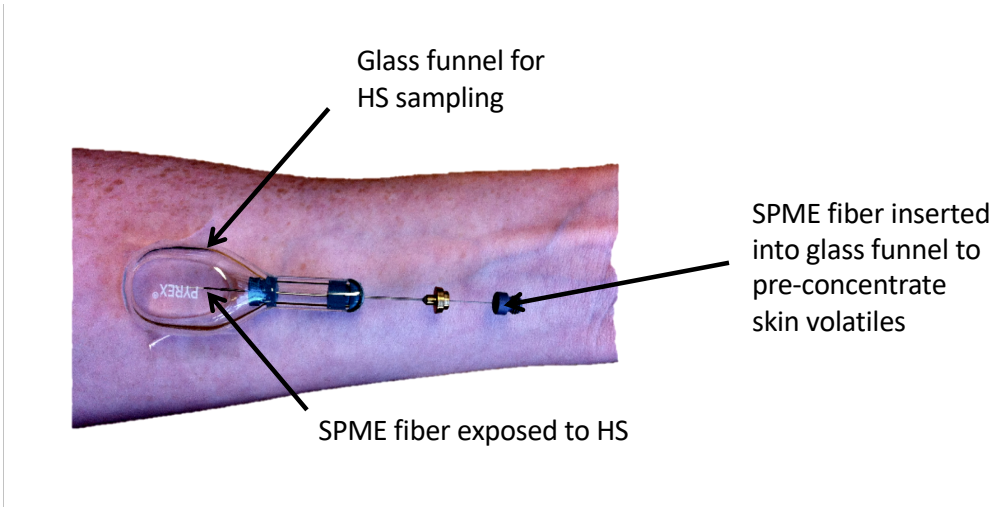


**Figure 2.1** Set up for skin VOC sampling using SPME fiber housed in a glass funnel serving to define the headspace (HS).

*2.2.4 Skin surface pH measurements*

Skin surface pH was taken for all participants and measured on the volar forearm or forehead as specified using a pH meter with a flat probe (Meter 2210, Probe HI1413; Hanna instruments Inc.). The pH probe was calibrated before skin surface pH measurement was taken. All pH measurements were carried out in triplicate.

*2.2.5 GC-MS Analysis*

For GC-MS analysis, two instruments were used as given in **Table 2.1**. The male and female volatile samples were analysed on; an Agilent 6890 GC connected to an Agilent 5973 mass selective detector (MSD) or an Agilent 7820A with MSD 5977B, respectively. **Table 2.2** summarises the chromatographic and MS conditions used for both GC-MS instruments.

**Table 2.1**: Instrumentation used for the analysis of the males and females volatile samples.

| GC-model | Agilent 6890 GC | Agilent 7820A |
|---|---|---|
| Mass selective detector | Agilent 597 | MSD 5977B |
| Type of samples analysed | Male samples | Female samples |

**Table 2.2**: chromatographic and MS conditions for both GC-MS instruments.

| | |
|---|---|
| Coloumn type | SLB-5ms |
| Column dimensions | 30 m×0.25 mm×0.25 μm $d_f$ |
| Carrier gas | Helium |
| Flow rate | 1 mL $min^{-1}$. |
| Inlet temperature | 250 °C |
| Injection type | Splitless |
| Oven temperature | 40 °C hold for 5 min<br>Ramp at 15 °C $min^{-1}$ to 270 °C |
| MS scan rate | 3.94 $s^{-1}$ |
| MS scan range | 35-400 m/z |
| Ion source temperature | 230 °C |
| Ionising energy | 70 eV |

The identification of compounds and structures was performed using the National Institute of Standards and Technology (NIST) library and was supported by a visual comparison of the unknown mass spectra, with previous literature reports and with retention index (RI) matching with a tolerance of ±15 RI units. A standard mixture of saturated alkanes (C7-C30, Sigma Aldrich, Arklow, Ireland) was used for RI matching. All the raw chromatograms were processed using Openchrom software. First, an identification step was applied to identify the peaks followed by a an integration step to calculate the area under each peak. In terms of data processing, peak area data was normalised were specified, where individual compound peak areas in a sample were divided by total peak area of the sample and referred to in this work as *normalised peak area*.

## 2.3 Results and discussion

This research aims to understand the link between the skin VFA emission and skin acidity. As skin pH play an important role in determining the pathogenesis of many skin diseases and conditions, the approach of monitoring skin surface pH via the skin VOC emission was explored.

### *2.3.1 Skin volatile emission profile*

Skin volatile emissions were collected on the forehead (females only) and volar forearm (male & female) using HS-SPME and analysed using GC-MS, as outlined in the Methods Section *2.2.5*. Typical chromatograms of the volatile emission of the forehead (F), and forearm (M & F) subjects, obtained from this study is shown in **Figure 2.2.** Results show that all samples; forehead (F), forearm (F) and forearm (M) had different volatile profiles. This suggests that discrimination based on gender and site (forehead and forearm) for volatile profiles is possible. Site discrimination based on the volatile profile sequence of the forehead (F) and forearm (F) showed that unlike the forearm (F), the forehead (F) showed a clear recovery of possibly heavier or more complex volatiles that appear 15 mins into the sample run (**Figure 2.2** top and middle). As well as that the forehead (F) had a volatile recovery that was greater than the forearm (F) as depicted by the higher peak intensities seen for the former site. Similarly, gender discrimination showed the same trend, in that the forearm (M) showed a slightly higher volatile recovery relative to the forearm (F) (**Figure 2.2** middle and bottom). It is however, important to note that the forearm (M & F) samples were analysed on different GC-MS instruments which may have influenced the recovery of volatiles.

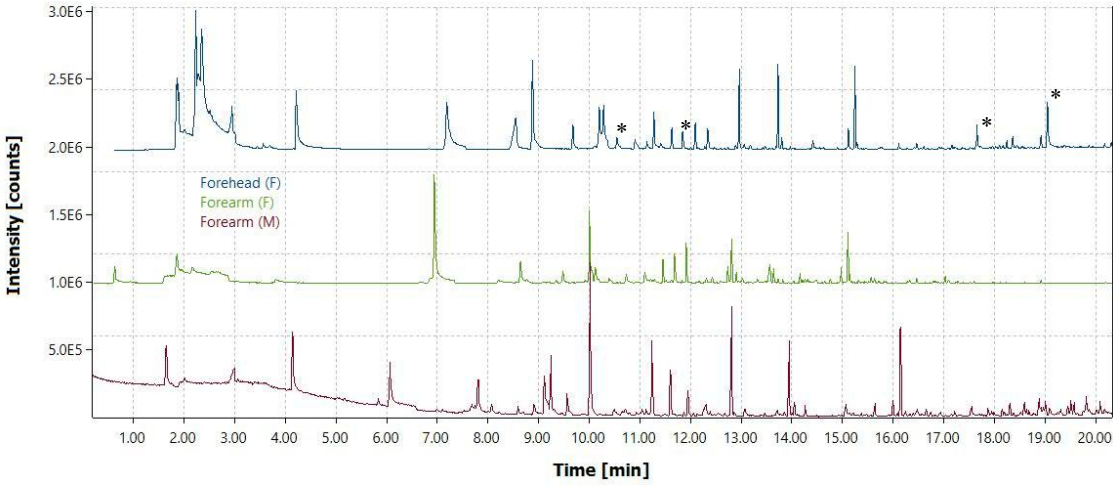


**Figure 2.2** Chromatograms for recovered volatiles from the female forehead (top), female forearm (middle) and male forearm (bottom). Asterix mark high abundant volatile compounds released from skin.

**Table 2.3** lists the identified volatile compounds along with their retention times. To better understand the differences in these profiles, the recovered volatiles were grouped and visualised based on chemical class. A stacked bar chart showing VOC composition for the forehead (F) and the forearm (M and F) is shown in **Figure 2.3**. Note that VOCs were not sampled from the male forehead for this aspect of the study. Acids, alcohols, aldehydes, ketones and esters were recovered from all sites. Unidentified compounds or compounds attributed to external sources such as the SPME fibre were classed as Other. Differences in composition across the different sites were noted. The forehead (F) and forearm (F) differed in profile, most notably in terms of the acidic emission. This is likely predominantly due to differing densities of sebaceous glands. A big difference between the studied skin regions is in their sebaceous gland densities. Sebaceous glands are found in a significantly higher concentration in the forehead (approx. 400-900 glands/cm$^2$) compared to any other site on the skin (approx. 100 glands/cm$^2$).[74,154] FFAs make up 15% of sebum secreted by these glands and their higher abundance in the forehead could explain the higher acid recovery from this region as compared to the forearm. In fact using TS to sample the skin and HPLC for sample analysis, Ludovici *et al*. were able to prove the presence of a strong positive correlation between the sebaceous gland density and the abundance of FFAs on the SC.[74]

Acids, alcohols and aldehydes found in skin secretions are said to originate from the interactions between sebaceous gland secretions and cutaneous bacteria.[155,156] Propionibacteria and staphylococci are the dominant microbial habitats of the forehead and forearm, respectively.[126] Propionibacteria found on the forehead is referred to as an "acidogenic" organism meaning that it produces acidic end products.[126] These acidic metabolites are likely contributing to the overall greater acid emission from the forehead as compared to the forearm. Anaerobic bacteria such as propionibacteria colonise hair follicle/sebaceous gland duct. They use lipases to breakdown triglycerides releasing long-chain-fatty acids which are further metabolised via aerobic bacteria into longer, saturated and unsaturated acids and smaller volatile acids, aldehydes and alcohols.[156]

Differences related to gender were also observed in the forearm (M & F) data. Of the acids, aldehydes, and ketones were recovered in a higher abundant in samples from male participants, while esters and alcohols were recovered in a higher abundance in samples from female participants (**Figure 2.3**)**.** The higher recovery of esters and alcohols in samples from female participants may be attributed to a higher use of cosmetic products. Other studies have also examined the effect of gender on volatile emissions and different observations have been reported. For example, Dormont *et al*. concluded no significant differences between male and female foot volatiles, although some quantitative differences in nonanal, undecanal and geranyl acetone were noted.[135] Curran *et al*. reported minor qualitative differences between male and female axillary sweat samples.[157]

**Table 2.3**: Volatile compounds identified from the HS of skin along with their retention time. Asterisked compounds have been attributed to a peak on **Figure 2.2**.

| Retention time | Compound |
|---|---|
| 6.651 | Hexanal |
| 10.290 | 5-hepten-2-one, 6-methyl |
| 10.557 | Octanal * |
| 10.912 | 1-Hexanol, 2-Ethyl- |
| 11.843 | Nonanal * |
| 12.958 | Decanal |
| 13.476 | Nonanoic acid |
| 13.973 | Undecanal |
| 14.906 | Dodecanal |
| 15.231 | Geranyl acetone |
| 16.134 | Dodecanoic acid |
| 16.480 | 1-Tridecanol |
| 16.654 | E-14-Hexadecanol |
| 17.637 | Tetradecanoic acid * |
| 18.358 | Pentadecanoic acid |
| 18.912 | 9-Hexadecenoic acid |
| 19.033 | n-Hexadecanoic acid * |
| 20.917 | Phthalate |

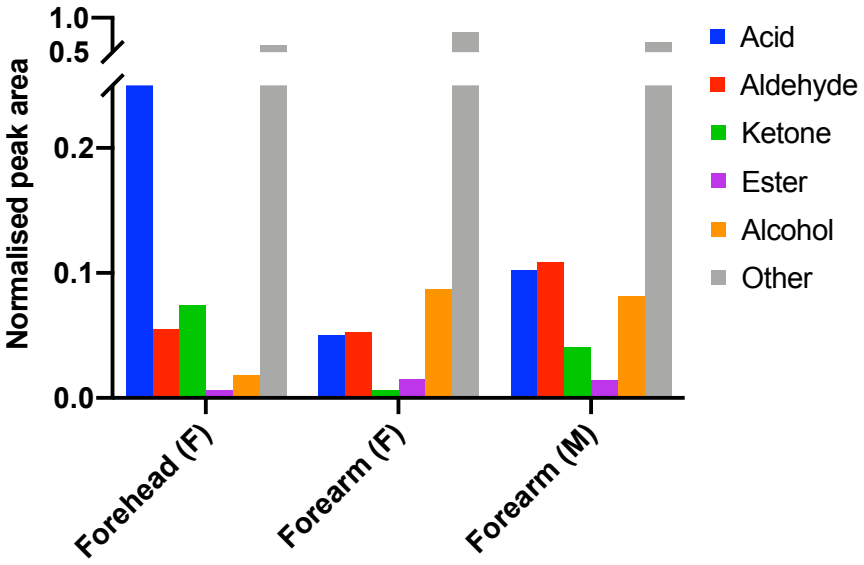


**Figure 2.3** Grouped bar chart showing normalised peak areas for compound classes recovered from skin volatile samples collected from the female forehead (n=10 participants), female forearm (n=10 participants) and male forearm (n=9 participants).

*2.3.2 Kinetic study of skin volatile emissions*

A kinetic study was conducted to investigate if skin volatile emissions, especially the VFA, changed with time. pH values and volatiles samples were collected every h for 4-5 h from the volar forearm of female participants (n=3).The total peak area, total acidic peak area and n-hexadecanoic peak area of skin volatile samples were quantified and plotted against time **Figure 2.4** .Only minor variation in peak areas were noted over time for each participant. The minor variations in peak areas may be attributed to the degradation of fibre or/and column coating.

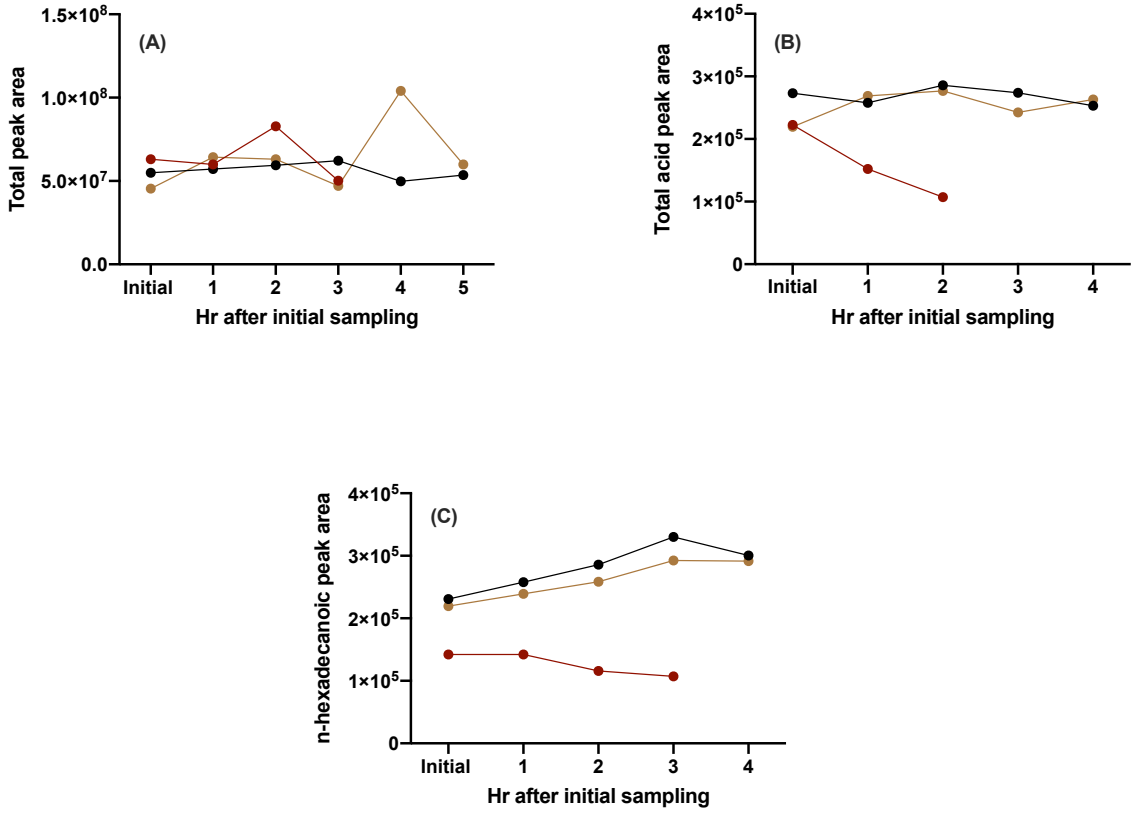


**Figure 2.4** Skin volatile emission abundances over time recovered from the volar forearm (n= 3 female participants). The x-axis represents (A) total peak area, (B) total acid peak area and (C) peak area of n-hexadecanoic acid. Different colours represent different participants.

*2.3.3 Effect of application of isopropyl alcohol to skin on the VFA emission and skin surface pH*

Numerous studies have implemented skin pre-treatment protocols before sampling the skin volatiles to reduce environmental contributions. Participants are generally requested to avoid using cosmetics on the day of sampling, and the skin site is often washed with water or with fragrance-free soap prior to sampling.[135,157,158] In our case, participants are asked not to apply cosmetics on day of sampling but no physical pre-treatment of the skin is carried out typically. As can be seen from the stacked bar graph (**Figure 2.2**), exogeneous skin VOCs are present typically in the data we obtain as cosmetic product tends to persist in the skin leading to their detection in the recovered samples.

In this work, the impact of pre-treating the skin with isopropyl alcohol (IPA) was investigated to see if the presence of exogenous compounds could be reduced. Skin volatile samples along with skin surface pH measurements were collected from the volar forearm before and after pre-treatment with IPA as described in the Methods Section *2.2.2*. The samples recovered before and immediately after IPA application to the skin were observed to be different (**Figure 2.5**). It can be seen that application of IPA results in a IPA peak at a retention time (Rt) of 2.31 min with a large peak area and a small reduction in areas of later eluting peaks. This reduction in peak area is likely due to a physical removal of compounds from the surface of the skin upon wiping with IPA. No significant change in skin surface pH was observed after applying IPA (n=4, average pH before IPA: 4.70 ± 0.21; after IPA: 4.73 ± 0.03, p-value: 0.0984).

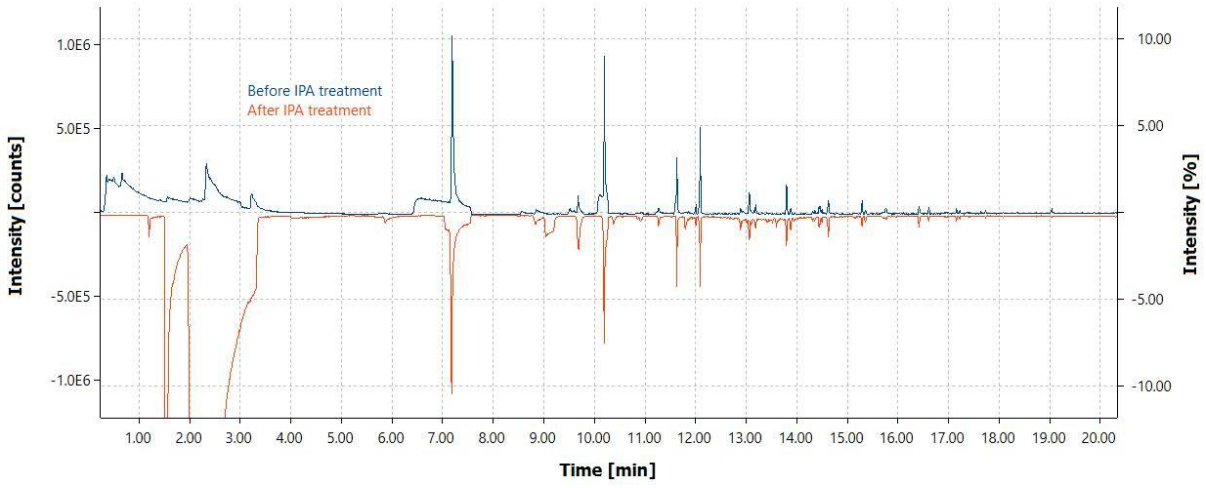


**Figure 2.5** Overlayed chromatograms for a recovered volatile sample taken before (brown) and immediately after (blue) application of IPA on the volar forearm.

2.3.4 Investigation of volatile profile stability after application of IPA to skin

As depicted in **Figure 2.5** the skin volatile profile was shown to be impacted by the application of IPA when the volatile emission is collected immediately after the IPA application. Here a kinetic study was conducted to monitor the volatile emission profile over time to determine how long it takes to re-establish itself after IPA application (**Figure 2.6**).

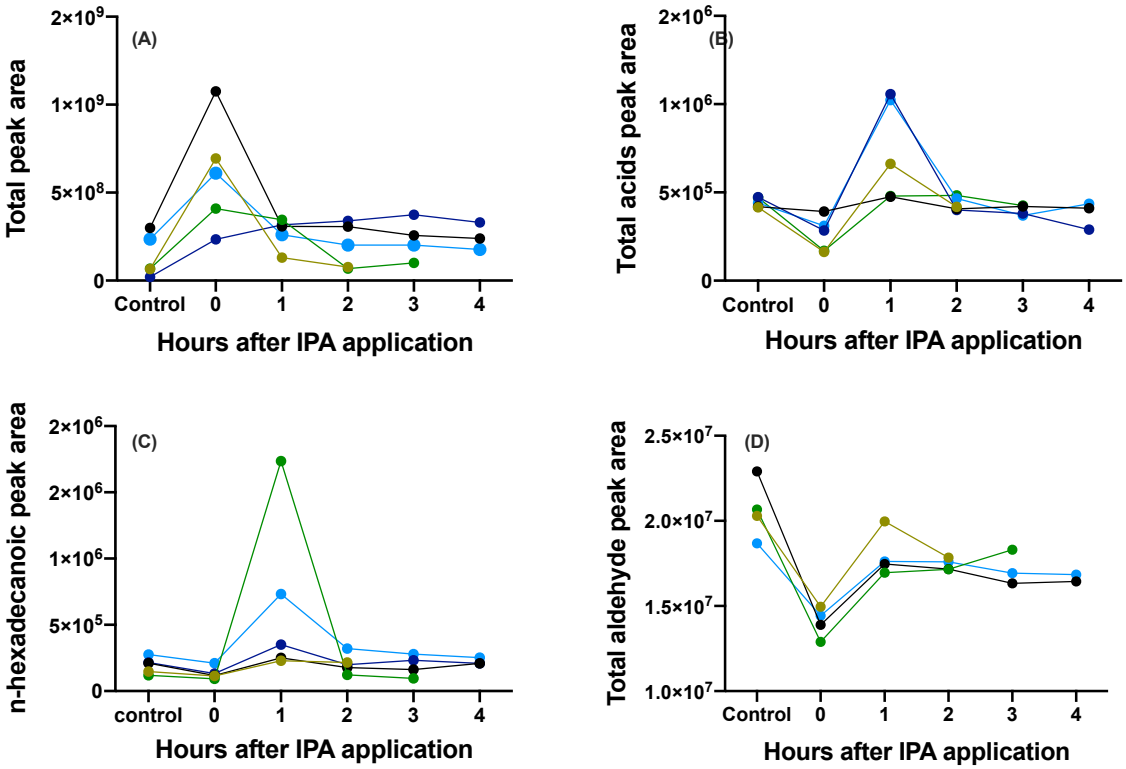


**Figure 2.6** Chromatographic peak areas for volatile emissions sampled from the volar forearm over time post application of IPA. (A) total peak area, (B) peak area of total identified acids, (C) peak area of n-hexadecanoic acid and (D) peak area of total identified aldehydes. One participant was sampled multiple times for this study where different colours represent different samples.

The results show that directly after IPA application (t=0), there is an increase in total peak area recovered which can be attributed to the IPA peak (**Figure 2.6 (A)**). Over time, the IPA evaporates and the total peak area reduces and stabilises. The most abundant VFA, n-hexadecanoic acid, was also tracked and it was observed that following application of IPA, the

peak area of this acid reduced a small bit, before increasing dramatically in abundance 1 h after application (**Figure 2.6 (B)**). This same trend is seen when quantifying the total acids before and after application of IPA. Beyond this timepoint, the abundance decreases again and re-establishes to baseline levels. This is an interesting phenomena and the reason for this spike in VFA emission is currently unknown. It would be useful to track the skin surface pH at the same time intervals to investigate if this event correlates with a significant decrease in pH. This spike was not observed for aldehyde compounds where it can be seen that the total aldehyde peak area was reduced following application of IPA (**Figure 2.6 (D)**) which is likely on account of the physical removal of content from the SC. The abundance of aldehydes is seen to increase over time as the skin presumably re-establishes homeostasis.

There are limited reports that describe the effect of skin pre-treatment methods on skin volatile emission. A publication by Dormont *et al*. showed that washing of the skin with water affected volatile composition.[135] This pre-treatment step led to a reduction in terpenes and alkanes. Bommannan *et al*. showed that in humans, ethanol enters the skin and removes measurable quantities of lipids found on the SC.[159] The reduction of acidic peak abundances immediately following IPA application (**Figure 2.6 (B)**) represents the physical removal of IPA from the SC. The mechanism by which alcohols such as ethanol remove SC lipids is not yet fully understood however it is believed that it occurs via the disruption of the lipid bi-layer.[160] Using molecular dynamics Guapta *et al*. showed that ethanol disrupt the FFA environment eg lipid bilayers, leading to a response from the glands to produce high amounts of FFAs to correct for this disruption.[160] The same phenomenon was observed in this study where an increase in FFA emissions was detected 1 h following application of IPA possible due to the accelerated production of FFA from the glands. Tracking the pH at the same time points could help very this observation as it could show that the FFA spike correlated temporarily with lowering of the pH. As mentioned earlier, Not only can alcohols affect the quantity of lipids on the SC but also the structure of the SC lipid phase becomes disrupted.[161] Another report examined the influence of alcohols on SC maturation enzymes.[162] Alcohols like isopropanol led to an abnormal expression of TNF-alpha and IL-1-alpha enzymes, known to irritate skin keratinocytes when over-expressed.[162] These proteins are essential in fighting microbial infections on the skin, and any variation in skin microbes can alter the composition of the volatiles emitted from the skin. PLA2 is another critical enzyme for normal SC barrier formation that is vital for degrading residual phospholipids to free fatty acids.[103] Results suggest that alcohols have the potential to inhibit SC enzyme activities in the order ethanol <

isopropanol < n-propanol.[162] Based on this and due to the significant observed effect of IPA on the skin volatile emission, all experiments discussed henceforth do not include a pre-treatment step.

*2.3.5 Skin acid volatile emission*

Here the acidic nature of the skin surface was examined in the context of considering the VFA composition of skin volatile emission. Volatiles were sampled from the HS above the forehead (F) and volar forearm (M & F) using SPME as seen in **Figure 2.1** of the Methods Section *2.2.3* and the samples collected were then analysed using GC-MS. VFAs that were identified in the majority of participants (>70%) were analysed quantitatively. In total, five VFAs were identified in the C9-C16 range which were present across all sites studied and have all been observed previously in skin volatile studies and are known to be primary metabolic products.[74,86,163,164]

Normalised peak area data for these VFAs for forehead (F) and forearm (M & F) is shown in **Figure 2.7**. Several observations are noted. Recovery of the individual VFAs was consistently lowest on the female forearm site while the normalised individual saturated VFA peak areas for the male forearm were highest for all VFAs. This can be explained in the context of gland density, whereby of all sites sampled, the female forearm has the lowest density of sebaceous glands and hence the lowest rate of production of FAs. The female forehead and male forearm have significantly higher densities of these glands, explaining the higher recoveries of VFAs. Despite the absolute differences in peak areas observed, all sets of data followed the similar general trend whereby long-chain VFAs (C14, C15, C16, C16:1) were recovered in higher amounts relative to the medium-chain VFAs (C9, C12).

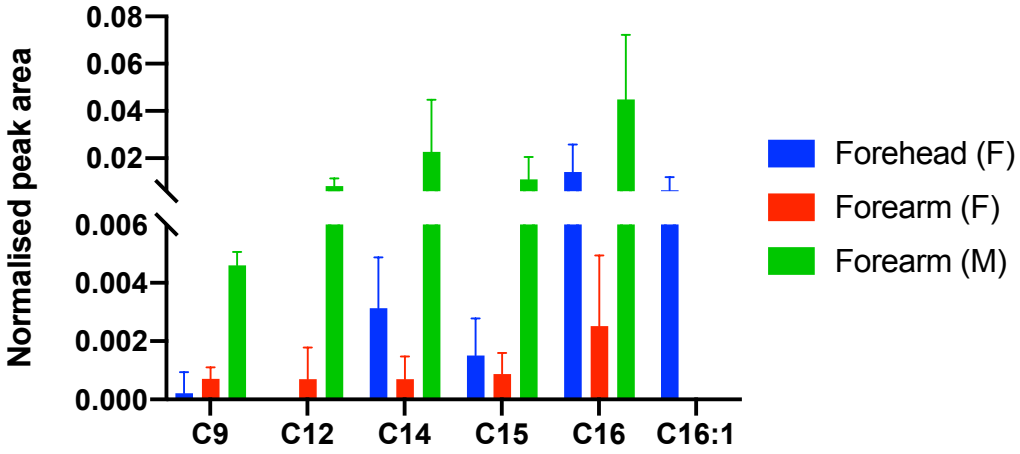


**Figure 2.7** Box plot showing normalised median peak areas of individual VFAs emitted from the female forehead (n=10 participants), female forearm (n=10 participants) and male forearm (n=9 participants).

Skin surface pH measurements were also taken for all participants sites prior to VOC sampling. A bar chart showing the collected skin surface pH data for the forehead (F), forearm (F) and forearm (M) is seen in **Figure 2.8**. It can be seen that median skin surface pH was measured to be lowest for the forehead (F) and highest for forearm (F), where sebaceous glands and their production of FAs is known to play an important role in skin acidity.[106] Consistent with this, similar observation was made by Fluhr *et al*. in a participant study where skin barrier was assessed via non-invasive measurements of six skin functions including skin surface pH using flat glass electrode. Skin surface pH at the forehead was the lowest relative to the other 6 anatomical sites studied.[165] In another study carried out by Ansari *et al*. forehead skin surface pH was determined to fall between 4.0-5.5 and the forearm between 4.4-5.1.[166] However, in a large participant study (n=712) carried out amongst an Asian population skin surface pH did not vary with anatomical site.[167,168] This observation may be true for this ethnic group only. However as the participant ethnicity was not stated in the two previously motioned studies carried out by Fluhr *et al*. and Ansari *et al*. it is difficult to draw conclusion.

The gender difference seen here for skin surface pH is consistent with that reported previously.[169] whereby the median skin surface pH for females is higher than that of males for the equivalent site. It is noted that the spread of male skin surface pH was much greater than that of females. Overall however, all values measured are within the expected normal pH range for a healthy skin surface taking gender and site into account.[169,170] In the presented study, it

was noted that the lower skin surface pH values in the forehead were accompanied by increased recovery of acidic VOC emissions relative to the forearm (**Figure 2.3**).

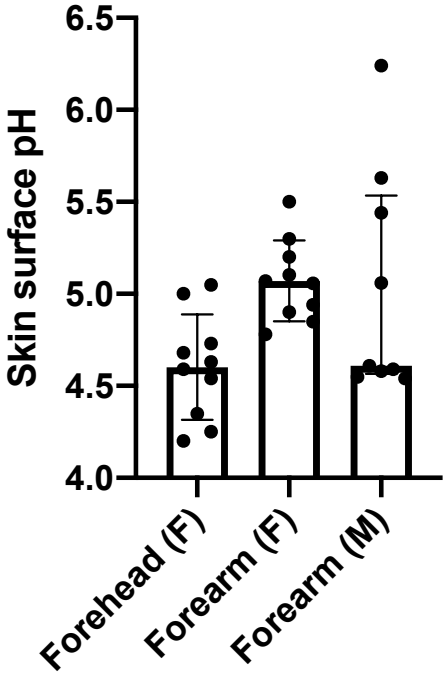


**Figure 2.8** Box plot showing skin surface pH measurements collected using a flat glass pH probe for the female forehead, female forearm and male forearm (n=10 participants for female forehead and forearm sample sets and n=9 participants for male forearm sample set). Box height represents median values and the error bars represent the 95% confidence interval.

*2.3.6 Association of skin surface pH with VFA emission*

Based on this data, the correlation between the abundances of VFAs recovered and skin acidity for each participant group was investigated. To do this, the total peak area of the considered VFAs was divided by the total chromatographic peak area for total volatiles recovered for each participant sample. This provided a normalised peak area for total VFAs which was plotted as a function of hydrogen ion concentration (as computed from a skin surface pH measurement) for each sample (**Figure 2.9 (A-C)**). Regression was performed and strong linear correlations with hydrogen ion concentration was observed within each group (female forehead: $r^2$=0.680; female forearm: 0.776; male forearm: $r^2$=0.791) and the associated P-values showed significance in all cases. The VFA peak area dependence on skin surface pH is likely primarily

driven by the already established association between skin FFA content (both exogenous and endogenous sources) and skin acidity. However, it is proposed here that the sensitivity of this association may be further amplified due to the link between the equilibrium vapour pressure of the FFAs and the skin surface pH. As the range of FFA pKa values are approx. 4.9-5.0, over the range of measured skin surface pH in this study (approx. 4.0-5.5) the proportion of undissociated FFA (relative to dissociated FFA) will vary significantly. Therefore, the undissociated FFAs will exhibit a vapour pressure above skin that will be dependent on skin surface pH. It should be noted that factors including SC water and ionic contents will influence the partitioning of the FFAs and therefore will have an effect on FFA equilibrium vapour pressures, which indeed may well account for some of the variability seen in the participant data.

The magnitude of normalised peak areas of recovered VFAs differs for all groups and was in the order of male forearm>female forehead>female forearm. The slopes of the regression lines fitted to the data for each site represents the sensitivity of the response (i.e. change in peak area per molar change in hydrogen ion concentration) (**Figure 2.9**). This measure for sensitivity of the response follows the same trend as seen for the magnitude of the response (i.e. greater sensitivity correlates with higher amounts of recovered VFAs). This behaviour is likely governed by different levels of glandular activities at each site but endogenous factors related to FFA production may also play a role.

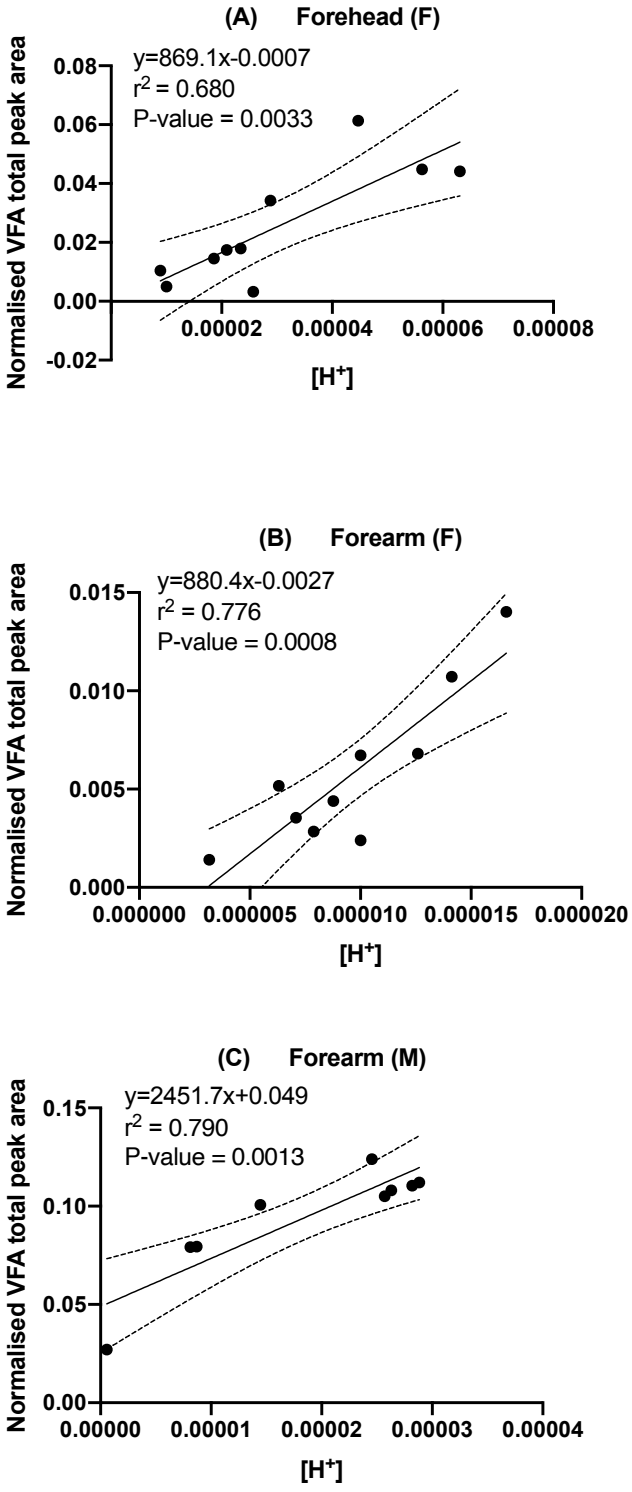


**Figure 2.9** Normalised total peak area of identified VFAs recovered from participants' skin samples plotted against hydrogen ion concentration as measured using a skin surface glass pH probe. Sites sampled: (A) female forehead (n=10 participants); (B) female forearm (n=10 participants); (C) male forearm (n=9 participants). Dashed lines shows the 95% confidence intervals of the regression models.

Although the literature demonstrates the important contribution of FFAs to SC acidification whereby FFAs are derived from sebum secretions, and hydrolyzation of SC phospholipids, FFAs are not the only species in the SC that contributes to the acidity. Various non-volatile acidic species including urocanic acid, lactic acid, carbonic acids and other weak organic acids, all generated via various cellular and metabolic pathways are also known to play a role in the maintenance of skin physiological pH. Despite FFAs being just one of several species contributing to SC acidity, it is clear that the FFA content, as measured by the VFA emission can provide a measure of total acidity.

In order to investigate if there were specific VFA emissions for which correlation with skin surface pH was greatest over the different sites, normalised peak areas for the individual VFAs were also plotted against hydrogen ion concentration (**Figure 2.10 - 2.12**). Although regression models had positive correlations at all sites investigated, correlation coefficients were low for each individual VFA considered. These low correlation coefficients may reflect low precision in sampling (e.g. inter-fibre variability, small changes in environmental temperature or humidity during sampling, etc). whereby the effect is minimised when total VFA peak area for identified VFAs is considered instead. Alternatively, it may indicate a complex interplay and dependency between the individual VFAs themselves that is not yet fully understood. Carlo et al. show that generally SPME fibre coatings containing Carboxen had very low repeatability associated with them. As well as that, the fibre-life seems mainly to be influenced by frequency of usage for sampling and by both the nature of the matrix under investigation and sampling conditions. [171,172] It was also observed that in general, the longer carbon chain VFAs had higher slope values for the regression models, indicating that these VFAs may be more significant than the shorter VFAs in terms of their association with skin acidity.

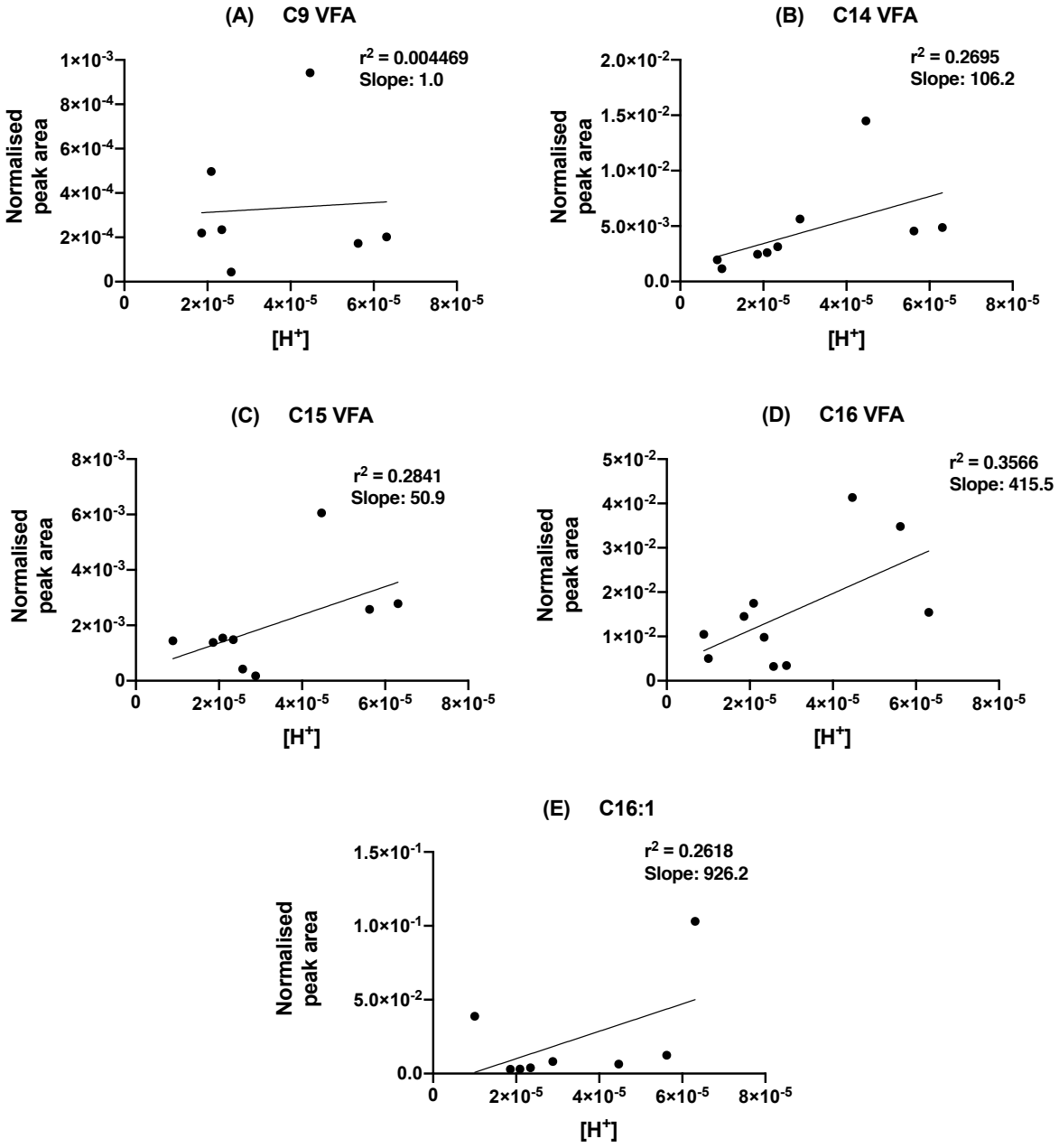


**Figure 2.10** Normalised peak areas for (A) nonanoic acid, (B) tetradecanoic acid, (C) pentadecanoic acid and (D) n-hexadecanoic acid (E) cis-7-hexadecenoic acid for the female forehead plotted against hydrogen ion concentration as measured using a skin surface glass pH probe.

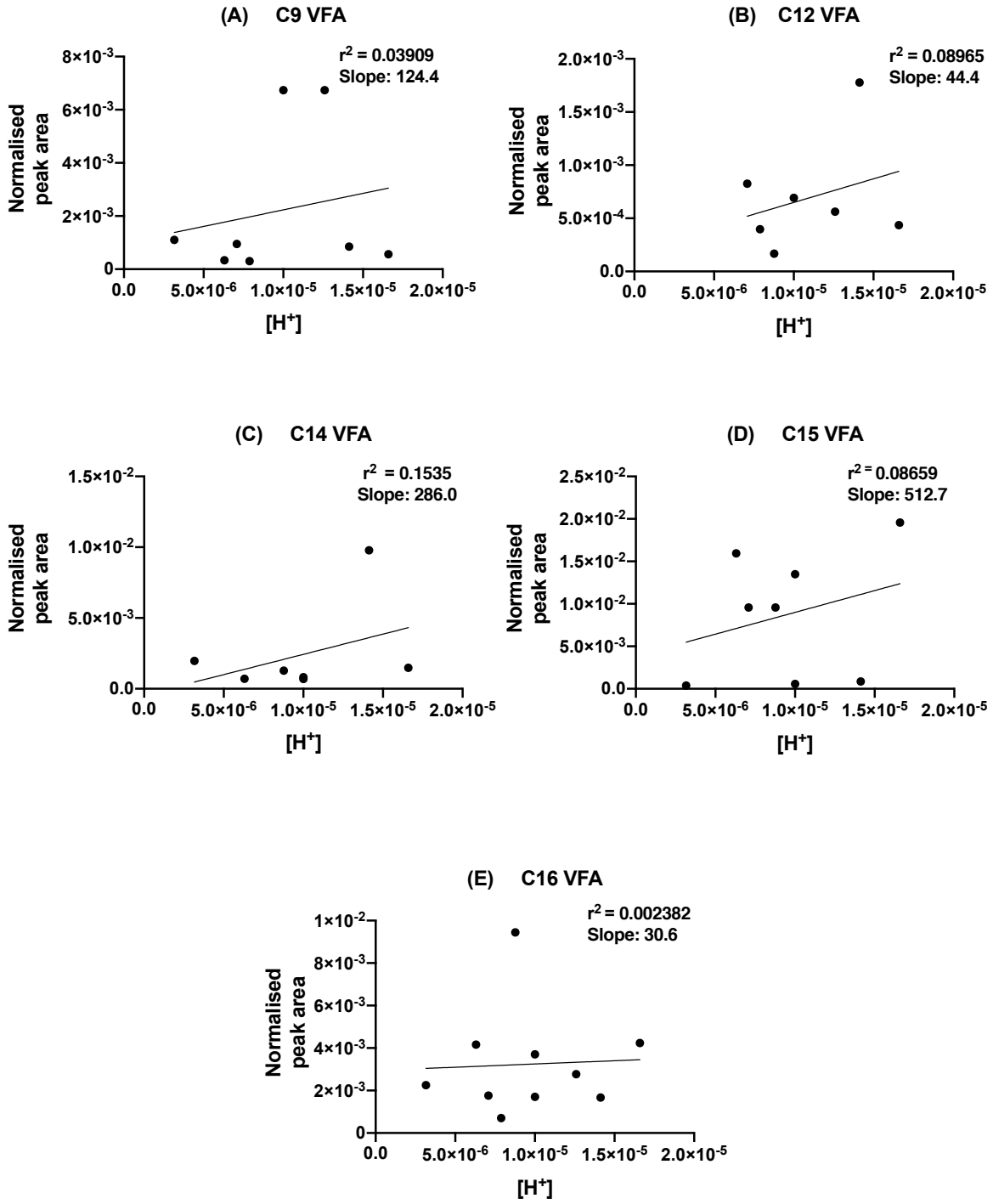


**Figure 2.11** Normalised peak areas for (A) nonanoic acid, (B) dodecanoic acid, (C) tetradecanoic acid, (D) pentadecanoic acid and (E) n-hexadecanoic acid for the female forearm plotted against hydrogen ion concentration as measured using a skin surface glass pH probe.

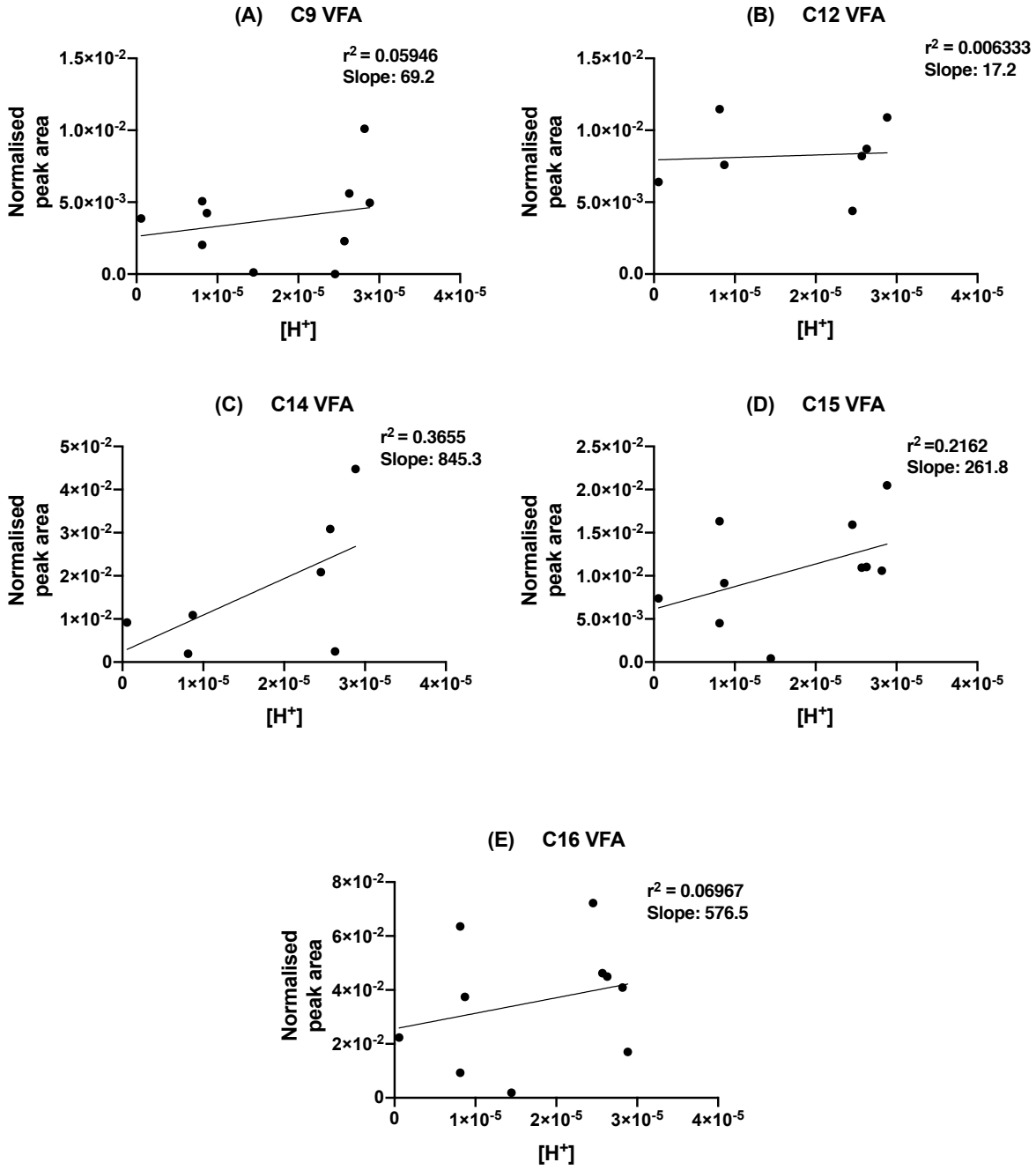


**Figure 2.12** Normalised peak areas for (A) nonanoic acid, (B) dodecanoic acid (C) tetradecanoic acid, (D) pentadecanoic acid and (E) n-hexadecanoic acid for the male forearm plotted against hydrogen ion concentration as measured using a skin surface glass pH probe.

As control data, in order to ensure it was specifically the VFA content in the VOC profile that demonstrated a correlation with skin acidity, total chromatographic peak area was plotted as a function of hydrogen ion concentration for all sites and no significant correlations established (**Figure 2.13**), supporting the hypothesis that peak area of the recovered skin-emitted VFAs selectively correlates with skin acidity.

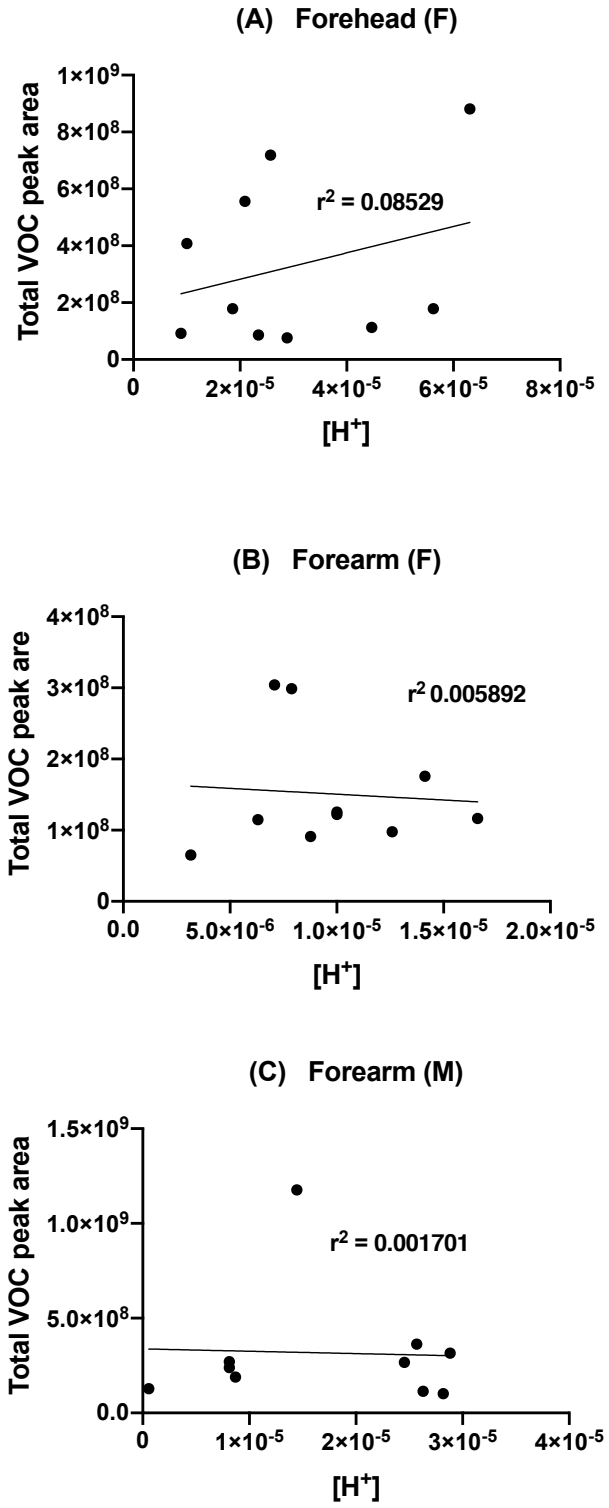


**Figure 2.13** Total VOC peak area recovered from (A) female forehead (B) female forearm and (C) male forehead plotted against hydrogen ion concentration as measured using a skin surface glass pH probe.

In summary, given the strong linear VFA correlation with hydrogen ion concentration observed across multiple sites and for both genders, the supporting literature regarding the acidification role of FFAs in the SC, and the proposed significant effect of pH on the VFA equilibrium vapour pressures, there is good rationale to suggest that the skin VFA emission is dependent of skin surface pH. Indeed the fundamental relationship between VFA concentration and pH for other matrices have been previously reported and complex models proposed.[173–175] As with other matrices, a more complex model to describe the VFA relationship with pH could be developed for the skin surface to consider factors including SC water and ionic contents. However, the simplistic linear models fitted in this work serve to initially highlight that quantifying the VFA emission, which can be sampled from skin in a contactless manner, could be a viable approach to get a measure of skin surface pH.

## 2.4 Conclusion

The work presented here focused on the analysis of VFA profiles recovered from healthy participant skin volatile samples. Several saturated medium- and long-chain fatty acids were identified as being present in participant samples, irrespective of gender and site. The amount of recovered VFA differed across the studied sites (forearm and forehead) and this was attributed to differences in sebaceous gland densities and hence sebum secretions and metabolic activity. The association of recovered VFA peak areas with skin surface acidity was examined in a pilot study in females (forehead and forearm) and males (forehead) and strong linear correlations in the data were found. This correlation is likely related to VFAs playing a significant role in influencing SC acidity but also the equilibrium vapour pressures of the VFAs being modulated by skin surface pH. This finding opens up the possibility that a measure of skin surface pH could be obtained by quantifying the volatile acid emission. This is the first time a direct link between VFA emission and surface pH has been demonstrated in skin to our knowledge, which represents a potentially useful finding for personalised monitoring of inflammatory skin disease where changes in skin surface pH are closely linked with disease flare-ups.

**2.5 References**


1. Kolarsick, P. A. J., Kolarsick, M. A. & Goodwin, C. Anatomy and Physiology of the Skin. *J. Dermatol. Nurses Assoc.* **3**, 203–213 (2011).
2. Sahle, F. F., Gebre-Mariam, T., Dobner, B., Wohlrab, J. & Neubert, R. H. H. Skin Diseases Associated with the Depletion of Stratum Corneum Lipids and Stratum Corneum Lipid Substitution Therapy. *Skin Pharmacol. Physiol.* **28**, 42–55 (2015).
3. Proksch, E., Brandner, J. M. & Jensen, J.-M. The skin: an indispensable barrier. *Exp. Dermatol.* **17**, 1063–1072 (2008).
4. Kanitakis, J. Anatomy, histology and immunohistochemistry of normal human skin. *Eur. J. Dermatol. EJD* **12**, 390–399; quiz 400–401 (2002).
5. Takahashi, M., Kawasaki, K., Tanaka, M., Ohta, S. & Tsuda, Y. The mechanism of stratum corneum plasticization with water. in *Bioengineering and the Skin: Based on the Proceedings of the European Society for Dermatological Research Symposium, held at the Welsh National School of Medicine, Cardiff, 19–21 July 1979* (eds. Marks, R. & Payne, P. A.) 67–73 (Springer Netherlands, 1981). doi:10.1007/978-94-009-7310-7_8.
6. Hoover, E. & Krishnamurthy, K. Physiology, Sebaceous Glands. in *StatPearls* (StatPearls Publishing, 2020).
7. Hodge, B. D. & Brodell, R. T. Anatomy, Skin Sweat Glands. in *StatPearls* (StatPearls Publishing, 2020).
8. Rippke, F., Berardesca, E. & Weber, T. M. pH and Microbial Infections. *Curr. Probl. Dermatol.* **54**, 87–94 (2018).
9. Drislane, C. & Irvine, A. D. The role of filaggrin in atopic dermatitis and allergic disease. *Ann. Allergy Asthma Immunol. Off. Publ. Am. Coll. Allergy Asthma Immunol.* **124**, 36–43 (2020).
10. Kubo, A., Nagao, K. & Amagai, M. Epidermal barrier dysfunction and cutaneous sensitization in atopic diseases. *J. Clin. Invest.* **122**, 440–447 (2012).

11. Smeden, J. van *et al.* The importance of free fatty acid chain length for the skin barrier function in atopic eczema patients. *Exp. Dermatol.* **23**, 45–52 (2014).

12. Del Rosso, J. Q. & Levin, J. The Clinical Relevance of Maintaining the Functional Integrity of the Stratum Corneum in both Healthy and Disease-affected Skin. *J. Clin. Aesthetic Dermatol.* **4**, 22–42 (2011).

13. Schmid-Wendtner, M.-H. & Korting, H. C. The pH of the Skin Surface and Its Impact on the Barrier Function. *Skin Pharmacol. Physiol.* **19**, 296–302 (2006).

14. Shirasu, M. & Touhara, K. The scent of disease: volatile organic compounds of the human body related to disease and disorder. *J. Biochem. (Tokyo)* **150**, 257–266 (2011).

15. Rondanelli, M. *et al.* Volatile Organic Compounds as Biomarkers of Gastrointestinal Diseases and Nutritional Status. *J. Anal. Methods Chem.* **2019**, e7247802 (2019).

16. Mochalski, P., King, J., Unterkofler, K., Hinterhuber, H. & Amann, A. Emission rates of selected volatile organic compounds from skin of healthy volunteers. *J. Chromatogr. B Analyt. Technol. Biomed. Life. Sci.* **959**, 62–70 (2014).

17. Kataoka, H., Saito, K., Kato, H. & Masuda, K. Noninvasive analysis of volatile biomarkers in human emanations for health and early disease diagnosis. *Bioanalysis* **5**, 1443–1459 (2013).

18. Samant, P. P. & Prausnitz, M. R. Mechanisms of sampling interstitial fluid from skin using a microneedle patch. *Proc. Natl. Acad. Sci. U. S. A.* **115**, 4583–4588 (2018).

19. Samant, P. P. *et al.* Sampling interstitial fluid from human skin using a microneedle patch. *Sci. Transl. Med.* **12**, (2020).

20. Liu, Y., Pharr, M. & Salvatore, G. A. Lab-on-Skin: A Review of Flexible and Stretchable Electronics for Wearable Health Monitoring. *ACS Nano* **11**, 9614–9635 (2017).

21. Jayathilaka, W. A. D. M. *et al.* Significance of Nanomaterials in Wearables: A Review on Wearable Actuators and Sensors. *Adv. Mater.* **31**, 1805921 (2019).

22. Jin, H., Abu-Raya, Y. S. & Haick, H. Advanced Materials for Health Monitoring with Skin-Based Wearable Devices. *Adv. Healthc. Mater.* (2017) doi:10.1002/adhm.201700024.

23. Maibach, H. & Honari, G. *Applied Dermatotoxicology: Clinical Aspects*. (Academic Press, 2014).

24. Wong, R., Geyer, S., Weninger, W., Guimberteau, J.-C. & Wong, J. K. The dynamic anatomy and patterning of skin. *Exp. Dermatol.* **25**, 92–98 (2016).

25. Kern, F., Niault, T. & Baccarini, M. Ras and Raf pathways in epidermis development and carcinogenesis. *Br. J. Cancer* **104**, 229–234 (2011).

26. Amisten, S. *et al.* An atlas of G-protein coupled receptor expression and function in human subcutaneous adipose tissue. *Pharmacol. Ther.* **146**, 61–93 (2015).

27. Vitorino, C., Sousa, J. & Pais, A. Overcoming the skin permeation barrier: challenges and opportunities. *Curr. Pharm. Des.* **21**, 2698–2712 (2015).

28. Kubo, A., Nagao, K. & Amagai, M. 3D Visualization of Epidermal Langerhans Cells. in *Molecular Dermatology* (eds. Has, C. & Sitaru, C.) vol. 961 119–127 (Humana Press, 2013).

29. Benson, H. A. E. Skin Structure, Function, and Permeation. in *Topical and Transdermal Drug Delivery* 1–22 (John Wiley & Sons, Ltd, 2012).

30. Behne, M. *et al.* Omega-hydroxyceramides are required for corneocyte lipid envelope (CLE) formation and normal epidermal permeability barrier function. *J. Invest. Dermatol.* **114**, 185–192 (2000).

31. Elias, P. M. *et al.* Formation and Functions of the Corneocyte Lipid Envelope (CLE). *Biochim. Biophys. Acta* **1841**, 314–318 (2014).

32. Yang, G. *et al.* Skin Barrier Abnormalities and Immune Dysfunction in Atopic Dermatitis. *Int. J. Mol. Sci.* **21**, 2867 (2020).

33. Zhang, B. *et al.* Chapter 52 - Bioengineering Skin Constructs. in *Stem Cell Biology and Tissue Engineering in Dental Sciences* (eds. Vishwakarma, A., Sharpe, P., Shi, S. & Ramalingam, M.) 703–719 (Academic Press, 2015). doi:10.1016/B978-0-12-397157-9.00056-4.

34. Skin Tissue Engineering and Regenerative Medicine - 1st Edition. https://www.elsevier.com/books/skin-tissue-engineering-and-regenerative-medicine/albanna/978-0-12-801654-1.

35. Baswan, S. *et al.* Understanding the Formidable Nail Barrier: A Review of the Nail Microstructure, Composition and Diseases. *Mycoses* **60**, 284–295 (2017).

36. Murphrey, M. B. & Vaidya, T. Histology, Apocrine Gland. in *StatPearls* (StatPearls Publishing, 2020).

37. Saga, K. Structure and function of human sweat gland studied with histochemistry an cytochemistry. *Prog. Histochem. Cytochem.* **37**, 323–86 (2002).

38. Chen, Y.-L., Kuan, W.-H. & Liu, C.-L. Comparative Study of the Composition of Sweat from Eccrine and Apocrine Sweat Glands during Exercise and in Heat. *Int. J. Environ. Res. Public. Health* **17**, (2020).

39. Baker, L. B. Physiology of sweat gland function: The roles of sweating and sweat composition in human health. *Temp. Multidiscip. Biomed. J.* **6**, 211–259 (2019).

40. Cui, C.-Y. & Schlessinger, D. Eccrine sweat gland development and sweat secretion. *Exp. Dermatol.* **24**, 644–650 (2015).

41. Esteves, C. Z. *et al.* Skin Biomarkers for Cystic Fibrosis: A Potential Non-Invasive Approach for Patient Screening. *Front. Pediatr.* **5**, (2018).

42. Rigopoulos, D., Larios, G. & Katsambas, A. Skin signs of systemic diseases. *Clin. Dermatol.* **29**, 531–540 (2011).

43. Crowther, J. M. *et al.* Measuring the effects of topical moisturizers on changes in stratum corneum thickness, water gradients and hydration in vivo. *Br. J. Dermatol.* **159**, 567–577 (2008).

44. Horii, I., Nakayama, Y., Obata, M. & Tagami, H. Stratum corneum hydration and amino acid content in xerotic skin. *Br. J. Dermatol.* **121**, 587–592 (1989).

45. Hoste, E. *et al.* Caspase-14 Is Required for Filaggrin Degradation to Natural Moisturizing Factors in the Skin. *J. Invest. Dermatol.* **131**, 2233–2241 (2011).

46. Nakagawa, N. *et al.* Relationship Between NMF (Lactate and Potassium) Content and the Physical Properties of the Stratum Corneum in Healthy Subjects. *J. Invest. Dermatol.* **122**, 755–763 (2004).

47. Watanabe, M., Tagami, H., Horii, I., Takahashi, M. & Kligman, A. M. Functional Analyses of the Superficial Stratum Corneum in Atopic Xerosis. *Arch. Dermatol.* **127**, 1689–1692 (1991).

48. Taylor, N. A. & Machado-Moreira, C. A. Regional variations in transepidermal water loss, eccrine sweat gland density, sweat secretion rates and electrolyte composition in resting and exercising humans. *Extreme Physiol. Med.* **2**, 4 (2013).

49. Watabe, A. *et al.* Sweat constitutes several natural moisturizing factors, lactate, urea, sodium, and potassium. *J. Dermatol. Sci.* **72**, 177–182 (2013).

50. Bernengo, J. & de Rigal, J. Physical Methods to Measure Stratum Corneum Water Content In Vivo. in *Agache's Measuring the Skin: Non-invasive Investigations, Physiology, Normal Constants* (eds. Humbert, P., Fanian, F., Maibach, H. I. & Agache, P.) 299–340 (Springer International Publishing, 2017). doi:10.1007/978-3-319-32383-1_29.

51. Querleux, B. *et al.* In vivo Hydration Profile in Skin Layers by High-Resolution Magnetic Resonance Imaging. *Skin Pharmacol. Physiol.* **7**, 210–216 (1994).

52. Caspers, P. J., Bruining, H. A., Puppels, G. J., Lucassen, G. W. & Carter, E. A. In Vivo Confocal Raman Microspectroscopy of the Skin: Noninvasive Determination of Molecular Concentration Profiles. *J. Invest. Dermatol.* **116**, 434–442 (2001).

53. Narasimha Murthy, S. & Shivakumar, H. N. CHAPTER 1 - Topical and Transdermal Drug Delivery. in *Handbook of Non-Invasive Drug Delivery Systems* (ed. Kulkarni, V. S.) 1–36 (William Andrew Publishing, 2010). doi:10.1016/B978-0-8155-2025-2.10001-0.

54. Hansen, J. R. & Yellin, W. NMR and Intrared Spectroscopic Studies of Stratum Corneum Hydration. in *Water Structure at the Water-Polymer Interface* (ed. Jellinek, H. H. G.) 19–28 (Springer US, 1972). doi:10.1007/978-1-4615-8681-4_4.

55. Darlenski, R., Sassning, S., Tsankov, N. & Fluhr, J. W. Non-invasive in vivo methods for investigation of the skin barrier physical properties. *Eur. J. Pharm. Biopharm. Off. J. Arbeitsgemeinschaft Pharm. Verfahrenstechnik EV* **72**, 295–303 (2009).

56. Plessis, J. du *et al.* International guidelines for the in vivo assessment of skin properties in non-clinical settings: Part 2. transepidermal water loss and skin hydration. *Skin Res. Technol.* **19**, 265–278 (2013).

57. Blank, I. H. Further observations on factors which influence the water content of the stratum corneum. *J. Invest. Dermatol.* **21**, 259–271 (1953).

58. Lu, F. *et al.* Review of Stratum Corneum Impedance Measurement in Non-Invasive Penetration Application. *Biosensors* **8**, 31 (2018).

59. Kohli, R., Archer, W. I., Roberts, J. M. C., Cochran, A. J. & Li Wan Po, A. Impedance measurements for the non-invasive monitoring of skin hydration: a reassessment. *Int. J. Pharm.* **26**, 275–287 (1985).

60. Björklund, S. *et al.* Skin Membrane Electrical Impedance Properties under the Influence of a Varying Water Gradient. *Biophys. J.* **104**, 2639–2650 (2013).

61. Kabiri Ameri, S. *et al.* Graphene Electronic Tattoo Sensors. *ACS Nano* **11**, 7634–7641 (2017).

62. Yao, S. *et al.* A Wearable Hydration Sensor with Conformal Nanowire Electrodes. *Adv. Healthc. Mater.* **6**, 1601159 (2017).

63. Ye, L., Wang, Z., Li, Z., Lv, C. & Man, M.-Q. Validation of GPSkin Barrier® for assessing epidermal permeability barrier function and stratum corneum hydration in humans. *Skin Res. Technol. Off. J. Int. Soc. Bioeng. Skin ISBS Int. Soc. Digit. Imaging Skin ISDIS Int. Soc. Skin Imaging ISSI* **25**, 25–29 (2019).

64. De Guzman, K. & Morrin, A. Screen-printed Tattoo Sensor towards the Non-invasive Assessment of the Skin Barrier. *Electroanalysis* **29**, 188–196 (2017).

65. Guzman, K. D., Al-Kharusi, G., Levingstone, T. & Morrin, A. Robust epidermal tattoo electrode platform for skin physiology monitoring. *Anal. Methods* **11**, 1460–1468 (2019).

66. Wang, Y. *et al.* Low-cost, μm-thick, tape-free electronic tattoo sensors with minimized motion and sweat artifacts. *Npj Flex. Electron.* **2**, 1–7 (2018).

67. Swisher, S. L. *et al.* Impedance sensing device enables early detection of pressure ulcers in vivo. *Nat. Commun.* **6**, 6575 (2015).

68. van Smeden, J. & Bouwstra, J. A. Stratum Corneum Lipids: Their Role for the Skin Barrier Function in Healthy Subjects and Atopic Dermatitis Patients. *Curr. Probl. Dermatol.* **49**, 8–26 (2016).

69. Norlén, L., Nicander, I., Lundsjö, A., Cronholm, T. & Forslind, B. A new HPLC-based method for the quantitative analysis of inner stratum corneum lipids with special reference to the free fatty acid fraction. *Arch. Dermatol. Res.* **290**, 508–516 (1998).

70. Cui, L. *et al.* Advancements in the maintenance of skin barrier/skin lipid composition and the involvement of metabolic enzymes. *J. Cosmet. Dermatol.* **15**, 549–558 (2016).

71. Ansari, M. N., Nicolaides, N. & Fu, H. C. Fatty acid composition of the living layer and stratum corneum lipids of human sole skin epidermis. *Lipids* **5**, 838–845 (1970).

72. Fluhr, J. W. *et al.* Generation of Free Fatty Acids from Phospholipids Regulates Stratum Corneum Acidification and Integrity. *J. Invest. Dermatol.* **117**, 44–51 (2001).

73. Picardo, M., Ottaviani, M., Camera, E. & Mastrofrancesco, A. Sebaceous gland lipids. *Dermatoendocrinol.* **1**, 68–71 (2009).

74. Ludovici, M. *et al.* Influence of the sebaceous gland density on the stratum corneum lipidome. *Sci. Rep.* **8**, 11500 (2018).

75. Freinkel, R. K. & Shen, Y. The origin of free fatty acids in sebum. II. Assay of the lipases of the cutaneous bacteria and effects of pH. *J. Invest. Dermatol.* **53**, 422–427 (1969).

76. Gray, G. M. & White, R. J. Glycosphingolipids and ceramides in human and pig epidermis. *J. Invest. Dermatol.* **70**, 336–341 (1978).

77. Camera, E. *et al.* Use of lipidomics to investigate sebum dysfunction in juvenile acne. *J. Lipid Res.* **57**, 1051–1058 (2016).

78. Masukawa, Y. *et al.* Comprehensive quantification of ceramide species in human stratum corneum. *J. Lipid Res.* **50**, 1708–1719 (2009).

79. van Smeden, J. *et al.* LC/MS analysis of stratum corneum lipids: ceramide profiling and discovery. *J. Lipid Res.* **52**, 1211–1221 (2011).

80. Shin, J.-H. *et al.* A lipidomic platform establishment for structural identification of skin ceramides with non-hydroxyacyl chains. *Anal. Bioanal. Chem.* **406**, 1917–1932 (2014).

81. Chiu, H.-H. & Kuo, C.-H. Gas chromatography-mass spectrometry-based analytical strategies for fatty acid analysis in biological samples. *J. Food Drug Anal.* **28**, 60–73 (2020).

82. Michael-Jubeli, R., Bleton, J. & Baillet-Guffroy, A. High-temperature gas chromatography-mass spectrometry for skin surface lipids profiling. *J. Lipid Res.* **52**, 143–151 (2011).

83. Pappas, A., Johnsen, S., Liu, J.-C. & Eisinger, M. Sebum analysis of individuals with and without acne. *Dermatoendocrinol.* **1**, 157–161 (2009).

84. Smith, R. N., Braue, A., Varigos, G. A. & Mann, N. J. The effect of a low glycemic load diet on acne vulgaris and the fatty acid composition of skin surface triglycerides. *J. Dermatol. Sci.* **50**, 41–52 (2008).

85. Croxton, R. S., Baron, M. G., Butler, D., Kent, T. & Sears, V. G. Variation in amino acid and lipid composition of latent fingerprints. *Forensic Sci. Int.* **199**, 93–102 (2010).

86. Martin, H. J., Reynolds, J. C., Riazanskaia, S. & Thomas, C. L. P. High throughput volatile fatty acid skin metabolite profiling by thermal desorption secondary electrospray ionisation mass spectrometry. *The Analyst* **139**, 4279–4286 (2014).

87. Berdyshev, E. *et al.* Lipid abnormalities in atopic skin are driven by type 2 cytokines. *JCI Insight* **3**, (2018).

88. Sadowski, T. *et al.* Large-scale human skin lipidomics by quantitative, high-throughput shotgun mass spectrometry. *Sci. Rep.* **7**, 43761 (2017).

89. Souza, S. L., Graça, G. & Oliva, A. Characterization of sweat induced with pilocarpine, physical exercise, and collected passively by metabolomic analysis. *Skin Res. Technol. Off. J. Int. Soc. Bioeng. Skin ISBS Int. Soc. Digit. Imaging Skin ISDIS Int. Soc. Skin Imaging ISSI* **24**, 187–195 (2018).

90. Delgado-Povedano, M. M., Calderón-Santiago, M., Luque de Castro, M. D. & Priego-Capote, F. Metabolomics analysis of human sweat collected after moderate exercise. *Talanta* **177**, 47–65 (2018).

91. Jadoon, S. *et al.* Recent Developments in Sweat Analysis and Its Applications. *Int. J. Anal. Chem.* **2015**, e164974 (2015).

92. Agrawal, K., Sivamani, R. K. & Newman, J. W. Noninvasive profiling of sweat-derived lipid mediators for cutaneous research. *Skin Res. Technol.* **25**, 3–11 (2019).

93. Mastella, G., Cesare, G., Borruso, A., Menin, L. & Zanolla, L. Reliability of sweat-testing by the Macroduct® collection method combined with conductivity analysis in comparison with the classic Gibson and Cooke technique. *Acta Paediatr. Oslo Nor. 1992* **89**, 933–7 (2000).

94. Hammond, K. B., Turcios, N. L. & Gibson, L. E. Clinical evaluation of the macroduct sweat collection system and conductivity analyzer in the diagnosis of cystic fibrosis. *J. Pediatr.* **124**, 255–260 (1994).

95. Chung, M., Fortunato, G. & Radacsi, N. Wearable flexible sweat sensors for healthcare monitoring: a review. *J. R. Soc. Interface* **16**, 20190217 (2019).

96. Gao, W. *et al.* Fully integrated wearable sensor arrays for multiplexed in situ perspiration analysis. *Nature* **529**, 509–514 (2016).

97. Kim, J. *et al.* Noninvasive Alcohol Monitoring Using a Wearable Tattoo-Based Iontophoretic-Biosensing System. *ACS Sens.* **1**, 1011–1019 (2016).

98. Tai, L.-C. *et al.* Methylxanthine Drug Monitoring with Wearable Sweat Sensors. *Adv. Mater.* **30**, 1707442 (2018).

99. Tai, L.-C. *et al.* Wearable Sweat Band for Noninvasive Levodopa Monitoring. *Nano Lett.* **19**, 6346–6351 (2019).

100. Proksch, E. Lowering skin pH: improved barrier function, anti-ageing and beyond. *Br. J. Dermatol.* **179**, 254–255 (2018).

101. Elias, P. M. Stratum corneum acidification: how and why? *Exp. Dermatol.* **24**, 179–180 (2015).

102. Yosipovitch, G. & Papoiu, A. D. P. What causes itch in atopic dermatitis? *Curr. Allergy Asthma Rep.* **8**, 306–311 (2008).

103. Proksch, E. pH in nature, humans and skin. *J. Dermatol.* **45**, 1044–1052 (2018).

104. Koch, A. & Schwab, A. Cutaneous pH landscape as a facilitator of melanoma initiation and progression. *Acta Physiol.* **225**, e13105 (2019).

105. Hachem, J.-P. *et al.* pH directly regulates epidermal permeability barrier homeostasis, and stratum corneum integrity/cohesion. *J. Invest. Dermatol.* **121**, 345–353 (2003).

106. Prakash, C., Bhargava, P., Tiwari, S., Majumdar, B. & Bhargava, R. K. Skin Surface pH in Acne Vulgaris: Insights from an Observational Study and Review of the Literature. *J. Clin. Aesthetic Dermatol.* **10**, 33–39 (2017).

107. Krien, P. M. & Kermici, M. Evidence for the Existence of a Self-Regulated Enzymatic Process Within the Human Stratum Corneum –An Unexpected Role for Urocanic Acid. *J. Invest. Dermatol.* **115**, 414–420 (2000).

108. Kezic, S. *et al.* Levels of filaggrin degradation products are influenced by both filaggrin genotype and atopic dermatitis severity. *Allergy* **66**, 934–940 (2011).

109. Cabanillas, B. & Novak, N. Atopic dermatitis and filaggrin. *Curr. Opin. Immunol.* **42**, 1–8 (2016).

110. Hu, J., Stein, A. & Bühlmann, P. Rational design of all-solid-state ion-selective electrodes and reference electrodes. *TrAC Trends Anal. Chem.* **76**, 102–114 (2016).

111. Allen, J. R. pH Electrodes, Ion-Selective Electrodes, and Oxygen Sensors: Electrochemical Sensors Used in the Medical Field. *Lab. Med.* **34**, 544–547 (2003).

112. Antonov, D., Schliemann, S. & Elsner, P. Methods for the Assessment of Barrier Function. *Skin Barrier Funct.* **49**, 61–70 (2016).

113. du Plessis, J. L., Stefaniak, A. B. & Wilhelm, K.-P. Measurement of Skin Surface pH. *Curr. Probl. Dermatol.* **54**, 19–25 (2018).

114. Lindfors, T., Ervelä, S. & Ivaska, A. Polyaniline as pH-sensitive component in plasticized PVC membranes. *J. Electroanal. Chem.* **560**, 69–78 (2003).

115. Nyein, H. Y. Y. *et al.* A Wearable Electrochemical Platform for Noninvasive Simultaneous Monitoring of Ca(2+) and pH. *ACS Nano* **10**, 7216–7224 (2016).

116. Anastasova, S. *et al.* A wearable multisensing patch for continuous sweat monitoring. *Biosens. Bioelectron.* **93**, 139–145 (2017).

117. Choi, J. *et al.* Soft, Skin-Integrated Multifunctional Microfluidic Systems for Accurate Colorimetric Analysis of Sweat Biomarkers and Temperature. *ACS Sens.* **4**, 379–388 (2019).

118. He, X. *et al.* Flexible and Superwettable Bands as a Platform toward Sweat Sampling and Sensing. *Anal. Chem.* **91**, 4296–4300 (2019).

119. Koh, A. *et al.* A soft, wearable microfluidic device for the capture, storage, and colorimetric sensing of sweat. *Sci. Transl. Med.* **8**, 366ra165 (2016).

120. Bandodkar, A. J. *et al.* Battery-free, skin-interfaced microfluidic/electronic systems for simultaneous electrochemical, colorimetric, and volumetric analysis of sweat. *Sci. Adv.* **5**, eaav3294 (2019).

121. USA, L. L'Oréal Unveils Prototype Of First-Ever Wearable Microfluidic Sensor To Measure Skin pH Levels. https://www.prnewswire.com/news-releases/loreal-unveils-prototype-of-first-ever-wearable-microfluidic-sensor-to-measure-skin-ph-levels-300773342.html.

122. Pojmanová, P., Ladislavová, N., Škeříková, V., Kania, P. & Urban, Š. Human scent samples for chemical analysis. *Chem. Pap.* **74**, 1383–1393 (2020).

123. Jha, S. K. Characterization of human body odor and identification of aldehydes using chemical sensor. *Rev. Anal. Chem.* **36**, (2017).

124. Cuzuel, V. *et al.* Origin, Analytical Characterization, and Use of Human Odor in Forensics. *J. Forensic Sci.* **62**, 330–350 (2017).

125. Parlet, C. P., Brown, M. M. & Horswill, A. R. Commensal Staphylococci Influence Staphylococcus aureus Skin Colonization and Disease. *Trends Microbiol.* **27**, 497–507 (2019).

126. Bacteriology of Humans: An Ecological Perspective | Wiley. *Wiley.com* https://www.wiley.com/en-us/Bacteriology+of+Humans%3A+An+Ecological+Perspective-p-9781405161657.

127. Ellis, S. R. *et al.* The Skin and Gut Microbiome and Its Role in Common Dermatologic Conditions. *Microorganisms* **7**, 550 (2019).

128. Yamazaki, Y., Nakamura, Y. & Núñez, G. Role of the microbiota in skin immunity and atopic dermatitis. *Allergol. Int.* **66**, 539–544 (2017).

129. Timm, C. M., Lloyd, E. P., Egan, A., Mariner, R. & Karig, D. Direct Growth of Bacteria in Headspace Vials Allows for Screening of Volatiles by Gas Chromatography Mass Spectrometry. *Front. Microbiol.* **9**, 491 (2018).

130. Fitzgerald, S., Duffy, E., Holland, L. & Morrin, A. Multi-strain volatile profiling of pathogenic and commensal cutaneous bacteria. *Sci. Rep.* **10**, 17971 (2020).

131. Duffy, E. & Morrin, A. Endogenous and microbial volatile organic compounds in cutaneous health and disease. *Trends Anal. Chem.* **111**, 163–172 (2018).

132. Sethi, S., Nanda, R. & Chakraborty, T. Clinical Application of Volatile Organic Compound Analysis for Detecting Infectious Diseases. *Clin. Microbiol. Rev.* **26**, 462–475 (2013).

133. Duffy, E. & Morrin, A. Endogenous and microbial volatile organic compounds in cutaneous health and disease. *TrAC Trends Anal. Chem.* **111**, 163–172 (2019).

134. Dormont, L., Bessière, J.-M. & Cohuet, A. Human skin volatiles: a review. *J. Chem. Ecol.* **39**, 569–578 (2013).

135. Dormont, L., Bessière, J.-M., McKey, D. & Cohuet, A. New methods for field collection of human skin volatiles and perspectives for their application in the chemical ecology of human–pathogen–vector interactions. *J. Exp. Biol.* **216**, 2783–2788 (2013).

136. Grabowska-Polanowska, B. *et al.* Development of sampling method and chromatographic analysis of volatile organic compounds emitted from human skin. *Bioanalysis* **9**, 1465–1475 (2017).

137. Jiang, R., Cudjoe, E., Bojko, B., Abaffy, T. & Pawliszyn, J. A non-invasive method for in vivo skin volatile compounds sampling. *Anal. Chim. Acta* **804**, 111–119 (2013).

138. Duffy, E., Guzman, K. D., Wallace, R., Murphy, R. & Morrin, A. Non-Invasive Assessment of Skin Barrier Properties: Investigating Emerging Tools for In Vitro and In Vivo Applications. *Cosmetics* **4**, 44 (2017).

139. Duffy, E., Jacobs, M. R., Kirby, B. & Morrin, A. Probing skin physiology through the volatile footprint: Discriminating volatile emissions before and after acute barrier disruption. *Exp. Dermatol.* **26**, 919–925 (2017).

140. Duffy, E., Albero, G. & Morrin, A. Headspace Solid-Phase Microextraction Gas Chromatography-Mass Spectrometry Analysis of Scent Profiles from Human Skin. *Cosmetics* **5**, 62 (2018).

141. Schmidt, K. & Podmore, I. Current Challenges in Volatile Organic Compounds Analysis as Potential Biomarkers of Cancer. *J. Biomark.* **2015**, (2015).

142. Mochalski, P. *et al.* Monitoring of selected skin- and breath-borne volatile organic compounds emitted from the human body using gas chromatography ion mobility spectrometry (GC-IMS). *J. Chromatogr. B* **1076**, 29–34 (2018).

143. Reynolds, J. C. *et al.* Detection of volatile organic compounds in breath using thermal desorption electrospray ionization-ion mobility-mass spectrometry. *Anal. Chem.* **82**, 2139–2144 (2010).

144. Nazemi, H., Joseph, A., Park, J. & Emadi, A. Advanced Micro- and Nano-Gas Sensor Technology: A Review. *Sensors* **19**, (2019).

145. Núñez Carmona, E. *et al.* Detection of food and skin pathogen microbiota by means of an electronic nose based on metal oxide chemiresistors. *Sens. Actuators B Chem.* **238**, 1224–1230 (2017).

146. Güntner, A. T. *et al.* Sniffing Entrapped Humans with Sensor Arrays. *Anal. Chem.* **90**, 4940–4945 (2018).

147. Lawson, B. *et al.* Skin alcohol perspiration measurements using MOX sensors. *Sens. Actuators B Chem.* **280**, 306–312 (2019).

148. Dormont, L., Bessière, J.-M. & Cohuet, A. Human Skin Volatiles: A Review. *J. Chem. Ecol.* **39**, 569–578 (2013).

149. Stevens, D. *et al.* Spatial variations in the microbial community structure and diversity of the human foot is associated with the production of odorous volatiles. *FEMS Microbiol. Ecol.* (2015) doi:10.1093/femsec/fiu018.

150. Verhulst, N. O., Weldegergis, B. T., Menger, D. & Takken, W. Attractiveness of volatiles from different body parts to the malaria mosquito Anopheles coluzzii is affected by deodorant compounds. *Sci. Rep.* **6**, 27141 (2016).

151. Penn, D. J. *et al.* Individual and gender fingerprints in human body odour. *J. R. Soc. Interface* **4**, 331–340 (2007).

152. Elias, P. M. Primary role of barrier dysfunction in the pathogenesis of atopic dermatitis. *Exp. Dermatol.* **27**, 847–851 (2018).

153. Rippke, F., Schreiner, V., Doering, T. & Maibach, H. I. Stratum corneum pH in atopic dermatitis: impact on skin barrier function and colonization with Staphylococcus Aureus. *Am. J. Clin. Dermatol.* **5**, 217–223 (2004).

154. Piérard-Franchimont, C., Quatresooz, P. & Piérard, G. E. Sebum Production. in *Textbook of Aging Skin* (eds. Farage, M. A., Miller, K. W. & Maibach, H. I.) 343–352 (Springer, 2010). doi:10.1007/978-3-540-89656-2_33.

155. Bernier, U. R., Kline, D. L., Barnard, D. R., Schreck, C. E. & Yost, R. A. Analysis of human skin emanations by gas chromatography/mass spectrometry. 2. Identification of volatile compounds that are candidate attractants for the yellow fever mosquito (Aedes aegypti). *Anal. Chem.* **72**, 747–756 (2000).

156. Gallagher, M. *et al.* Analyses of volatile organic compounds from human skin. *Br. J. Dermatol.* **159**, 780–791 (2008).

157. Curran, A. M., Prada, P. A. & Furton, K. G. The differentiation of the volatile organic signatures of individuals through SPME-GC/MS of characteristic human scent compounds. *J. Forensic Sci.* **55**, 50–57 (2010).

158. Prada-Tiedemann, P. & Furton, K. Human Scent Detection: A Review of its Developments and Forensic Applications. *Rev. Cienc. Forenses* **1**, 81–87 (2008).

159. Bommannan, D., Potts, R. O. & Guy, R. H. Examination of the effect of ethanol on human stratum corneum in vivo using infrared spectroscopy. *J. Controlled Release* **16**, 299–304 (1991).

160. Gupta, R., Badhe, Y., Rai, B. & Mitragotri, S. Molecular mechanism of the skin permeation enhancing effect of ethanol: a molecular dynamics study. *RSC Adv.* **10**, 12234–12248 (2020).

161. Horita, D. *et al.* Molecular mechanisms of action of different concentrations of ethanol in water on ordered structures of intercellular lipids and soft keratin in the stratum corneum. *Biochim. Biophys. Acta BBA - Biomembr.* **1848**, 1196–1202 (2015).

162. Cartner, T. *et al.* Effect of different alcohols on stratum corneum kallikrein 5 and phospholipase A2 together with epidermal keratinocytes and skin irritation. *Int. J. Cosmet. Sci.* **39**, 188–196 (2017).

163. Filipiak, W. *et al.* A Compendium of Volatile Organic Compounds (VOCs) Released By Human Cell Lines. *Curr. Med. Chem.* **23**, 2112–2131 (2016).

164. James, A., Casey, J., Hyliands, D. & Mycock, G. Fatty acid metabolism by cutaneous bacteria and its role in axillary malodour. *World J. Microbiol. Biotechnol.* **20**, 787–793 (2004).

165. Kleesz, P., Darlenski, R. & Fluhr, J. W. Full-Body Skin Mapping for Six Biophysical Parameters: Baseline Values at 16 Anatomical Sites in 125 Human Subjects. *Skin Pharmacol. Physiol.* **25**, 25–33 (2012).

166. Farage, M. A., Hood, W., Berardesca, E. & Maibach, H. Intrinsic and Extrinsic Factors Affecting Skin Surface pH. *PH Skin Issues Chall.* **54**, 33–47 (2018).

167. Man, M. Q. *et al.* Variation of Skin Surface pH, Sebum Content and Stratum Corneum Hydration with Age and Gender in a Large Chinese Population. *Skin Pharmacol. Physiol.* **22**, 190–199 (2009).

168. Choi, S.-J. *et al.* Comparison of transepidermal water loss, capacitance and pH values in the skin between intrinsic and extrinsic atopic dermatitis patients. *J. Korean Med. Sci.* **18**, 93–96 (2003).

169. Jacobi, U., Gautier, J., Sterry, W. & Lademann, J. Gender-related differences in the physiology of the stratum corneum. *Dermatol. Basel Switz.* **211**, 312–317 (2005).

170. Lambers, H., Piessens, S., Bloem, A., Pronk, H. & Finkel, P. Natural skin surface pH is on average below 5, which is beneficial for its resident flora. *Int. J. Cosmet. Sci.* **28**, 359–370 (2006).

171. Bicchi, C., Cordero, C., Liberto, E., Sgorbini, B. & Rubiolo, P. Reliability of fibres in solid-phase microextraction for routine analysis of the headspace of aromatic and medicinal plants. *J. Chromatogr. A* **1152**, 138–149 (2007).

172. Spietelun, A., Pilarczyk, M., Kloskowski, A. & Namieśnik, J. Current trends in solid-phase microextraction (SPME) fibre coatings. *Chem. Soc. Rev.* **39**, 4524–4537 (2010).

173. Jiang, J. *et al.* Volatile fatty acids production from food waste: effects of pH, temperature, and organic loading rate. *Bioresour. Technol.* **143**, 525–530 (2013).

174. Lukitawesa, null, Patinvoh, R. J., Millati, R., Sárvári-Horváth, I. & Taherzadeh, M. J. Factors influencing volatile fatty acids production from food wastes via anaerobic digestion. *Bioengineered* **11**, 39–52 (2020).

175. Münch, E. v. & Greenfield, P. F. Estimating VFA concentrations in prefermenters by measuring pH. *Water Res.* **32**, 2431–2441 (1998).

176. Tang, Z., Yang, J., Yu, J. & Cui, B. A colorimetric sensor for qualitative discrimination and quantitative detection of volatile amines. *Sensors* **10**, 6463–6476 (2010).

177. Mazumder, S., Ahamed, R. A., McGahee, E., Wang, L. & Seyler, T. H. A New Automated Method for the Analysis of Aromatic Amines in Human Urine by GC–MS/MS. *J. Anal. Toxicol.* **43**, 25–35 (2019).

178. Ng, T. W., Chan, P. Y., Chan, T. T., Wu, H. & Lai, K. M. Skin squames contribute to ammonia and volatile fatty acid production from bacteria colonizing in air-cooling units with odor complaints. *Indoor Air* **28**, 258–265 (2018).

179. Visciano, P., Schirone, M. & Paparella, A. An Overview of Histamine and Other Biogenic Amines in Fish and Fish Products. *Foods Basel Switz.* **9**, (2020).

180. Doeun, D., Davaatseren, M. & Chung, M.-S. Biogenic amines in foods. *Food Sci. Biotechnol.* **26**, 1463–1474 (2017).

181. Lucaire, V., Schwartz, J.-J., Delhomme, O., Ocampo-Torres, R. & Millet, M. A sensitive method using SPME pre-concentration for the quantification of aromatic amines in indoor air. *Anal. Bioanal. Chem.* **410**, 1955–1963 (2018).

182. Sandlers, Y. Amino Acids Profiling for the Diagnosis of Metabolic Disorders. *Biochem. Test. - Clin. Correl. Diagn.* (2019) doi:10.5772/intechopen.84672.

183. Claes, L., Janssen, M. & De Vos, D. E. Organocatalytic Decarboxylation of Amino Acids as a Route to Bio-based Amines and Amides. *ChemCatChem* **11**, 4297–4306 (2019).

184. Thorn, R. M. S. & Greenman, J. Microbial volatile compounds in health and disease conditions. *J. Breath Res.* **6**, (2012).

185. Mohiuddin, S. S. & Khattar, D. Biochemistry, Ammonia. in *StatPearls* (StatPearls Publishing, 2021).

186. Li, M. *et al.* Human Ammonia Emission Rates under Various Indoor Environmental Conditions. *Environ. Sci. Technol.* **54**, 5419–5428 (2020).

187. Smallegange, R. C., Verhulst, N. O. & Takken, W. Sweaty skin: an invitation to bite? *Trends Parasitol.* **27**, 143–148 (2011).

188. Keller, R. W., Bailey, J. L., Wang, Y., Klein, J. D. & Sands, J. M. Urea transporters and sweat response to uremia. *Physiol. Rep.* **4**, (2016).

189. Nose, K. *et al.* Identification of Ammonia in Gas Emanated from Human Skin and Its Correlation with That in Blood. *Anal. Sci. Int. J. Jpn. Soc. Anal. Chem.* **21**, 1471–4 (2006).

190. Ferrer, F. M., Hobart, K. & Bailey, J. V. Detection of urease and carbonic anhydrase activity using a rapid and economical field test to assess microbially-induced carbonate precipitation. *bioRxiv* 2020.01.10.902379 (2020) doi:10.1101/2020.01.10.902379.

191. Neofotistos, A.-D. G., Tsagkaris, A. S. & Proestos, G. P. D. and C. Emerging Trends in Biogenic Amines Analysis. *Biog. Amines* (2019) doi:10.5772/intechopen.81274.

192. Jamalabadi, H., Mani-Varnosfaderani, A. & Alizadeh, N. PPy-Metal Oxide Hybrid Nanocomposite Sensor Array for Simultaneous Determination of Volatile Organic Amines in High Humid Atmosphere. *IEEE Sens. J.* **17**, 8282–8289 (2017).

193. Xiao-wei, H., Xiao-bo, Z., Ji-yong, S., Zhi-hua, L. & Jie-wen, Z. Colorimetric sensor arrays based on chemo-responsive dyes for food odor visualization. *Trends Food Sci. Technol.* **81**, 90–107 (2018).

194. Rakow, N. A., Sen, A., Janzen, M. C., Ponder, J. B. & Suslick, K. S. Molecular Recognition and Discrimination of Amines with a Colorimetric Array. *Angew. Chem. Int. Ed.* **44**, 4528–4532 (2005).

195. Oh, H. J. *et al.* Washable Colorimetric Nanofiber Nonwoven for Ammonia Gas Detection. *Polymers* **12**, 1585 (2020).

196. Helmy, S. *et al.* Photoswitching Using Visible Light: A New Class of Organic Photochromic Molecules. *J. Am. Chem. Soc.* **136**, 8169–8172 (2014).

197. Helmy, S., Oh, S., Leibfarth, F. A., Hawker, C. J. & Read de Alaniz, J. Design and Synthesis of Donor–Acceptor Stenhouse Adducts: A Visible Light Photoswitch Derived from Furfural. *J. Org. Chem.* **79**, 11316–11329 (2014).

198. Diaz, Y. J. *et al.* A Versatile and Highly Selective Colorimetric Sensor for the Detection of Amines. *Chem. – Eur. J.* **23**, 3562–3566 (2017).

199. Schmidt, F. M. *et al.* Ammonia in breath and emitted from skin. *J. Breath Res.* **7**, 017109 (2013).

200. Martínez-Lozano, P. Mass spectrometric study of cutaneous volatiles by secondary electrospray ionization. *Int. J. Mass Spectrom.* **282**, 128–132 (2009).

201. Furukawa, S. *et al.* Simultaneous and multi-point measurement of ammonia emanating from human skin surface for the estimation of whole body dermal emission rate. *J. Chromatogr. B Analyt. Technol. Biomed. Life. Sci.* **1053**, 60–64 (2017).

202. Bigi, F. *et al.* Clean synthesis in water. Part 2: Uncatalysed condensation reaction of Meldrum's acid and aldehydes. *Tetrahedron Lett.* **42**, 5203–5205 (2001).

203. Palmer, L. I. & Alaniz, J. R. de. Lewis Acid Catalyzed Rearrangement of Furylcarbinols: The Aza- and Oxa-Piancatelli Cascade Reaction. *Synlett* **25**, 08–11 (2014).

204. Piutti, C. & Quartieri, F. The Piancatelli Rearrangement: New Applications for an Intriguing Reaction. *Molecules* **18**, 12290–12312 (2013).

205. Šafář, P. *et al.* Dichotomy in the Ring Opening Reaction of 5-[(2-Furyl)methylidene]-2,2-dimethyl-1,3-dioxane-4,6-dione with Cyclic Secondary Amines. *Collect. Czechoslov. Chem. Commun.* **65**, 1911–1938 (2000).

206. Sidman, J. W. Electronic Transitions Due To Nonbonding Electrons Carbonyl, Aza-Aromatic, And Other Compounds. https://pubs.acs.org/doi/pdf/10.1021/cr50022a004 (2002) doi:10.1021/cr50022a004.

207. Bailey, D. C. Not Normal: the uncertainties of scientific measurements. *R. Soc. Open Sci.* **4**, (2017).

208. Sahu, P. K. & Lee, S.-L. Hydrogen-bond interaction in 1:1 complexes of tetrahydrofuran with water, hydrogen fluoride, and ammonia: A theoretical study. *J. Chem. Phys.* **123**, 044308 (2005).

209. Lam, T. H. *et al.* Understanding the microbial basis of body odor in pre-pubescent children and teenagers. *Microbiome* **6**, (2018).

210. Dekaboruah, E., Suryavanshi, M. V., Chettri, D. & Verma, A. K. Human microbiome: an academic update on human body site specific surveillance and its possible role. *Arch. Microbiol.* **202**, 2147–2167 (2020).

211. Luqman, A. *et al.* Trace amines produced by skin bacteria accelerate wound healing in mice. *Commun. Biol.* **3**, 1–10 (2020).

212. Luqman, A., Nega, M., Nguyen, M.-T., Ebner, P. & Götz, F. SadA-Expressing Staphylococci in the Human Gut Show Increased Cell Adherence and Internalization. *Cell Rep.* **22**, 535–545 (2018).

213. Shetewi, T. *et al.* Investigation of the relationship between skin-emitted volatile fatty acids and skin surface acidity in healthy participants - a pilot study. *J. Breath Res.* (2021) doi:10.1088/1752-7163/abf20a.

214. Lang, W., Blöck, T. M. & Zander, R. Solubility of NH3 and apparent pK of NH4+ in human plasma, isotonic salt solutions and water at 37 degrees C. *Clin. Chim. Acta Int. J. Clin. Chem.* **273**, 43–58 (1998).

# Chapter 3

# Wearable colorimetric sensor development for the detection of volatile amines in skin

### 3.1 Introduction

In the human body, volatile amines including ammonia are produced by growing cells, decomposition of proteins and through microbial activity.[176–178] Their existence and concentrations are good indicators of food spoilage, indoor air pollution and biomarkers in metabolic diseases.[179–182] In metabolism, one route to forming amines is via the decarboxylation of neutral amino acids. Amination of carbonyl compounds is another route for forming amines like ethylamine, diethylamine and trimethylamine.[183] Trimethylamine is also produced by many species of bacteria from the breakdown of choline or trimethylamine oxide sourced from fish, eggs and cruciferous vegetables.[184] Another interesting nitrogen-containing compound produced by bacterial breakdown of proteins in the gut is the ammonium ion that can be converted to ammonia. Ammonia is also produced via the enzymatic break down of urea by urease (eq.1). Ammonia produced is transported to the liver where it get converted to urea and excreted in urine.[185] Ammonia in the blood can diffuse via the skin or from breath.[186] The skin ammonia emission originates from (i) sweat secreted by glands particularly eccrine sweat that contains ammonia, and (ii) microbial activity that involves release of ammonia via microbial metabolic activity or microbial activity on urea secreted on the skin by eccrine glands.[187,188] Correlation has been demonstrated between skin and blood ammonia levels.[189] Along with ammonia, urease enzyme also produces carbon dioxide (eq.1) which coupled with ammonia hydrolysis and carbon dioxide hydration catalysed via carbonic anhydrase (eq. 2), produces basic compounds like hydroxide, bicarbonate and ammonium (eq. 3).[190]

$$(NH_2)_2CO_{(aq)} + H_2O_{(l)} \rightarrow CO_{2(g)} + 2NH_{3(g)} \quad (1)$$

$$CO_{2(g)} + H_2O_{(l)} \rightleftharpoons HCO_3^-{}_{(aq)} + H^+{}_{(aq)} \quad (2)$$

$$(NH_2)_2CO_{(aq)} + 3H_2O_{(l)} \rightarrow HCO_3^-{}_{(aq)} + 2NH_4^+{}_{(aq)} + OH^-{}_{(aq)} \quad (3)$$

Ammonium production is balanced by acid production but in the absence of fermentable products for acid production, the produced ammonium ion gets converted to ammonia which causes an increase in skin surface pH.[184] Carbonic anhydrase found in many microbial species like *E.coli* is associated with skin disorders such as eczema, known to be linked to an increase in skin surface pH.[184] Thus, ammonia is an important species to consider for skin health because it can influence skin surface pH and thus skin barrier function.

The detection and quantification of amines in solution and gas phase has been performed using a variety of methods including gas chromatography (GC), liquid chromatography (LC) and mass spectrometry (MS) techniques.[191] While very sophisticated and have high sensitivities, these methods employ bulky and expensive instrumentation, are time consuming and require trained personnel to operate them. For volatile amine (and other volatile compound classes) sensing these traditional methods are being replaced by gas sensors that are smaller in size and easier to use. These sensors can comprise a range of dye arrays that can react with different analytes. This creates unique patterns that can be interpreted by pattern recognition programs to differentiate between different related analytes or even different concentrations of the same analyte.[192] Among the different gas sensors, metal oxide materials have been used extensively for amine detection.[192] Although they are advantageous over instrumentation-based methods, the high operating temperature, poor selectivity and low sensitivity associated with metal oxide sensors are some of the challenges of deploying these for particular sensing application e.g. wearable sensors.[192] Another useful and simple method for gas sensing is through colorimetric sensors that contain dyes or materials that change in colour in response to exposures to specific analyte. The chemo-responsive dye contains a centre that can interact strongly with the analyte. The dye-analyte interaction at the active centre can occur through strong chemical interactions (forming/breaking of chemical bonds) or via simple physical adsorption, both of which can result in a colorimetric change.[176,193] For example, in the case of strong chemical interaction, when a dye reacts with a gas molecule, their vacant frontier orbitals can react with each other which leading to a shift in transition energy resulting in a new product with a different colour.[176] The product of this chemical reaction can have different electronic and chemical properties as well as molecular structure and stereo shapes. For chemo-responsive dyes, this change in colour carries the information regarding the molecular properties of the gaseous analyte.

Using common basic imagining equipment such as a camera, the response of the chemo-sensor dye to analyte can be quantified by monitoring the colour change (before and after exposure). In colour imaging, there are three signal channels (red, green and blue) for each pixel imaged that can be used to quantify this colour change.[176] Tracking the change in these signal channels before and after exposure to the gaseous analyte offers a means for developing a powerful transduction methodology. Although not as sophisticated as instrumental methods mentioned previously, colorimetric sensors using dyes are of great interest for their simplicity, low-cost, visual response and ease of fabrication and interpretation without need for a power source. Rakow *et al*. for example have reported the development of a colorimetric sensor array capable of discriminating between a variety of amines including cyclic and branched amines.[194] The

sensor showed limits of detection well below 1 part per million (ppm) for volatile amines that were generated by flowing nitrogen through the neat liquid analyte in a thermostated, glass-fritted bubbler. Recently, Ju Oh *et al*. described the development of a fabric-based washable colorimetric sensor (a vest) for detection and monitoring of ammonia in industrial sites.[195] The sensor was fabricated using electrospinning and contained meta-aramid/dye 3 nanofibers for ammonia gas sensing. When exposed to ammonia, the dye is deprotonated and a bathochromic shift occurs in the absorption band accompanied by a change in dye colour from orange to brown (**figure 3.1**). While the ammonia concentration limit set by the health and safety administration is 25 ppm this sensor had an LOD of 50 ppb and was capable of quatifying ammonia concentration between 1-10 ppm within 10 s of exposure at room temperature and showed sensing properties and reversibility following washing with detergent.

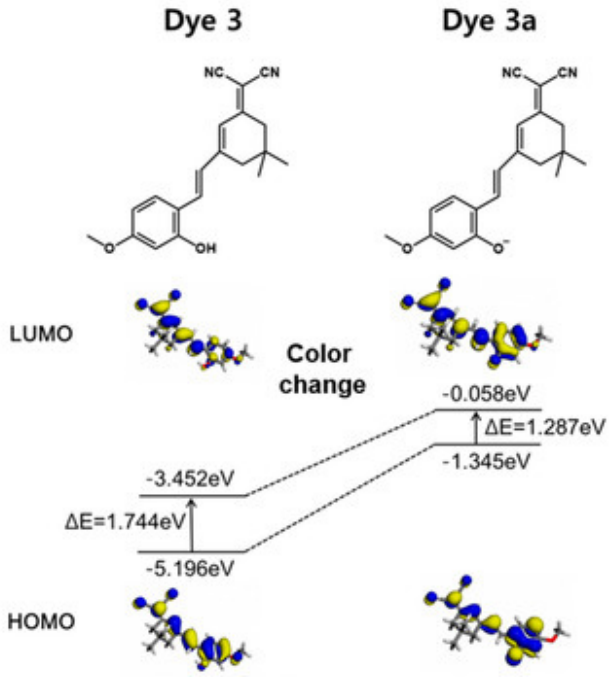


**Figure 3.1** Electron distribution in HOMO and LUMO energy levels in dye 3 and dye 3a following exposure to ammonia that results in a colour change.[195]

Helmy *et al*. exploited amine-selective ring opening of photochromes, known as donor-acceptor Stenhouse adducts (**Figure 3.2 (A)** ).[196,197] One interesting compound belonging to this class of photochromes is Meldrum's activated furan (MAF). The bi-carbonyl moiety of this MAF dye, helps to create a push-pull electron system which activates the dye towards attack via nitrogen lone pair of amines. This leads to the ring opening of MAF dye (**Figure 3.2**

**(A)**).[197] The group demonstrated the successful application of this dye as a sensor to detect fish spoilage.[198]

Research on the sensing approaches for detection of skin-emitted amines are quite limited due to the low concentration rates at which amines are emitted from the skin.[199] However, there are several research papers that have looked at ammonia emissions from skin. For example, Martinez-lorenzo *et al*. used on-line electron spray ionisation-MS set in the positive ionisation mode to study cutaneous volatiles in the headspace above the hand. This approach allowed for the focused detection of amines from the skin including trimethylamine, piperideine and heptylamine.[200] Schmidt *et al* reported the use of a commercial cavity ring-down spectrometer to measure ammonia emissions in skin and in breath. They reported a median concentration of ammonia emitted from the forearm of healthy subjects to be 0.3 ng cm $^{-2}$, approx. less than 10 ppb.[199] Furukawa *et al*. used a passive flux sampler to collect skin volatiles and ion-exchange chromatography for volatile analysis to determine the levels of ammonia emitted from different parts of the body. The results showed ammonia emission from the feet was the highest relative to all other sites possibly due to the high densities of eccrine glands found here.[201]

This chapter describes the synthesis of a colorimetric dye and its fabrication into a wearable sensors that can be used for the colorimetric detection of volatile amines released from skin. This type of sensor can be useful for healthcare monitoring of various skin conditions. Inspired by the work of Helmy et al. (**Figure 3.2 (A)**), a colorimetric dye approach was used where the synthesis of a Meldrum's activated pyrrole (MAP) was achieved (**Figure 3.2 (B)**).[197]

(A) Read de Alaniz's work

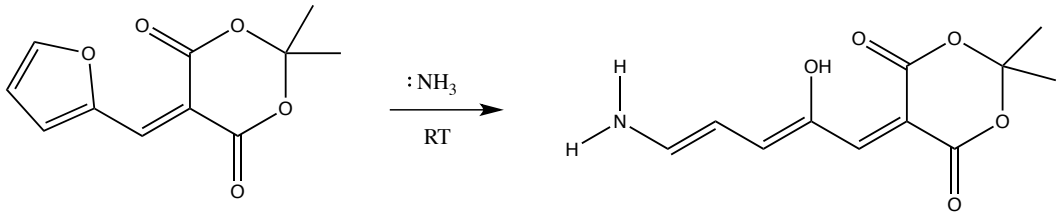


MAF

(B) This work

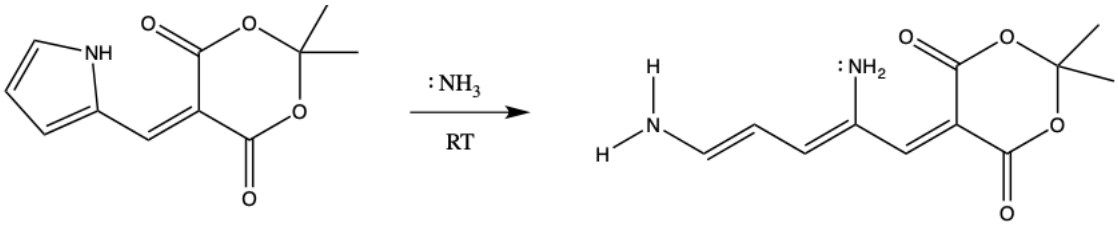


MAP

**Figure 3.2** Reaction scheme showing the structure of the (A) MAF dye synthesised by Helmy *et al*. and (B) MAP dye synthesised in the current work and the proposed products upon their reaction with ammonia at room temperature (RT).

A mechanism for the synthesis of the MAP dye as well as evidence for its reaction with ammonia are proposed in this work. Physical and chemical properties of the dye were assessed in solution and in solid state. The dye was drop-cast to flexible silica substrates as sensor spots and its response to ammonia characterised. This platform was then developed into a wearable sensor for the detection of volatile skin amines in the headspace above the skin. The response of the new sensor to the skin emissions at different body sites (forearm, forehead, abdomen, and foot) was measured and emission rates of ammonia at each site were estimated based on the data. The sensors showed promising discriminatory results where different colorimetric responses (colour intensities (CIs)) were produced for different body parts which were linked to gland distribution and microbial flora densities. Skin surface pH values were also recorded along with sensor response to investigate possible correlation between skin pH and amine-based emission from skin. Our initial results show that the sensor response to the amine emission does not correlate closely to skin surface pH as was observed for the VFA emission in the previous chapter. Nevertheless, this sensor demonstrates potential for use in amine monitoring from skin and with further development and refinement, could be ultimately used

to monitor changes in amine emissions in skin which may have an impact for skin barrier health. As well as that quantifying amines from the skin emission, these sensors can also be useful for other types of wearable applications whereby personalised exposures to amines in different environments could be tracked.

## 3.2 Materials & Methods

### *3.2.1 Materials*

All chemical reagents were purchased from Sigma, Ireland and used without further purification. Solvents used were bench-grade except for the HPLC grade tetrahydrofuran (THF) which was used for ultraviolet-visible spectroscopy (UV-Vis) experiments. UV-Vis absorption spectroscopy studies were carried out on a Shimadzu UV-2600 spectrophotometer. 1H, NMR spectra were obtained on a Bruker AC 600 MHz NMR spectrometer. Imaging of MAP sensors was carried out using a flatbed scanner (Epson XP-322) and image processing was done using ImageJ software.

### *3.2.2 Synthesis of Meldrum-activated pyrrole (MAP) dye*

MAP dye was synthesised according to a procedure previously reported by de Alaniz *et al*. To produce MAF, 2-dimethyl-1,3-dioxane-4,6-dione (1 mmol, 144.36 mg, 1.0 equiv.) was dissolved in DI water (20 mL). To this, pyrrole-2-carboxaldehyde (1 mmol, 95.1 mg, 1.0 equiv.) was added, and the solution turned yellow. The solution was heated to 75 ℃ and left to stir for 2 h (**Figure 3.3**). The resulting mixture was filtered under vacuum to yield a yellow solid (0.12365 g, 56.2%).

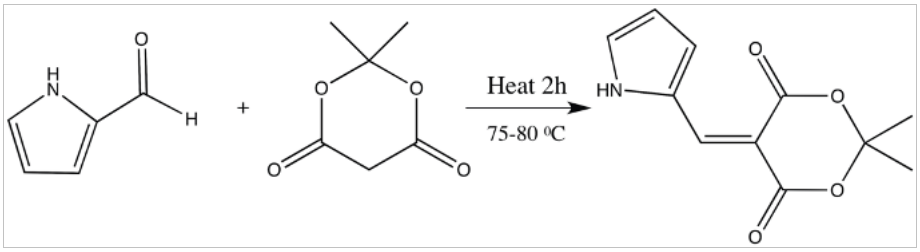


**Figure 3.3** Reaction scheme for the synthesis of the MAP dye.

*3.2.3 Chemical analysis*

Proton Nuclear Magnetic Resonance ($^1$HNMR) characterisation was carried out to confirm the structure of the dye. The synthesised compound (20 mg) was dissolved in deuterated dimethyl sulfoxide (DMSO-$d_6$) for HNMR analysis.

$^1$H NMR (600 MHz, DMSO-$d_6$) $\delta$ 8.30 (s, 1H), 7.45 (s, 1H), 7.3, (s, 1H), 7.15 (d, 1H), 6.51-6.55 (M, 1H), 1.7 (s, 6H). **Figure 3.9** shows the HNMR spectrum of the dye.

UV-Vis analysis was performed on dilutions of the MAP dye in THF (20 mM) in the absence and presence of ammonia. Aliquots of the stock solution (2 mL) whereas transferred to volumetric flasks (10 ml) and exposed to different volumes of neat ammonia (2, 4, 6, 8, 10, 20, 40, 60, 80 and 100 ppm). The absorbance of the resulting solution was recorded over the wavelength range of 190-500 nm.

*3.2.4 MAP selectivity study*

A stock solution of the dye (20 mM) was prepared by dissolving the MAP (110 mg) in THF (25 mL). Aliquots (2 mL) of this stock solution were transferred to glass vials. To each respective vial, the following solvents: acetone, methanol, acetic acid, hexane and ammonia were added and the vials capped. Vials were allowed to sit at room temperature for 1 h after which the colour of the solution in the vials was reassessed.

*3.2.5 MAP dye colorimetric response to ammonia in solution phase*

Using the stock solution prepared in Section *3.2.4*, aliquots (2 mL) were transferred to vials (7 mL) and an image of the vials was taken using the camera on a Huawei P20 phone. Each respective vial was exposed to a specific volumes (2, 4, 6, 8, 10, 20, 40, 60, 80 and 100 $\mu$L) of neat ammonia. The vials were left at room temperature for 1 h to equilibrate and after which another image of the vials was taken and processed as described in Section *3.2.10*.

*3.2.6 MAP deposition on solid supports*

To identify the most suitable solid support for sensor fabrication, MAP in THF stock solution (110 mg /25 ml) as prepared in Section *3.2.4*, and drop-cast (1 $\mu$L) on three different solid substrates - silica TLC plates, acylated TLC plates and cellulose filter paper. The substrates were then allowed to dry in a vacuum desiccator (SP Bel-Art, USA) for at least 1 h, after which the shape and uniformity of the spots were assessed. To assess the impact of dye encapsulation, sol-gel films comprising dye were prepared to encapsulate the dye before drop-casting it on solid supports. MAP dye (22 mg) was placed in a glass vials containing methyltriethoxysilane (0.199 mL) triethoxy(octyl)silane (0.314 mL) 2-methoxymethanol (1.971 mL) propylene glycol monomethyl ether acetate (1.362 mL), THF (1.265 mL) and hydrochloric acid (0.1 M, 0.00152 mL). The vial was then mixed at room temperature until the dye was fully dissolved. 1 $\mu$L of this solution was deposited on a silica TLC plate and allowed to dry in a vacuum desiccator, after which the shape and uniformity of the spot were assessed. These encapsulated dye spots were tested for ammonia response.

To prepare the sensor spots for skin volatile testing, MAP dye (100 mg) was dissolved in THF (0.5 mL) and vortexed until fully dissolved. The dye solution (1 µL) was drop-cast onto a silica TLC plate and allowed to dry in the vacuum desiccator for 1 h before use. Up to six spots (diameter: 2.4 ± 0.3 cm) were drop-cast on a piece of silica.

*3.2.7 Kinetic study of MAP dye sensor reaction with ammonia*

MAP sensors (comprising 6 spots drop-cast on silica) were prepared, scanned and the colour intensity (CI) of the individual spots quantified before exposing them to ammonia and the image processed using ImageJ. In order to monitor the kinetic reaction of the MAP dye with ammonia, the sensor was adhered to the inner lid surface of a glass container (1.8 L) using Blu-Tac. A piece of Whatman filter paper (diameter: 4.7 cm) was placed inside the vial and 2$\mu L$ of neat ammonia was dropped directly onto the filter paper. The vials were closed using the lid and sealed around the edges with parafilm. 5 vials containing MAP sensors were prepared in total. Each vial was sealed for a specified period (e,g vial containing sensor 1 exposed for 1 h, vial containing sensor 2 exposed for 2 h, etc) after which the sensor was removed from the vial and scanned again. Processing of the sensor images before and after exposure to ammonia was carried out using ImageJ and is described in Section *3.2.10*

*3.2.8 Quantitative study of MAP dye sensor spot to ammonia*

MAP sensors (comprising 6 spots drop-cast on silica) were prepared, scanned and the CI of the individual spots quantified using ImageJ. In order to measure the response of the sensor to ammonia, the sensor was adhered to the inner lid surface of a glass container (1.8 L) using Blu-Tack. A piece of filter paper (Whatman, diameter: 4.70 cm) was placed inside the container and a precise volume of neat ammonia solution (1-10 $\mu L$) was dropped directly onto the filter paper. The containers were closed using the lid and sealed around the edges with parafilm. The containers with the MAP sensors were exposed to ammonia (for 5 h, after which the sensor was removed from the container and scanned. Processing of the sensor image before and after exposure to ammonia was carried out using ImageJ and is described in Section *3.2.10*

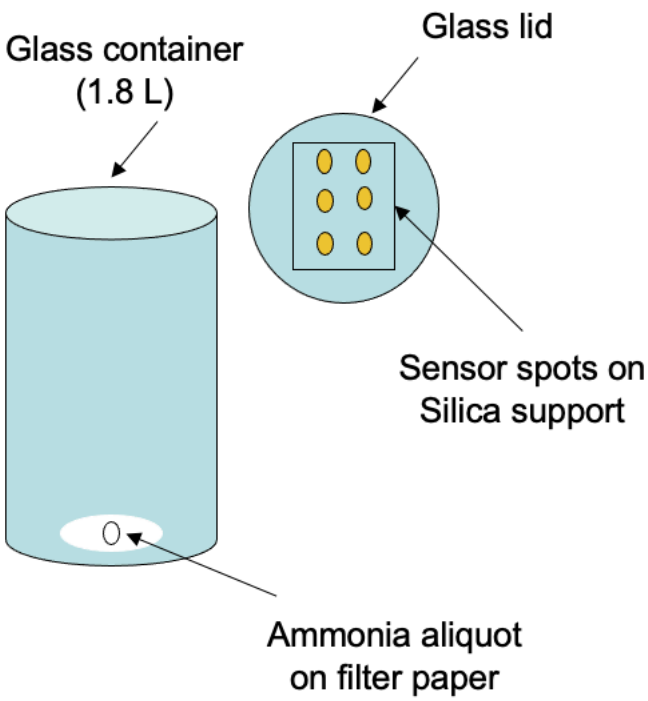


**Figure 3.4** Experimental set up for testing the MAP dye sensor spots response to ammonia.

*3.2.9 Application of MAP sensor for skin volatile emission in a participant study*

Two healthy female volunteers (F1 and F2) aged 20-25 were recruited for colorimetric MAP dye sensor testing on skin. Participants were informed of the aim and purpose of the study and asked to provide written informed consent. The participants were instructed not to apply perfumes or cosmetics on the days of sample collection.

The wearable format of the MAP sensor is shown in **Figure 3.5**. The sensor substrate (2.5 x 2.5 cm) comprised of 6 MAP dye spots and was applied to the skin surface using a stainless woven wire mesh (Inoxia Ltd, UK) as a spacer, to define the headspace and prevent direct contact with skin. The sensor was covered with a polyethylene terephthalate (PET) film and the complete platform was enclosed (**Figure 3.6**) and secured to the skin with surgical tape (BSN medical Leukosilk, Germany).

The MAP sensor was worn by participants for 5 h at a time as they went about normal everyday activities (working, walking etc). The MAP sensor was applied to different body sites as specified (volar forearm, forehead, abdomen and foot). The sensors were imaged before and after wearing on the skin as described. Sensors were imaged using an Epson XP-322 flatbed scanner. Images were processed using ImageJ to measure intensity of MAP dye colour before and after exposure to the skin and is described in Section *3.2.10*

Skin surface pH (Meter 2210, Probe HI1413; Hanna instruments Inc.) was also collected where specified, before application of sensor.

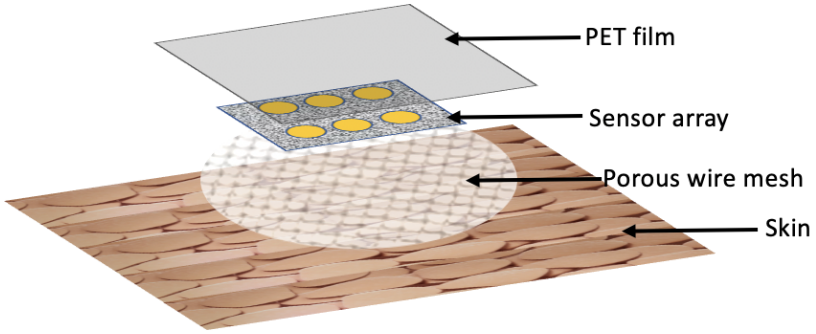


**Figure 3.5** Schematic of the different layers comprising the MAP dye sensor spots applied to the skin surface.

**Figure 3.6** Image showing the MAP sensor as worn on the skin in the participant study.

*3.2.10 Image analysis of MAP sensors*

All scanned sensor images were processed using ImageJ to quantify a CI for each individual dye spot on the MAP sensor. To do this, a region in the centre of the dye spot was highlighted and using the CI function, an intensity value was obtained. This process was carried out for each dye spot on the MAP sensor (up to 6) and an average CI (also standard deviation) value calculated. The average CI of the dye spots before ammonia exposure was subtracted from the average CI of dye spots after exposure. The difference between these values (ΔCI) represents the response of the MAP sensor to volatile amines.

The Red Green Blue (RGB) values were also obtained using ImageJ where specified. Again, a region in centre of a single spot was highlighted and using the RGB function, the RGB values were obtained. This process was carried out for each dye spot on the MAP sensor (up to 6) and an average and standard deviation value calculated for a sensor. These RGB values for the sensors before and after exposure to the skin were used to replicate the dye colour for analysis tables below.

### 3.3 Results and discussion

*3.3.1 MAP synthesis*

Previous literature describes the synthesis of a new class of photochromes by reacting Meldrum's acid and furfural to form a colorimetric dye known as Meldrum's activated furan (MAF). The general reaction involves the condensation of furfural with 1,3-dicarbonyl compounds to provide the dye compound that can undergo ring opening at room temperature RT with a variety of amines (cyclic, branched and aliphatic).[197] It was decided to employ this synthetic route to generate ammonia-responsive dyes for our work. However, although furfural (**Figure 3.7 (A)**) is a readily available chemical, due to the toxicity associated with this compound, It was decided to use an analog for our work. Pyrrole-2-carboxaldehyde (**Figure 3.7 (B)**) was selected as the analog in our case and substituted for furfural.

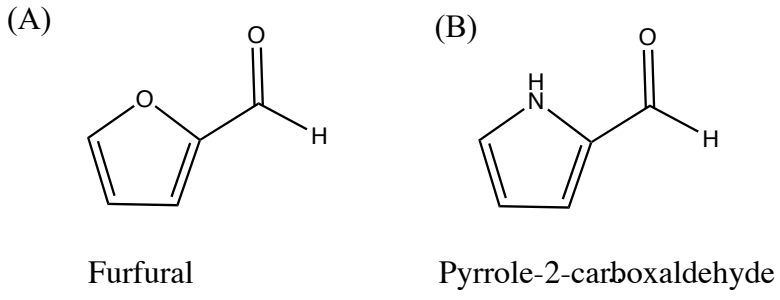


**Figure 3.7** Structure of (A) furfural and (B) pyrrole-2-carboxaldehyde.

The MAP dye was synthesised via a Knoevenagel condensation reaction between two carbonyl-containing compounds (Meldrum's acid and pyrrole-2-carboxaldehyde), in the presence of heat.[202] The first step (1) of the synthesis involved the protonation of the aldehyde carbonyl to form the highly electrophilic intermediate 1 as seen in **Figure 3.8**. This reaction is catalysed by the acidic protons on the di-carbonyl Meldrum's acid compound. An enol is formed that is nucleophilic at the α-carbon. This enol then reacts with intermediate 1 to form the aldol produced which undergoes spontaneous dehydration to form the MAP dye as the final product.

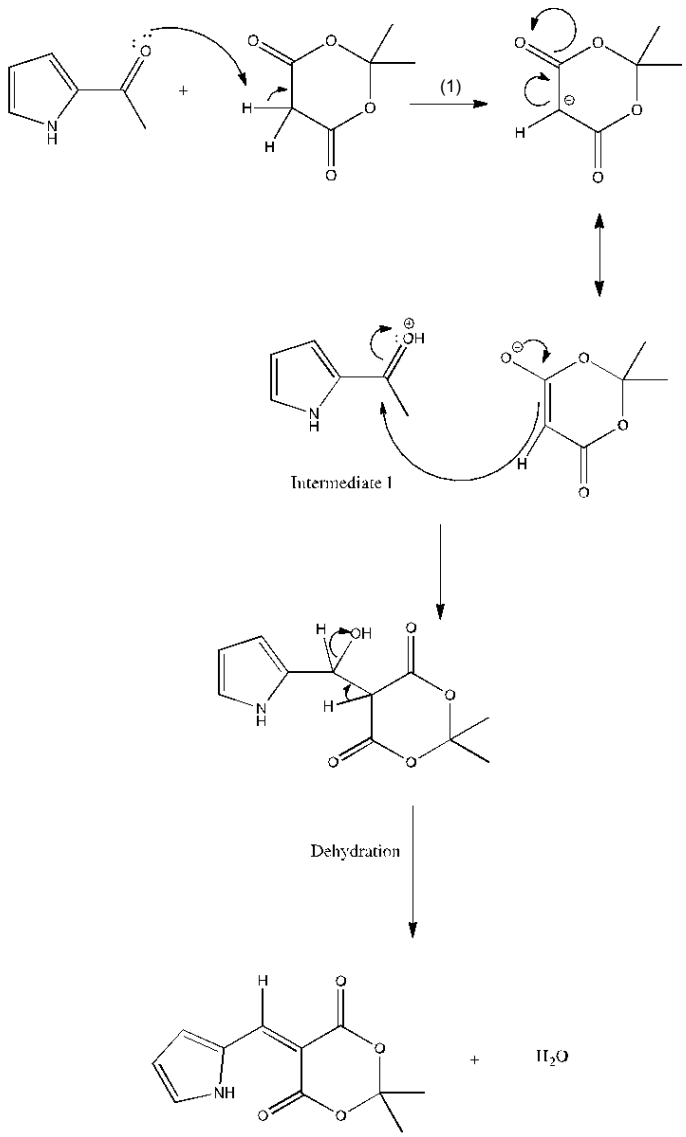


**Figure 3.8** Mechanism for the synthesis of the MAP dye via Knoevenagel condensation reaction between pyrrole-2-carboxaldehyde and Meldrum's acid.

*3.3.2 MAP physical and chemical characterisation*

Firstly, the physical properties of the dye were assessed (**Table 3.1**). The isolated powder was yellow in colour. Based on the fact the dye product precipitates out of water after synthesis highlights the insolubility of the MAP dye in water. Furthermore, solubility tests were carried out to confirm that the dye was insoluble in water, which is attributed to the fact that the aromatic characteristic of the dye is stronger than its polar properties. The dye was also observed to be insoluble in non-polar solvents like diethyl ether, hexane and toluene but soluble

in polar aprotic solvents like dichloromethane (DCM) and THF. Based on this, it was proposed that the MAP dye behaves as a proton donor as it dissolved in polar aprotic compounds.[196]

**Table 3.1** Physical properties of the MAP dye.

| Physical parameter | |
|---|---|
| Colour | Light yellow |
| State | Powdered solid |
| Solubility | Soluble in polar aprotic solvents, insoluble in $H_2O$ and non-polar solvents |

To confirm the structure of the dye NMR studies were carried out. **Figure 3.9** shows the HNMR spectrum of the dye dissolved in deuterated dimethyl sulfoxide (DMSO-$d_6$). The peak at 2.2 ppm was that of the solvent. The remaining peaks highlight the presence of a compound that contains 6 protons that are in a chemically different environment. A singlet at 7.3 ppm confirms the formation of the dye as it represents the shift associated with the proton attached to the newly formed C=C unit. Moreover, the obtained spectrum of this MAP dye is similar to the spectrum obtained by Diaz *et al*. who synthesised the related MAF dye- 5-[(2-furyl)methylidene]-2,2-dimethyl-1,3-dioxane-4,6-dione- derived from furfural.[198] (**Figure 3.6 (a)**)

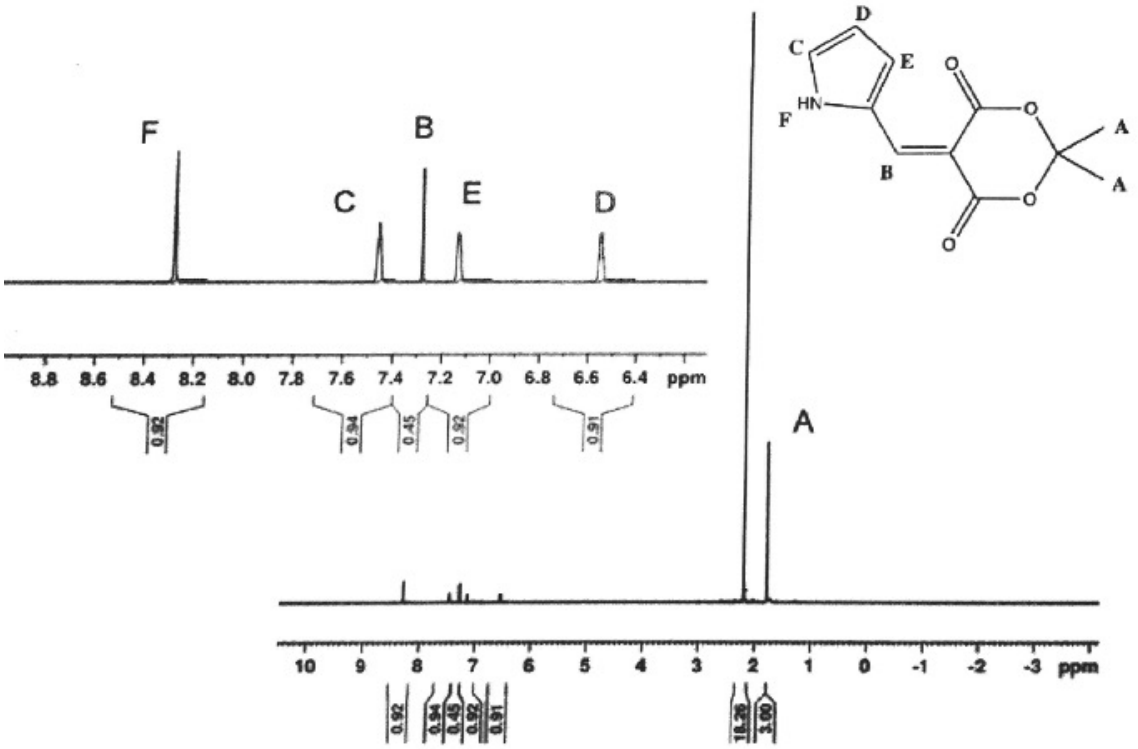


**Figure 3.9** HNMR spectrum of MAP dye in DMSO-$d_6$.

$^1$H NMR (600 MHz, DMSO-$d_6$) $\delta$ 8.30 (s, 1H), 7.45 (s, 1H), 7.3, (s, 1H), 7.15 (d, 1H), 6.51-6.55 (M, 1H), 1.7 (s, 6H)

UV-vis analysis of MAP dye in THF (2 mM) was also performed (**Figure 3.10**). The spectrum showed an absorbance band at 385 nm. The cyclic aromaticity of the pyrrole ring on the dye molecule is responsible for the absorbance band at this wavelength. The effect of ammonia on this absorbance band is discussed later.

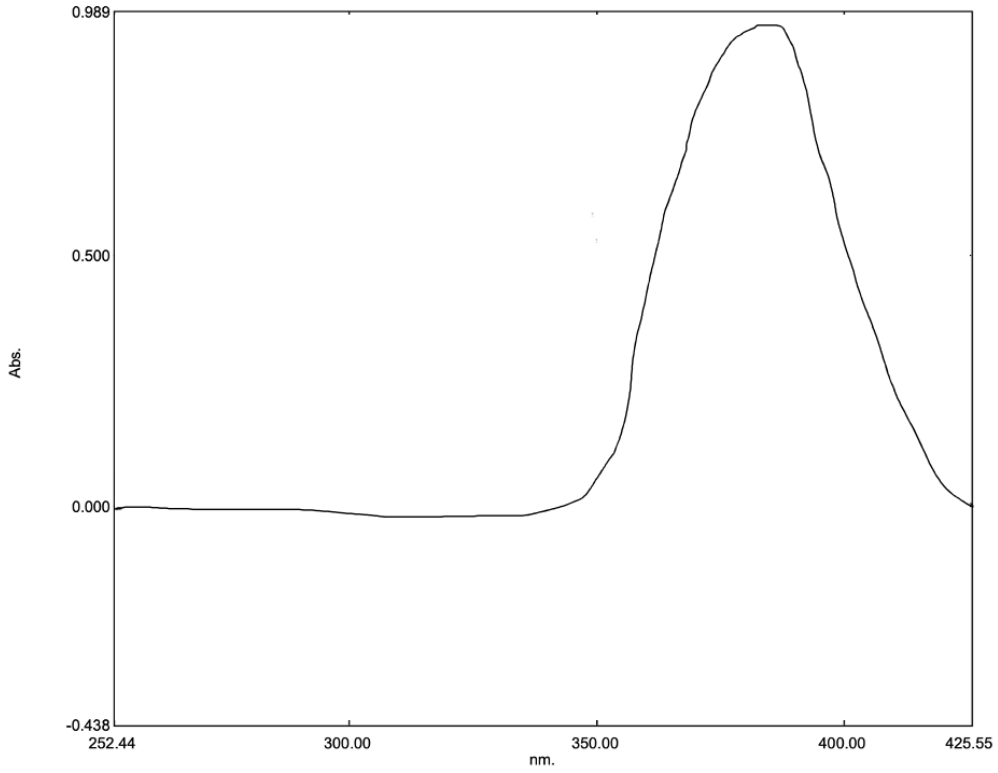


**Figure 3.10** UV-Vis spectra for the MAP dye in THF (2 mM).

The reactivity of the dye (20 mM in THF) was tested as outlined in the Methods Section *3.4.2*. Acetone, methanol, acetic acid and hexane were added to the solution and no colour change was observed indicating that the ring opening did not occur. Upon addition of ammonia however, the solution changed (within 5 min) from a yellow to a dark brown colour. The same colour change response was observed when diethylamine was added to the dye solution, demonstrating the amine selectivity of the dye. This amine selectivity was also observed by Diaz *et al*. for the related MAF dye.[198] Based on this observation and the reaction pathway of MAP with ammonia, the mechanism for the reaction of the MAP dye with ammonia is hypothesised to be (**Figure 3.11**) as follows:[203–205] Activation of the pyrrole ring towards ring opening is believed to occur in the presence of a basic donor. In this case, ammonia behaves as a basic donor, whereby the lone pair of electrons on its nitrogen atom attack the pyrrole ring leading to ring opening (step 1, **Figure 3.11**). This nucleophilic attack occurs on C-2 of the pyrrole ring as it is highly electropositive. Typically, pyrrole reacts with electrophiles (positively charges species as it's an electron rich ring). However, in this case the ethylene

(C=C) on the MAP dye is an electron withdrawing substituent which pulls away the negative charge from the pyrrole ring thus activating the ring towards nucleophilic attack.[196]

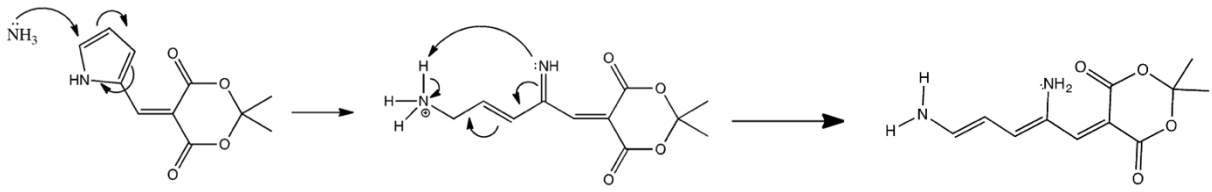

**Figure 3.11** Proposed mechanism for the reaction of MAP dye with ammonia.

The ability of the MAP dye to respond quantitatively to ammonia was investigated. The dye solution (20 mM) was exposed to ammonia between concentrations of 1 - 52 ppm and following 1 h of exposure, the colour of the solution was noted. The colour intensity (CI) of the dye solution increased with increasing concentrations of ammonia (**Figure 3.12**). Visible changes in dye intensity was detected for ammonia concentrations as low as 5 ppm and lower. In the work of Diaz *et al*. a similar experiment was carried out however, in this experiment the colour change was only detectable at 100 ppm ammonia and higher.[198] One possible reason for increased sensitivity for the MAP dye could relate to steric hindrance of the active site on the dye. In the MAF dye compound, the oxygen atom of the furan ring has a greater atomic radius than the nitrogen of the pyrrole ring found on the MAP dye. This larger oxygen atom could potentially sterically hinder attack by ammonia leading to reduced sensitivity of the MAF dye relative to MAP.

(A)

(B)

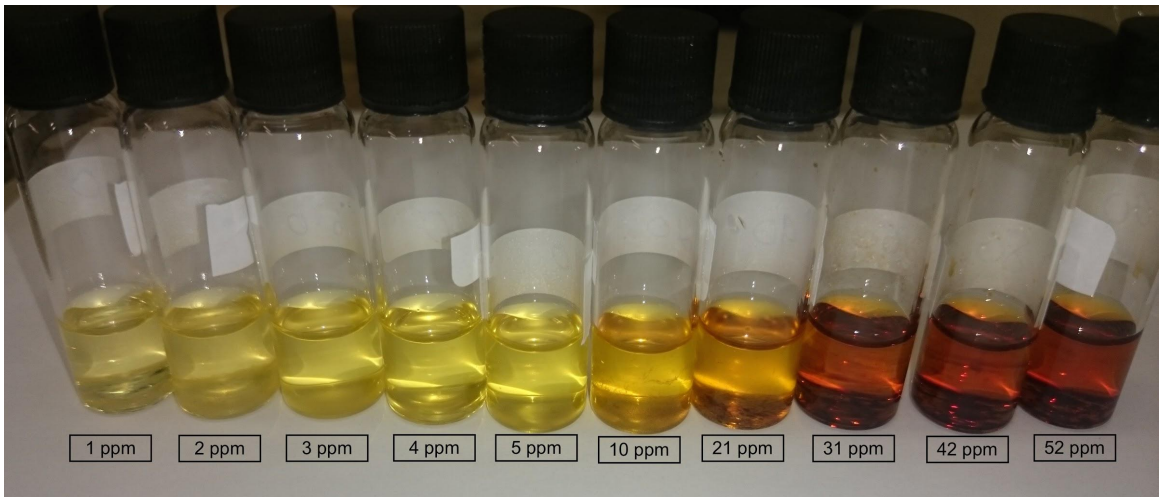


**Figure 3.12** Images of MAP dye (20 mM) in THF (A) left vial: 1 h after preparation; right vial: 24 h after preparation and (B) in the presence of increasing concentrations (from left to right) of ammonia.

To investigate this further, UV-Vis analysis of the MAP dye-ammonia interactions in solution (**Figure 3.13**) was performed. Samples were diluted (2 mM in THF) prior to UV-Vis analysis. The UV-Vis absorbance was recorded over a wavelength range of 190-500 nm. An isosbestic point was determined at 320 nm. The band at 270 nm corresponds to the transition (n→$\pi^*$) in C=O and increased in intensity with increasing concentrations of ammonia. In this transition there is overlap between a non-bonding orbital and an antibonding $\pi$ orital. Overlap between these type of orbitals is poor and so transition is weak.[206] The conjugation in the MAP-ammonia system leads to a spilt in the energy distribution of the orbitals. This allows for transitions to occur at higher wavelengths, and thus lower energy. Initially the aromaticity of the pyrrole increases the stability of the dye compound, allowing for absorption to happens at lower

energies accounting for the absorbance band at 385 nm. Addition of ammonia results in pyrrole ring opening and thus loss or aromaticity and stability. Cyclic conjugated systems are more stable than linear conjugated systems. This explains the decrease in band absorbance with increasing ammonia concentration at 385 nm and the subsequent increase in the absorbance band at 270 nm.

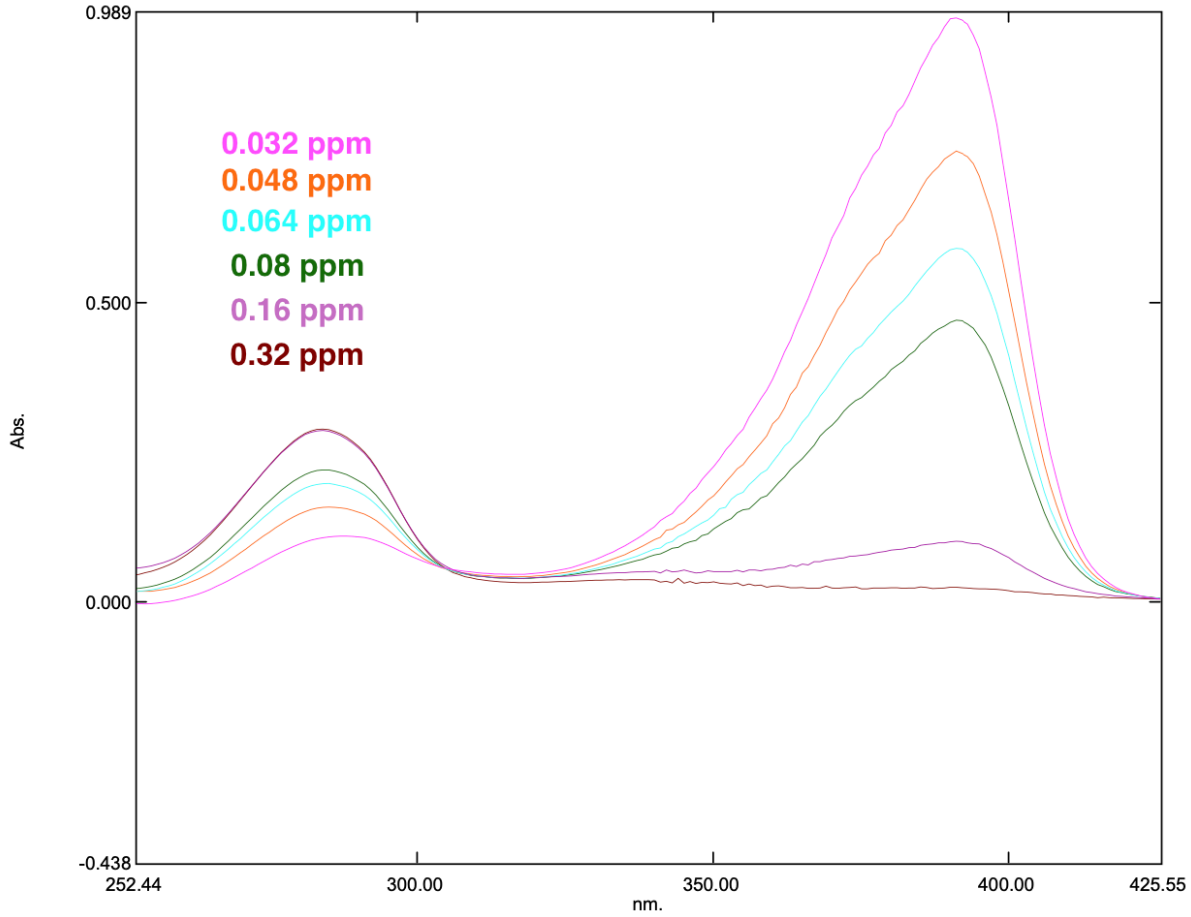


**Figure 3.13** Overlaid UV-Vis spectra for MAP dye (2 mM) in THF with varying ammonia concentrations (0.032-0.32 ppm).

Given the rapid colorimetric responsiveness of the solution phase of the dye to ammonia, the dye's performance as a solid film with respect to its responsiveness towards volatile ammonia was next investigated. These MAP sensors comprised 6 sensor spots and were fabricated according to Methods Section *3.2.6*. In order to develop these sensors, a suitable solid support had to be identified for drop-casting the MAP solution to form homogenous films that could be used as sensor spots. When deposited on acylated TLC plate (**Figure 3.14**) and cellulose

filter paper (no image available), the MAP dye spots formed leached and were inconsistent in shape. In an attempt to resolve this issue, the dye was encapsulated in a sol gel film (no image available) as described in Methods Section *3.2.6*. However, although this approach yielded homogenous and consistent spots, it was deemed unsuccessful as the encapsulated dyes spots did not show a colour response upon ammonia exposure and so were not explored further.

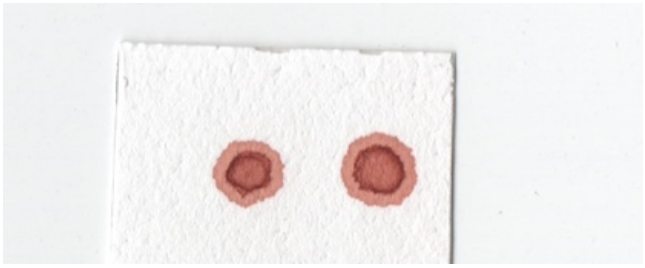

**Figure 3.14** Drop-cast MAP dye (1 uL) from a 20 mM MAP in THF solution on acylated TLC paper. Note: Image is following exposure to ammonia (30 ppm).

Silica TLC plates were also investigated and showed the most homogeneous film deposition (**Figure 3.14**) and so were chosen as a substrate to deposit MAP dye onto from a MAP in THF (20mM). Furthermore, these highly homogenous, regular dye spots underwent a colour change in response to ammonia (**Figure 3.15**). Silica TLC plates were also used by Diaz *et al*., as a substrates for their MAF dye.[198]

**Figure 3.15** Drop-cast MAP dye (1 uL) from a 20 mM THF solution on silica TLC paper. Note: Image is following exposure to ammonia (30 ppm).

The stability of the dye on silica is attributed to the interactions between the MAP dye and silica TLC plate which is assumed to occur through hydrogen bonds. The presence of double-bonded oxygen atoms in MAP allows for increased electronegativity of the oxygen atom leading to stronger interaction with the hydrogen atoms of the silica plate as shown in **Figure**

**3.16.** Thus for all experiments carried out from here on, MAP sensors were fabricated using silica as the substrate unless otherwise specified

------ = HYDROGEN BONDS

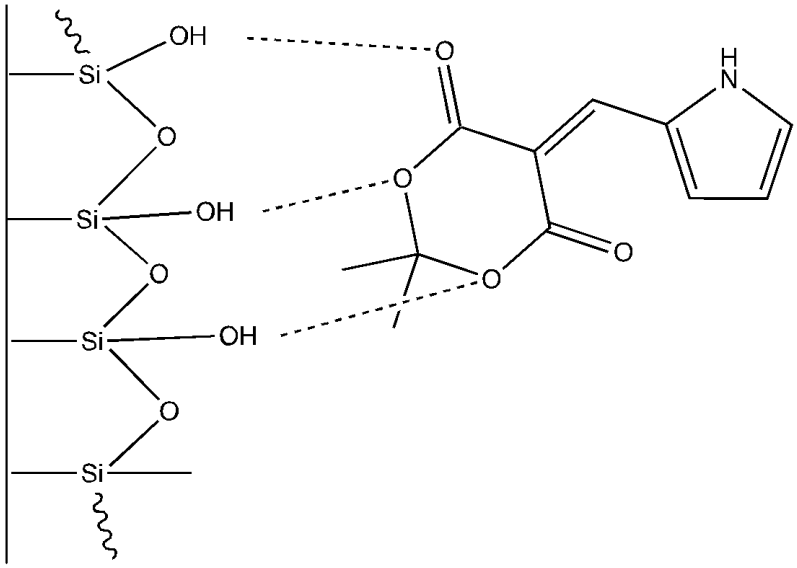


**Figure 3.16** Molecular Interactions of the MAP dye with the silanol groups on a silica TLC plate via hydrogen bonding.

*3.3.3 Kinetic study of MAP sensor reaction with ammonia*

To investigate the kinetics of the MAP sensor with ammonia, MAP sensors were prepared as per the Methods Section *3.2.7*. All sensors were exposed to the same concentration of ammonia (5 ppm) for different periods of time (0, 1, 2, 3, 4, 5 h) and sensor images processed in ImageJ. **Figure 3.17** shows that increased exposure time led to an increased change in CI (ΔCI). A steep response occurred in the first 3 h, followed by plateau from approx. 4 h indicating a partition equilibrium state reached for the ammonia between the headspace and sensor spot. Thus, to ensure equilibrium based sensor-analyte responses, 5 h was chosen as the sampling time. Read de Alaniz *et al*. observed a similar response kinetics for their MAF dye, albeit in solution. The solution-based MAF dye showed a steep change in dye solution absorbance at 532 nm for the first 6 hour followed by a steady increase and then a plateau in absorbance.[198]

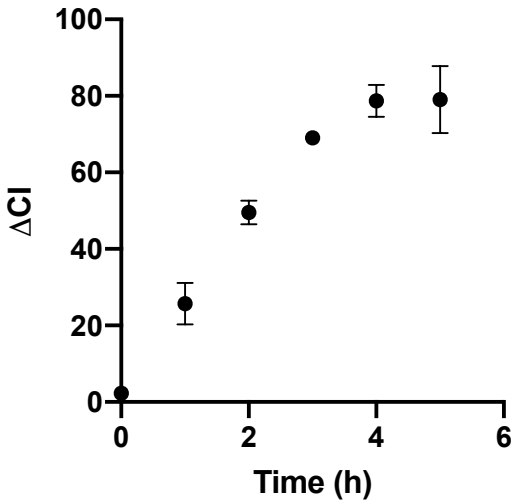


**Figure 3.17** ΔCI of the MAP sensor vs exposure time to ammonia ($2\mu L$). Error bars represent the standard deviation of replicate dye spots within the same vial (n=5).

The response range and limit of detection (LOD) of the MAP sensor were investigated as per Methods Section *3.2.8* where MAP sensors were exposed to a range of concentrations of ammonia in closed vials. Sensor responses was measured over a wide range of concentrations (0.00549 - 5.13 ppm; or $9.35 \times 10^{-5}$ - $9.35 \times 10^{-3}$ g). As seen in **Figure 3.18** (A & B), linear responses were obtained for ammonia concentrations in the lower range of 0.027- 0.055 ppm ($4.67 - 9.35 \times 10^{-4}$ g) and wider range 0.11- 0.55 ppm ($1.87 - 9.35 \times 10^{-3}$ g). These experiments were conducted using neat aliquots of ammonia. Solutions of ammonia in THF were also prepared (20 mM) and added as small volumes (0.1-0.9 $\mu$L) to vials containing MAP sensors. However the dye spots did not respond to these diluted ammonia solutions. Low ($\mu$L) volumes were used to prepare this stock solution, and along-side the low boiling point of ammonia, made it difficult to accurate transfer the desired ammonia volume into THF without loss of ammonia to air.[207] Furthermore, only weak hydrogen bonding exists between ammonia and THF which allows for ammonia to be readily evaporated.[208]

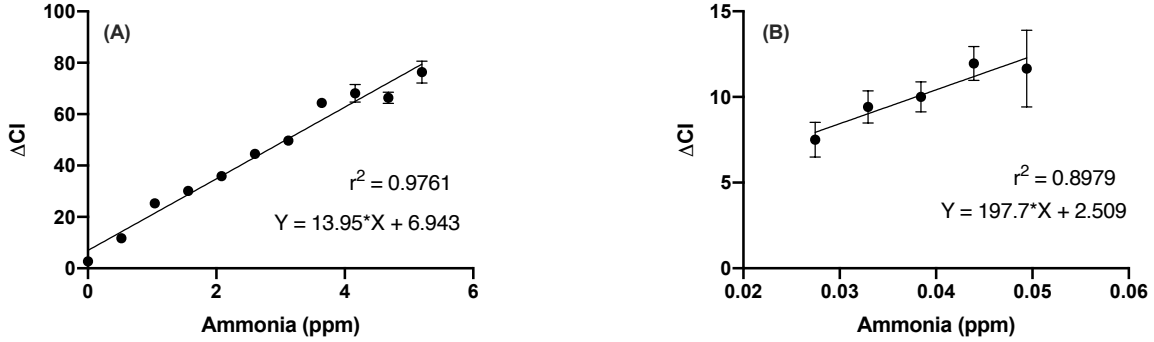


**Figure 3.18** ΔCI as a function of ammonia concentration over a (A) wide concentration range 0-6 ppm and (B) lower, narrow concentration range 0.02-0.05 ppm. Linear regression was applied. Error bars represent the standard deviation of replicate dye spots (n=5) on the sensor.

Once the linear range was identified LOD was calculated by dividing the standard deviation (SD) by the slope of the calibration curve (m) as given by the following formula:

$$LOD = 3.3\left(\frac{SD}{m}\right)$$

Taking the lower of these figures, the LOD for these MAP colorimetric sensor spots was deemed to be approx. 0.006 ppm.

*3.3.4 Participant study using MAP sensors for the detection of amines from skin*

In this research, the responsiveness of the MAP dye sensor towards volatile amines from skin emissions in the form of a MAP sensor was tested. The MAP sensors were prepared as described in the Methods Section *3.2.6* to contain multiple dye spots (n=6). The sensors were applied to the skin of participants as described earlier and shown in **Figure 3.6**. The MAP sensors were scanned before and after a 5 h skin exposure (**Figure 3.19**). In all cases, an average ΔCI ± SD were reported, based on 6 sensor spots for each MAP sensor

(A) Before application on skin (B) After application to skin (5 h)

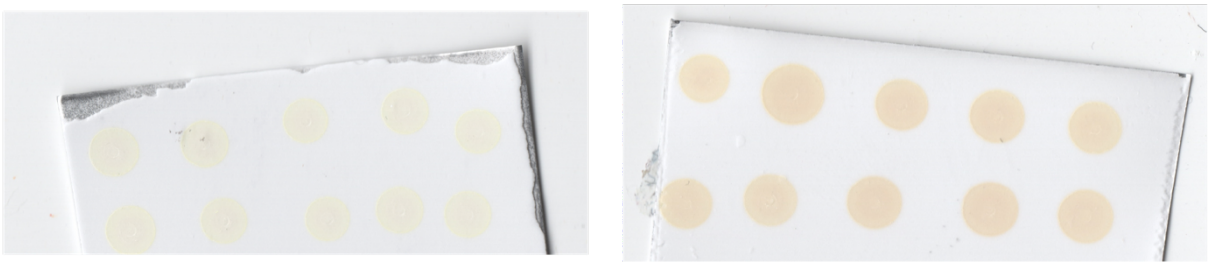

**Figure 3.19** : MAP dye sensor spots (A) before and (B) after applying to the axillae region for a participant for 5 h.

Using ImageJ to analyse the MAP sensor response to the skin volatile emission, the CI of the spot before and after exposure to the different sites was calculated. Control experiments were also carried out, whereby the sensor substrate was sandwiched between two plastic sheets before and applied to the skin as normal. ΔCI values were measured in these control experiments and responses < 7 were considered as background interference when assessing sensos applied to the skin.

MAP sensor responses were then obtained for a number of different sites on the body for a single participant and the colour **Table 3.2** shows the RGB colour of the dye spots before and after exposure to the different sites. Sites like the forehead axillae and feet have high densities of eccrine glands which release secretions that comprise ammonia and thus it was expected that ammonia emission from these sites would be high.[187] This correlates with a high MAP sensor response in the case of the axillae and the forehead, but not the foot (**Table 3.2**). As well as sweat, another reason for the high ammonia emissions from particular sites may relate to the microflora. The moist and warm environment of the axillae region for example makes a great niche for the flourishment of many types of microorganisms, in particular bacteria. The

metabolism of skin bacteria produces various microbial VOC compounds, including amines.[133] One of the microorganisms known to be abundant at this site are bacteria that belong to the staphylococcus genus.[209] Because the axillae is an occluded area, the density of Staphylococcus bacteria located here are much higher than other body parts like the hands.[210] Gotz *et al*. recently reported that Staphylococcus bacteria such as *S.epidermidis* produces amines via an enzyme called staphylococcal aromatic amino acid decarboxylase (SadA).[211,212] The potential generation of amines by these organisms at the axillae region in particular may be a factor in the high MAP sensor response from this site.

The MAP sensor applied to the base of the foot showed very low responses indicating low volatile amines emission from this site. This was not expected as the literature shows that the foot has a high ammonia emission due to the high density of eccrine glands found at this body part.[199] Indeed, a high ammonia emission from the foot was previously seen in a study carried out by Furukawa *et al*. who used a passive flux sampler to sample 13 different body sites. Analysis was via ion-exchange chromatography and showed that the ammonia emission from the feet was the highest relative to all other sites.[201] It should be noted however that the ion-exchange analysis performed was selective to ammonia, whereas in our case, the sensor spots is less selective and will respond to many volatile aminated compounds. This may be a factor related to the different trends observed.

**Table 3.2** Colour table showing the RGB colours of the MAP dye before and after exposure to the skin, and average ΔCI ± std dev after exposure to different body sites for F1.

| | |
|---|---|
| Before application | Forehead (7.1 ± 0.9) |
| Before application | Abdomen (13.1 ± 1.2) |
| Before application | Axillae (23.5 ± 0.3) |
| Before application | Foot (2.7 ± 1.6) |

**Figure 3.20** is a bar graph showing the different MAP dye response to the various sites on the body for the two female participants (F1 & F2). Results again show ΔCI of the dye is different from site to site. Both participants showed differences in MAP dye responses but trends across the sites was broadly similar whereby both participants showed higher responses at the forearm and abdomen relative to the foot and forehead. The sensor showed variable responses between participants especially at the axillae region where F1 showed significantly higher emissions than F2.

The skin axillae region contains a high density of bacteria. A study carried out by Takken *et al*. using anthrophilic mosquitoes - that are known to be attracted to various compounds one of which is ammonia - showed that human sweat incubated with bacteria it more attractive to anthrophilic mosquitos coinciding with an increase in ammonia levels.[187] Another reason for the varying response of the sensor to the axillae region could be related to the fact that this site has inherently variable emissions, seen previously in our group, which we attribute to the use of deodorants and other exogeneous products on a daily basis. It should be noted that this study was carried out in 2020 and due to COVID-19 infection control measures, the ability to recruit participants to this study was significantly hindered and thus the sample size for this study was small. More data collection is required to better understand the results obtained for this study.

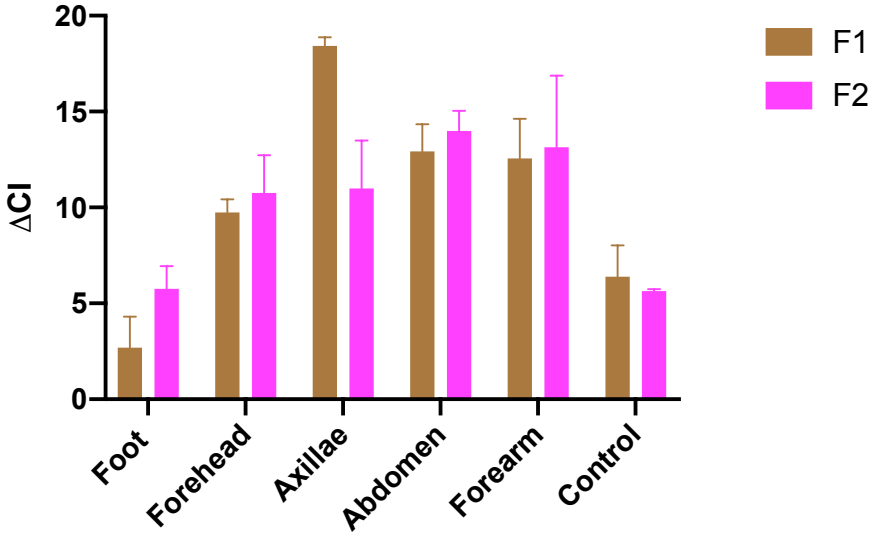


**Figure 3.20** Bar graph showing average dye response to different body sites for F1 and F2 collected over 5 days. Error bars represent standard deviation between replicate spots (n=6) for each MAP sensor.

Differences between the participants may be due to a myriad of factors including racial differences and dermal conditions including sweat, skin surface pH and diet. Further research is required to understand sensor response in more detail. Skin surface pH measurements were also taken in this study (**Figure 3.21**) to investigate if there was a correlation between skin surface pH and ammonia emissions at different sites. It can be seen that skin surface pH readings varied between participants at the same site especially for the axillae, abdomen and forearm regions.

Generally, sensor response and pH response are consistent whereby low skin surface pH gives a low sensor response and high skin surface pH gives a high sensor response. F1 showed a significantly higher pH at the axillae than any other site, correlating with the high MAP sensor ΔCI response at this site. Interestingly, the forehead showed a high sensor response for a very low skin surface pH. The forehead has a high concentration of sebaceous glands that create a thick layer of sebum at this site.[74] Sebum at this site is dominated by VFA that are responsible for the low pH of the forehead and possibly ammonia/amine as detected by the MAP sensor.[213] The skin surface pH on the foot was measured as reasonably acidic (approx. 5), correlating with the low amine response detected on the foot. This was discussed earlier and was not expected as it is believed that ammonia emissions and hence skin surface pH from this eccrine gland rich site would be high. A correlation with the skin surface pH was not seen whereby although pH at this site was high, sensor response was very low. Application of pressure (standing, waking) on the sensor by the foot may have induced high skin occlusion (compared to other sites where no pressure on the sensor would have been applied.

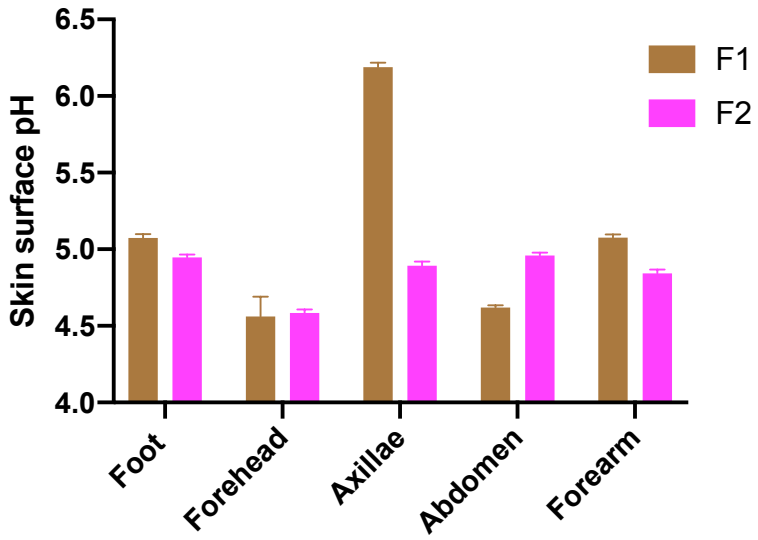


**Figure 3.21** Bar graph showing average skin surface pH values calculated by taking surface pH values daily over 5 days and taking an average for each participant, F1 & F2 at each site. Error bars represent the standard deviation of replicate pH measurements (n= 5).

As seen in **Figure 3.20**, average varying responses among participants for the same site were noted. To understand this effect better, variation in the daily emission of amines from a single participant at one site along with skin surface pH was studied. To no surprise, some daily fluctuation in the amine emission occurs (**Figure 3.22**). Apart from the factors mentioned above, daily change in ammonia emission can be affected by diet and exercise. Using a commercial cavity ring spectrometer, Schmidt *et al*. show that in a fasting state zero to little emission of ammonia is detected.[199] An increase in skin emission after food consumption (protein 60 g) was noted by Nose *et al*.[189] This increase is believed to either be directly related to the food consumption or due the metabolism of food that leads to an increase in body and subsequent release of sweat containing ammonia.[199]

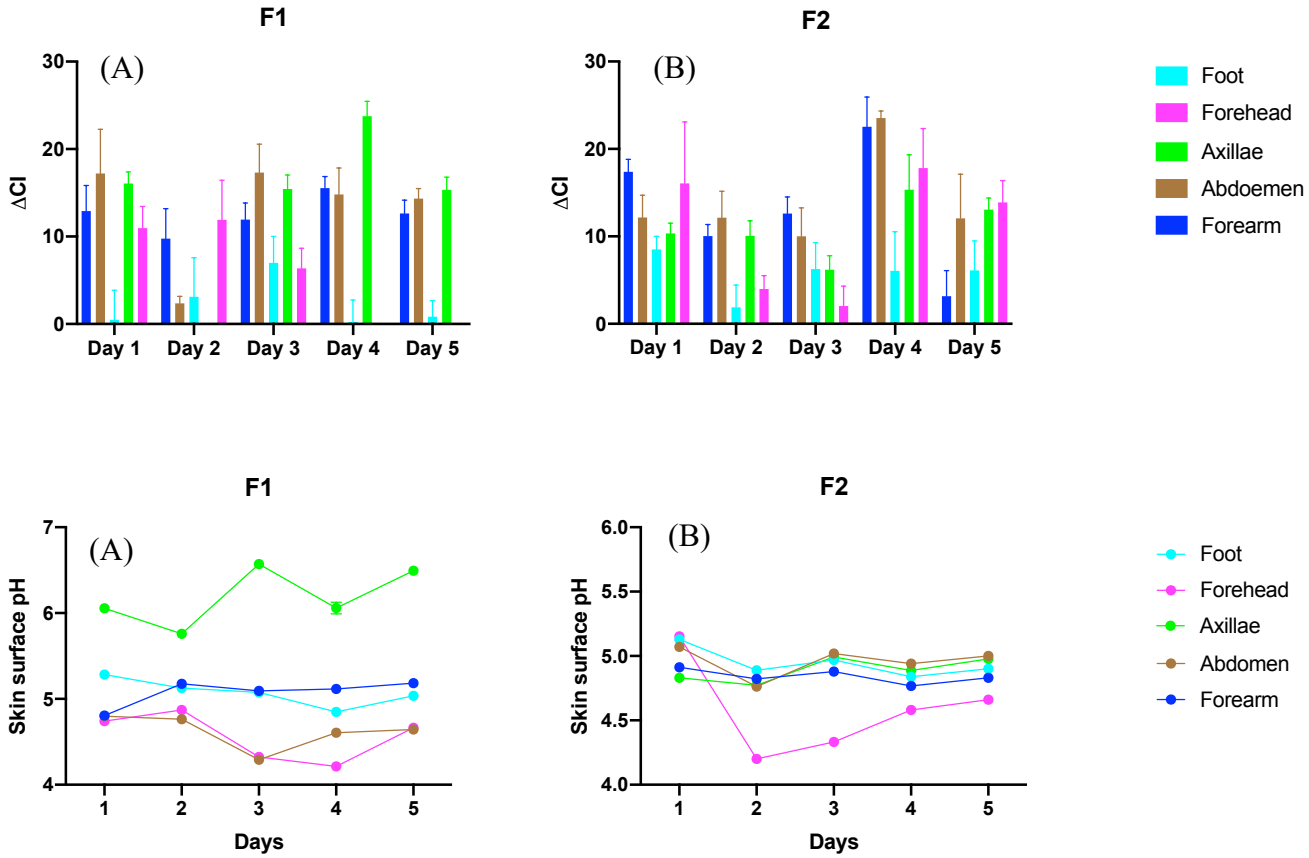


**Figure 3.22** Daily MAP dye ΔCI response to different sites (top) and corresponding daily skin surface pH values (bottom) for (A) F1 and (B) F2.

Furthermore, to better understand the relationship between skin surface pH and response of the dye to skin amines, a graph was plotted for the daily pH values and the corresponding ΔCI of dye spots on sensors for F1 and F2 at the different body sites **(Figure 3.23)**. Skin surface pH was observed to weakly correlate with ΔCI for the axillae and forehead regions, while no correlation was observed for the foot, abdomen or forearm. The purpose of this investigation was to test the sensor on real subjects. Without testing of the sensor on greater numbers of participants, it is difficult to draw a conclusion from this data. Further investigations are required to fully understand the response of the sensors in relation to skin surface pH.

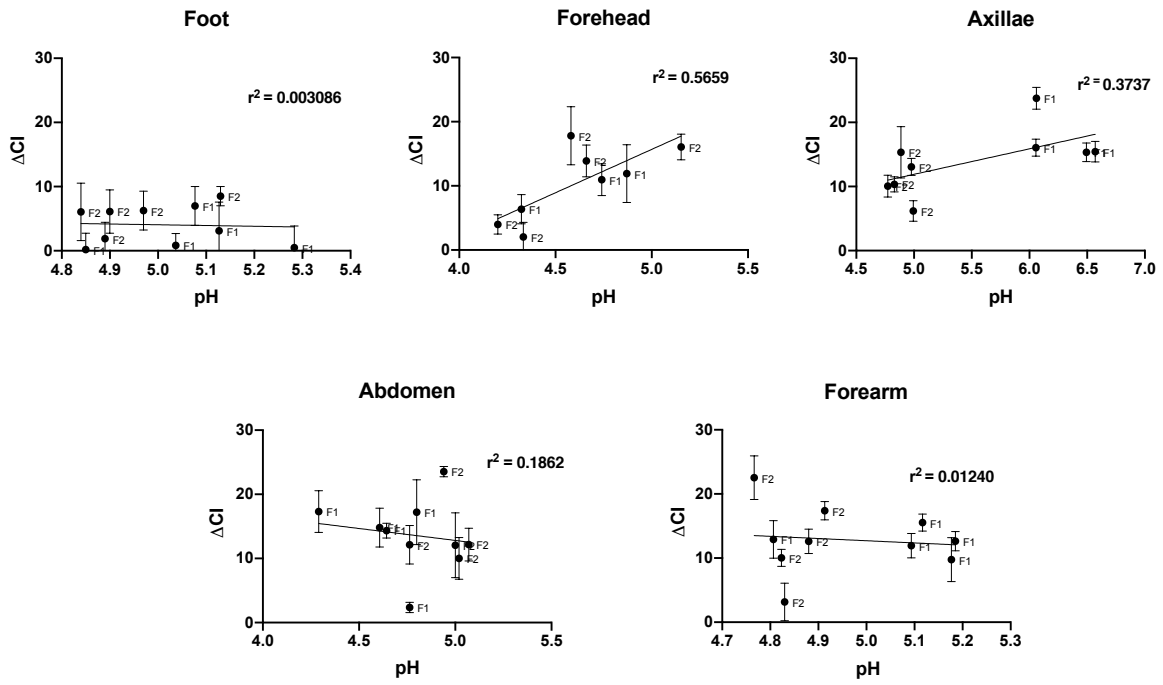


**Figure 3.23** ΔCI responses of the MAP dye plotted against corresponding skin surface pH values for n=2 participants (F1 and F2) sampled over 5 days.

The ΔCI response was used to extrapolate the corresponding amine-based emission rate from each site for each participant (**Table 3.3**). To calculate the emission rate, the MAP sensor response was related to an ammonia mass using the standard calibration curve generated earlier (**Figure 3.18 (B)**) this was then considered as mg per $cm^2$ area of the skin sampled per min of sampling time.

Sample calculation:

F1 axillae response (ΔCI) was approx. 23.5 (**Table 3.2** ) when interpolated using the calibration curve (**Figure 3.18 (B)**) you get an ammonia concentration of 0.087 ppm.

0.087 ppm = 0.087 mg 100 $cm^{-3}$ = 87 ng $cm^{-2}$.

The sensors were kept on the skin for a period of 5 h.

Thus the rate is 87 ng $cm^{-2}$ 5 $h^{-1}$ ≈ 1049 ng $min^{-1}$ $cm^{-2}$.

**Table 3.3** Calculated rate of ammonia from F1 and F2 for different body sites..

| | Amine-based emission rate (ng $min^{-1}$ $cm^{-2}$ ) | | | | |
|---|---|---|---|---|---|
| | Foot | Forehead | Axillae | Abdomen | Forearm |
| F1 | Below calibration range (< 7) | 315 | 1049 | 584 | 552 |
| F2 | Below calibration range (< 7) | 401 | 421 | 674 | 602 |

Using our colorimetric sensor, amine emission rates from the stomach and forearm for both participants were similar. Nose *et al*. found that the ammonia emission from the forearm of healthy participants averaged to 0.4 ng $min^{-1}$ $cm^2$.[189] This is very small compared to the values (F1; 552 and F2; 602) obtained in the presented study. The differences in methods between the two studies may be a reason for these differences. While a colorimetric method was used to assess ammonia emission from skin in the resented Nose *et al.* used a plastic skin sampler attached to the forearm and helium to flush the skin VOCs into a GC- flame thermionic detector for analysis. The group used water to clean the skin prior to collection of the skin VOCs. This may be because of Henry's law which states that the amount of gas dissolved in a liquid is proportional to its partial pressure above the liquid.[214] Ammonia has a high Henry's law constant meaning it is highly soluble in water which may have caused ammonia to partition into the water applied to the skin thus leading to reduced levels of volatile ammonia being detected.[189,199] It is also important to note that the colorimetric sensor described in this study is at its early development stage and requires more investigation and validation.

### 3.4 Conclusion

The dye presented in this study was synthesised via a simple one pot condensation reaction between two carbonyl-containing compounds; Meldrum's acid and pyrrole-2-carboxaldehyde. HNMR characterisation of the new dye showed the formation of a characteristic peak at 2.7 ppm confirming formation of MAP dye. UV-Vis analysis revealed the dye's selectivity and low sensitivity (10 ppm ammonia) towards amine-based compounds. A ring-opening mechanism for the reaction of ammonia with MAP dye was proposed which was supported by the UV-Vis study. Following solution-based characterisation, the dye was developed into a wearable skin colorimetric MAP sensor and the detection of volatile amines in the skin emission was demonstrated. The main aim of this study was to test on real subjects. Analysis of the colorimetric sensors after application to the skin revealed that MAP sensor response to various body sites across participants differed. However, further investigation and validation is required to understand the selectivity of the response from one participant to the other. With further improvements, the proposed MAP sensor could find application as a wearable colorimetric sensors for amine emissions which can be linked to kidney dysfunction, microbial activity changes, skin surface basicity potentially, or more broadly as a wearable sensor for monitoring ammonia levels in the environment e.g workplace safety (to detect ammonia or toxic volatile amines).

### 3.5 References


1. Kolarsick, P. A. J., Kolarsick, M. A. & Goodwin, C. Anatomy and Physiology of the Skin. *J. Dermatol. Nurses Assoc.* **3**, 203–213 (2011).
2. Sahle, F. F., Gebre-Mariam, T., Dobner, B., Wohlrab, J. & Neubert, R. H. H. Skin Diseases Associated with the Depletion of Stratum Corneum Lipids and Stratum Corneum Lipid Substitution Therapy. *Skin Pharmacol. Physiol.* **28**, 42–55 (2015).
3. Proksch, E., Brandner, J. M. & Jensen, J.-M. The skin: an indispensable barrier. *Exp. Dermatol.* **17**, 1063–1072 (2008).
4. Kanitakis, J. Anatomy, histology and immunohistochemistry of normal human skin. *Eur. J. Dermatol. EJD* **12**, 390–399; quiz 400–401 (2002).
5. Takahashi, M., Kawasaki, K., Tanaka, M., Ohta, S. & Tsuda, Y. The mechanism of stratum corneum plasticization with water. in *Bioengineering and the Skin: Based on the Proceedings of the European Society for Dermatological Research Symposium, held at the Welsh National School of Medicine, Cardiff, 19–21 July 1979* (eds. Marks, R. & Payne, P. A.) 67–73 (Springer Netherlands, 1981). doi:10.1007/978-94-009-7310-7_8.
6. Hoover, E. & Krishnamurthy, K. Physiology, Sebaceous Glands. in *StatPearls* (StatPearls Publishing, 2020).
7. Hodge, B. D. & Brodell, R. T. Anatomy, Skin Sweat Glands. in *StatPearls* (StatPearls Publishing, 2020).
8. Rippke, F., Berardesca, E. & Weber, T. M. pH and Microbial Infections. *Curr. Probl. Dermatol.* **54**, 87–94 (2018).
9. Drislane, C. & Irvine, A. D. The role of filaggrin in atopic dermatitis and allergic disease. *Ann. Allergy Asthma Immunol. Off. Publ. Am. Coll. Allergy Asthma Immunol.* **124**, 36–43 (2020).

10. Kubo, A., Nagao, K. & Amagai, M. Epidermal barrier dysfunction and cutaneous sensitization in atopic diseases. *J. Clin. Invest.* **122**, 440–447 (2012).

11. Smeden, J. van *et al.* The importance of free fatty acid chain length for the skin barrier function in atopic eczema patients. *Exp. Dermatol.* **23**, 45–52 (2014).

12. Del Rosso, J. Q. & Levin, J. The Clinical Relevance of Maintaining the Functional Integrity of the Stratum Corneum in both Healthy and Disease-affected Skin. *J. Clin. Aesthetic Dermatol.* **4**, 22–42 (2011).

13. Schmid-Wendtner, M.-H. & Korting, H. C. The pH of the Skin Surface and Its Impact on the Barrier Function. *Skin Pharmacol. Physiol.* **19**, 296–302 (2006).

14. Shirasu, M. & Touhara, K. The scent of disease: volatile organic compounds of the human body related to disease and disorder. *J. Biochem. (Tokyo)* **150**, 257–266 (2011).

15. Rondanelli, M. *et al.* Volatile Organic Compounds as Biomarkers of Gastrointestinal Diseases and Nutritional Status. *J. Anal. Methods Chem.* **2019**, e7247802 (2019).

16. Mochalski, P., King, J., Unterkofler, K., Hinterhuber, H. & Amann, A. Emission rates of selected volatile organic compounds from skin of healthy volunteers. *J. Chromatogr. B Analyt. Technol. Biomed. Life. Sci.* **959**, 62–70 (2014).

17. Kataoka, H., Saito, K., Kato, H. & Masuda, K. Noninvasive analysis of volatile biomarkers in human emanations for health and early disease diagnosis. *Bioanalysis* **5**, 1443–1459 (2013).

18. Samant, P. P. & Prausnitz, M. R. Mechanisms of sampling interstitial fluid from skin using a microneedle patch. *Proc. Natl. Acad. Sci. U. S. A.* **115**, 4583–4588 (2018).

19. Samant, P. P. *et al.* Sampling interstitial fluid from human skin using a microneedle patch. *Sci. Transl. Med.* **12**, (2020).

20. Liu, Y., Pharr, M. & Salvatore, G. A. Lab-on-Skin: A Review of Flexible and Stretchable Electronics for Wearable Health Monitoring. *ACS Nano* **11**, 9614–9635 (2017).

21. Jayathilaka, W. A. D. M. *et al.* Significance of Nanomaterials in Wearables: A Review on Wearable Actuators and Sensors. *Adv. Mater.* **31**, 1805921 (2019).

22. Jin, H., Abu-Raya, Y. S. & Haick, H. Advanced Materials for Health Monitoring with Skin-Based Wearable Devices. *Adv. Healthc. Mater.* (2017) doi:10.1002/adhm.201700024.

23. Maibach, H. & Honari, G. *Applied Dermatotoxicology: Clinical Aspects*. (Academic Press, 2014).

24. Wong, R., Geyer, S., Weninger, W., Guimberteau, J.-C. & Wong, J. K. The dynamic anatomy and patterning of skin. *Exp. Dermatol.* **25**, 92–98 (2016).

25. Kern, F., Niault, T. & Baccarini, M. Ras and Raf pathways in epidermis development and carcinogenesis. *Br. J. Cancer* **104**, 229–234 (2011).

26. Amisten, S. *et al.* An atlas of G-protein coupled receptor expression and function in human subcutaneous adipose tissue. *Pharmacol. Ther.* **146**, 61–93 (2015).

27. Vitorino, C., Sousa, J. & Pais, A. Overcoming the skin permeation barrier: challenges and opportunities. *Curr. Pharm. Des.* **21**, 2698–2712 (2015).

28. Kubo, A., Nagao, K. & Amagai, M. 3D Visualization of Epidermal Langerhans Cells. in *Molecular Dermatology* (eds. Has, C. & Sitaru, C.) vol. 961 119–127 (Humana Press, 2013).

29. Benson, H. A. E. Skin Structure, Function, and Permeation. in *Topical and Transdermal Drug Delivery* 1–22 (John Wiley & Sons, Ltd, 2012). doi:10.1002/9781118140505.ch1.

30. Behne, M. *et al.* Omega-hydroxyceramides are required for corneocyte lipid envelope (CLE) formation and normal epidermal permeability barrier function. *J. Invest. Dermatol.* **114**, 185–192 (2000).

31. Elias, P. M. *et al.* Formation and Functions of the Corneocyte Lipid Envelope (CLE). *Biochim. Biophys. Acta* **1841**, 314–318 (2014).

32. Yang, G. *et al.* Skin Barrier Abnormalities and Immune Dysfunction in Atopic Dermatitis. *Int. J. Mol. Sci.* **21**, 2867 (2020).

33. Zhang, B. *et al.* Chapter 52 - Bioengineering Skin Constructs. in *Stem Cell Biology and Tissue Engineering in Dental Sciences* (eds. Vishwakarma, A., Sharpe, P., Shi, S. & Ramalingam, M.) 703–719 (Academic Press, 2015). doi:10.1016/B978-0-12-397157-9.00056-4.

34. Skin Tissue Engineering and Regenerative Medicine - 1st Edition. https://www.elsevier.com/books/skin-tissue-engineering-and-regenerative-medicine/albanna/978-0-12-801654-1.

35. Baswan, S. *et al.* Understanding the Formidable Nail Barrier: A Review of the Nail Microstructure, Composition and Diseases. *Mycoses* **60**, 284–295 (2017).

36. Murphrey, M. B. & Vaidya, T. Histology, Apocrine Gland. in *StatPearls* (StatPearls Publishing, 2020).

37. Saga, K. Structure and function of human sweat gland studied with histochemistry an cytochemistry. *Prog. Histochem. Cytochem.* **37**, 323–86 (2002).

38. Chen, Y.-L., Kuan, W.-H. & Liu, C.-L. Comparative Study of the Composition of Sweat from Eccrine and Apocrine Sweat Glands during Exercise and in Heat. *Int. J. Environ. Res. Public. Health* **17**, (2020).

39. Baker, L. B. Physiology of sweat gland function: The roles of sweating and sweat composition in human health. *Temp. Multidiscip. Biomed. J.* **6**, 211–259 (2019).

40. Cui, C.-Y. & Schlessinger, D. Eccrine sweat gland development and sweat secretion. *Exp. Dermatol.* **24**, 644–650 (2015).

41. Esteves, C. Z. *et al.* Skin Biomarkers for Cystic Fibrosis: A Potential Non-Invasive Approach for Patient Screening. *Front. Pediatr.* **5**, (2018).

42. Rigopoulos, D., Larios, G. & Katsambas, A. Skin signs of systemic diseases. *Clin. Dermatol.* **29**, 531–540 (2011).

43. Crowther, J. M. *et al.* Measuring the effects of topical moisturizers on changes in stratum corneum thickness, water gradients and hydration in vivo. *Br. J. Dermatol.* **159**, 567–577 (2008).

44. Horii, I., Nakayama, Y., Obata, M. & Tagami, H. Stratum corneum hydration and amino acid content in xerotic skin. *Br. J. Dermatol.* **121**, 587–592 (1989).

45. Hoste, E. *et al.* Caspase-14 Is Required for Filaggrin Degradation to Natural Moisturizing Factors in the Skin. *J. Invest. Dermatol.* **131**, 2233–2241 (2011).

46. Nakagawa, N. *et al.* Relationship Between NMF (Lactate and Potassium) Content and the Physical Properties of the Stratum Corneum in Healthy Subjects. *J. Invest. Dermatol.* **122**, 755–763 (2004).

47. Watanabe, M., Tagami, H., Horii, I., Takahashi, M. & Kligman, A. M. Functional Analyses of the Superficial Stratum Corneum in Atopic Xerosis. *Arch. Dermatol.* **127**, 1689–1692 (1991).

48. Taylor, N. A. & Machado-Moreira, C. A. Regional variations in transepidermal water loss, eccrine sweat gland density, sweat secretion rates and electrolyte composition in resting and exercising humans. *Extreme Physiol. Med.* **2**, 4 (2013).

49. Watabe, A. *et al.* Sweat constitutes several natural moisturizing factors, lactate, urea, sodium, and potassium. *J. Dermatol. Sci.* **72**, 177–182 (2013).

50. Bernengo, J. & de Rigal, J. Physical Methods to Measure Stratum Corneum Water Content In Vivo. in *Agache's Measuring the Skin: Non-invasive Investigations, Physiology, Normal Constants* (eds. Humbert, P., Fanian, F., Maibach, H. I. & Agache, P.) 299–340 (Springer International Publishing, 2017). doi:10.1007/978-3-319-32383-1_29.

51. Querleux, B. *et al.* In vivo Hydration Profile in Skin Layers by High-Resolution Magnetic Resonance Imaging. *Skin Pharmacol. Physiol.* **7**, 210–216 (1994).

52. Caspers, P. J., Bruining, H. A., Puppels, G. J., Lucassen, G. W. & Carter, E. A. In Vivo Confocal Raman Microspectroscopy of the Skin: Noninvasive Determination of Molecular Concentration Profiles. *J. Invest. Dermatol.* **116**, 434–442 (2001).

53. Narasimha Murthy, S. & Shivakumar, H. N. CHAPTER 1 - Topical and Transdermal Drug Delivery. in *Handbook of Non-Invasive Drug Delivery Systems* (ed. Kulkarni, V. S.) 1–36 (William Andrew Publishing, 2010). doi:10.1016/B978-0-8155-2025-2.10001-0.

54. Hansen, J. R. & Yellin, W. NMR and Intrared Spectroscopic Studies of Stratum Corneum Hydration. in *Water Structure at the Water-Polymer Interface* (ed. Jellinek, H. H. G.) 19–28 (Springer US, 1972). doi:10.1007/978-1-4615-8681-4_4.

55. Darlenski, R., Sassning, S., Tsankov, N. & Fluhr, J. W. Non-invasive in vivo methods for investigation of the skin barrier physical properties. *Eur. J. Pharm. Biopharm. Off. J. Arbeitsgemeinschaft Pharm. Verfahrenstechnik EV* **72**, 295–303 (2009).

56. Plessis, J. du *et al.* International guidelines for the in vivo assessment of skin properties in non-clinical settings: Part 2. transepidermal water loss and skin hydration. *Skin Res. Technol.* **19**, 265–278 (2013).

57. Blank, I. H. Further observations on factors which influence the water content of the stratum corneum. *J. Invest. Dermatol.* **21**, 259–271 (1953).

58. Lu, F. *et al.* Review of Stratum Corneum Impedance Measurement in Non-Invasive Penetration Application. *Biosensors* **8**, 31 (2018).

59. Kohli, R., Archer, W. I., Roberts, J. M. C., Cochran, A. J. & Li Wan Po, A. Impedance measurements for the non-invasive monitoring of skin hydration: a reassessment. *Int. J. Pharm.* **26**, 275–287 (1985).

60. Björklund, S. *et al.* Skin Membrane Electrical Impedance Properties under the Influence of a Varying Water Gradient. *Biophys. J.* **104**, 2639–2650 (2013).

61. Kabiri Ameri, S. *et al.* Graphene Electronic Tattoo Sensors. *ACS Nano* **11**, 7634–7641 (2017).

62. Yao, S. *et al.* A Wearable Hydration Sensor with Conformal Nanowire Electrodes. *Adv. Healthc. Mater.* **6**, 1601159 (2017).

63. Ye, L., Wang, Z., Li, Z., Lv, C. & Man, M.-Q. Validation of GPSkin Barrier® for assessing epidermal permeability barrier function and stratum corneum hydration in humans. *Skin Res. Technol. Off. J. Int. Soc. Bioeng. Skin ISBS Int. Soc. Digit. Imaging Skin ISDIS Int. Soc. Skin Imaging ISSI* **25**, 25–29 (2019).

64. De Guzman, K. & Morrin, A. Screen-printed Tattoo Sensor towards the Non-invasive Assessment of the Skin Barrier. *Electroanalysis* **29**, 188–196 (2017).

65. Guzman, K. D., Al-Kharusi, G., Levingstone, T. & Morrin, A. Robust epidermal tattoo electrode platform for skin physiology monitoring. *Anal. Methods* **11**, 1460–1468 (2019).

66. Wang, Y. *et al.* Low-cost, μm-thick, tape-free electronic tattoo sensors with minimized motion and sweat artifacts. *Npj Flex. Electron.* **2**, 1–7 (2018).

67. Swisher, S. L. *et al.* Impedance sensing device enables early detection of pressure ulcers in vivo. *Nat. Commun.* **6**, 6575 (2015).

68. van Smeden, J. & Bouwstra, J. A. Stratum Corneum Lipids: Their Role for the Skin Barrier Function in Healthy Subjects and Atopic Dermatitis Patients. *Curr. Probl. Dermatol.* **49**, 8–26 (2016).

69. Norlén, L., Nicander, I., Lundsjö, A., Cronholm, T. & Forslind, B. A new HPLC-based method for the quantitative analysis of inner stratum corneum lipids with special reference to the free fatty acid fraction. *Arch. Dermatol. Res.* **290**, 508–516 (1998).

70. Cui, L. *et al.* Advancements in the maintenance of skin barrier/skin lipid composition and the involvement of metabolic enzymes. *J. Cosmet. Dermatol.* **15**, 549–558 (2016).

71. Ansari, M. N., Nicolaides, N. & Fu, H. C. Fatty acid composition of the living layer and stratum corneum lipids of human sole skin epidermis. *Lipids* **5**, 838–845 (1970).

72. Fluhr, J. W. *et al.* Generation of Free Fatty Acids from Phospholipids Regulates Stratum Corneum Acidification and Integrity. *J. Invest. Dermatol.* **117**, 44–51 (2001).

73. Picardo, M., Ottaviani, M., Camera, E. & Mastrofrancesco, A. Sebaceous gland lipids. *Dermatoendocrinol.* **1**, 68–71 (2009).

74. Ludovici, M. *et al.* Influence of the sebaceous gland density on the stratum corneum lipidome. *Sci. Rep.* **8**, 11500 (2018).

75. Freinkel, R. K. & Shen, Y. The origin of free fatty acids in sebum. II. Assay of the lipases of the cutaneous bacteria and effects of pH. *J. Invest. Dermatol.* **53**, 422–427 (1969).

76. Gray, G. M. & White, R. J. Glycosphingolipids and ceramides in human and pig epidermis. *J. Invest. Dermatol.* **70**, 336–341 (1978).

77. Camera, E. *et al.* Use of lipidomics to investigate sebum dysfunction in juvenile acne. *J. Lipid Res.* **57**, 1051–1058 (2016).

78. Masukawa, Y. *et al.* Comprehensive quantification of ceramide species in human stratum corneum. *J. Lipid Res.* **50**, 1708–1719 (2009).

79. van Smeden, J. *et al.* LC/MS analysis of stratum corneum lipids: ceramide profiling and discovery. *J. Lipid Res.* **52**, 1211–1221 (2011).

80. Shin, J.-H. *et al.* A lipidomic platform establishment for structural identification of skin ceramides with non-hydroxyacyl chains. *Anal. Bioanal. Chem.* **406**, 1917–1932 (2014).

81. Chiu, H.-H. & Kuo, C.-H. Gas chromatography-mass spectrometry-based analytical strategies for fatty acid analysis in biological samples. *J. Food Drug Anal.* **28**, 60–73 (2020).

82. Michael-Jubeli, R., Bleton, J. & Baillet-Guffroy, A. High-temperature gas chromatography-mass spectrometry for skin surface lipids profiling. *J. Lipid Res.* **52**, 143–151 (2011).

83. Pappas, A., Johnsen, S., Liu, J.-C. & Eisinger, M. Sebum analysis of individuals with and without acne. *Dermatoendocrinol.* **1**, 157–161 (2009).

84. Smith, R. N., Braue, A., Varigos, G. A. & Mann, N. J. The effect of a low glycemic load diet on acne vulgaris and the fatty acid composition of skin surface triglycerides. *J. Dermatol. Sci.* **50**, 41–52 (2008).

85. Croxton, R. S., Baron, M. G., Butler, D., Kent, T. & Sears, V. G. Variation in amino acid and lipid composition of latent fingerprints. *Forensic Sci. Int.* **199**, 93–102 (2010).

86. Martin, H. J., Reynolds, J. C., Riazanskaia, S. & Thomas, C. L. P. High throughput volatile fatty acid skin metabolite profiling by thermal desorption secondary electrospray ionisation mass spectrometry. *The Analyst* **139**, 4279–4286 (2014).

87. Berdyshev, E. *et al.* Lipid abnormalities in atopic skin are driven by type 2 cytokines. *JCI Insight* **3**, (2018).

88. Sadowski, T. *et al.* Large-scale human skin lipidomics by quantitative, high-throughput shotgun mass spectrometry. *Sci. Rep.* **7**, 43761 (2017).

89. Souza, S. L., Graça, G. & Oliva, A. Characterization of sweat induced with pilocarpine, physical exercise, and collected passively by metabolomic analysis. *Skin Res.*

*Technol. Off. J. Int. Soc. Bioeng. Skin ISBS Int. Soc. Digit. Imaging Skin ISDIS Int. Soc. Skin Imaging ISSI* **24**, 187–195 (2018).

90. Delgado-Povedano, M. M., Calderón-Santiago, M., Luque de Castro, M. D. & Priego-Capote, F. Metabolomics analysis of human sweat collected after moderate exercise. *Talanta* **177**, 47–65 (2018).

91. Jadoon, S. *et al.* Recent Developments in Sweat Analysis and Its Applications. *Int. J. Anal. Chem.* **2015**, e164974 (2015).

92. Agrawal, K., Sivamani, R. K. & Newman, J. W. Noninvasive profiling of sweat-derived lipid mediators for cutaneous research. *Skin Res. Technol.* **25**, 3–11 (2019).

93. Mastella, G., Cesare, G., Borruso, A., Menin, L. & Zanolla, L. Reliability of sweat-testing by the Macroduct® collection method combined with conductivity analysis in comparison with the classic Gibson and Cooke technique. *Acta Paediatr. Oslo Nor. 1992* **89**, 933–7 (2000).

94. Hammond, K. B., Turcios, N. L. & Gibson, L. E. Clinical evaluation of the macroduct sweat collection system and conductivity analyzer in the diagnosis of cystic fibrosis. *J. Pediatr.* **124**, 255–260 (1994).

95. Chung, M., Fortunato, G. & Radacsi, N. Wearable flexible sweat sensors for healthcare monitoring: a review. *J. R. Soc. Interface* **16**, 20190217 (2019).

96. Gao, W. *et al.* Fully integrated wearable sensor arrays for multiplexed in situ perspiration analysis. *Nature* **529**, 509–514 (2016).

97. Kim, J. *et al.* Noninvasive Alcohol Monitoring Using a Wearable Tattoo-Based Iontophoretic-Biosensing System. *ACS Sens.* **1**, 1011–1019 (2016).

98. Tai, L.-C. *et al.* Methylxanthine Drug Monitoring with Wearable Sweat Sensors. *Adv. Mater.* **30**, 1707442 (2018).

99. Tai, L.-C. *et al.* Wearable Sweat Band for Noninvasive Levodopa Monitoring. *Nano Lett.* **19**, 6346–6351 (2019).

100. Proksch, E. Lowering skin pH: improved barrier function, anti-ageing and beyond. *Br. J. Dermatol.* **179**, 254–255 (2018).

101. Elias, P. M. Stratum corneum acidification: how and why? *Exp. Dermatol.* **24**, 179–180 (2015).

102. Yosipovitch, G. & Papoiu, A. D. P. What causes itch in atopic dermatitis? *Curr. Allergy Asthma Rep.* **8**, 306–311 (2008).

103. Proksch, E. pH in nature, humans and skin. *J. Dermatol.* **45**, 1044–1052 (2018).

104. Koch, A. & Schwab, A. Cutaneous pH landscape as a facilitator of melanoma initiation and progression. *Acta Physiol.* **225**, e13105 (2019).

105. Hachem, J.-P. *et al.* pH directly regulates epidermal permeability barrier homeostasis, and stratum corneum integrity/cohesion. *J. Invest. Dermatol.* **121**, 345–353 (2003).

106. Prakash, C., Bhargava, P., Tiwari, S., Majumdar, B. & Bhargava, R. K. Skin Surface pH in Acne Vulgaris: Insights from an Observational Study and Review of the Literature. *J. Clin. Aesthetic Dermatol.* **10**, 33–39 (2017).

107. Krien, P. M. & Kermici, M. Evidence for the Existence of a Self-Regulated Enzymatic Process Within the Human Stratum Corneum –An Unexpected Role for Urocanic Acid. *J. Invest. Dermatol.* **115**, 414–420 (2000).

108. Kezic, S. *et al.* Levels of filaggrin degradation products are influenced by both filaggrin genotype and atopic dermatitis severity. *Allergy* **66**, 934–940 (2011).

109. Cabanillas, B. & Novak, N. Atopic dermatitis and filaggrin. *Curr. Opin. Immunol.* **42**, 1–8 (2016).

110. Hu, J., Stein, A. & Bühlmann, P. Rational design of all-solid-state ion-selective electrodes and reference electrodes. *TrAC Trends Anal. Chem.* **76**, 102–114 (2016).

111. Allen, J. R. pH Electrodes, Ion-Selective Electrodes, and Oxygen Sensors: Electrochemical Sensors Used in the Medical Field. *Lab. Med.* **34**, 544–547 (2003).

112. Antonov, D., Schliemann, S. & Elsner, P. Methods for the Assessment of Barrier Function. *Skin Barrier Funct.* **49**, 61–70 (2016).

113. du Plessis, J. L., Stefaniak, A. B. & Wilhelm, K.-P. Measurement of Skin Surface pH. *Curr. Probl. Dermatol.* **54**, 19–25 (2018).

114. Lindfors, T., Ervelä, S. & Ivaska, A. Polyaniline as pH-sensitive component in plasticized PVC membranes. *J. Electroanal. Chem.* **560**, 69–78 (2003).

115. Nyein, H. Y. Y. *et al.* A Wearable Electrochemical Platform for Noninvasive Simultaneous Monitoring of Ca(2+) and pH. *ACS Nano* **10**, 7216–7224 (2016).

116. Anastasova, S. *et al.* A wearable multisensing patch for continuous sweat monitoring. *Biosens. Bioelectron.* **93**, 139–145 (2017).

117. Choi, J. *et al.* Soft, Skin-Integrated Multifunctional Microfluidic Systems for Accurate Colorimetric Analysis of Sweat Biomarkers and Temperature. *ACS Sens.* **4**, 379–388 (2019).

118. He, X. *et al.* Flexible and Superwettable Bands as a Platform toward Sweat Sampling and Sensing. *Anal. Chem.* **91**, 4296–4300 (2019).

119. Koh, A. *et al.* A soft, wearable microfluidic device for the capture, storage, and colorimetric sensing of sweat. *Sci. Transl. Med.* **8**, 366ra165 (2016).

120. Bandodkar, A. J. *et al.* Battery-free, skin-interfaced microfluidic/electronic systems for simultaneous electrochemical, colorimetric, and volumetric analysis of sweat. *Sci. Adv.* **5**, eaav3294 (2019).

121. USA, L. L'Oréal Unveils Prototype Of First-Ever Wearable Microfluidic Sensor To Measure Skin pH Levels. https://www.prnewswire.com/news-releases/loreal-unveils-

prototype-of-first-ever-wearable-microfluidic-sensor-to-measure-skin-ph-levels-300773342.html.

122. Pojmanová, P., Ladislavová, N., Škeříková, V., Kania, P. & Urban, Š. Human scent samples for chemical analysis. *Chem. Pap.* **74**, 1383–1393 (2020).

123. Jha, S. K. Characterization of human body odor and identification of aldehydes using chemical sensor. *Rev. Anal. Chem.* **36**, (2017).

124. Cuzuel, V. *et al.* Origin, Analytical Characterization, and Use of Human Odor in Forensics. *J. Forensic Sci.* **62**, 330–350 (2017).

125. Parlet, C. P., Brown, M. M. & Horswill, A. R. Commensal Staphylococci Influence Staphylococcus aureus Skin Colonization and Disease. *Trends Microbiol.* **27**, 497–507 (2019).

126. Bacteriology of Humans: An Ecological Perspective | Wiley. *Wiley.com* https://www.wiley.com/en-us/Bacteriology+of+Humans%3A+An+Ecological+Perspective-p-9781405161657.

127. Ellis, S. R. *et al.* The Skin and Gut Microbiome and Its Role in Common Dermatologic Conditions. *Microorganisms* **7**, 550 (2019).

128. Yamazaki, Y., Nakamura, Y. & Núñez, G. Role of the microbiota in skin immunity and atopic dermatitis. *Allergol. Int.* **66**, 539–544 (2017).

129. Timm, C. M., Lloyd, E. P., Egan, A., Mariner, R. & Karig, D. Direct Growth of Bacteria in Headspace Vials Allows for Screening of Volatiles by Gas Chromatography Mass Spectrometry. *Front. Microbiol.* **9**, 491 (2018).

130. Fitzgerald, S., Duffy, E., Holland, L. & Morrin, A. Multi-strain volatile profiling of pathogenic and commensal cutaneous bacteria. *Sci. Rep.* **10**, 17971 (2020).

131. Duffy, E. & Morrin, A. Endogenous and microbial volatile organic compounds in cutaneous health and disease. *Trends Anal. Chem.* **111**, 163–172 (2018).

132. Sethi, S., Nanda, R. & Chakraborty, T. Clinical Application of Volatile Organic Compound Analysis for Detecting Infectious Diseases. *Clin. Microbiol. Rev.* **26**, 462–475 (2013).

133. Duffy, E. & Morrin, A. Endogenous and microbial volatile organic compounds in cutaneous health and disease. *TrAC Trends Anal. Chem.* **111**, 163–172 (2019).

134. Dormont, L., Bessière, J.-M. & Cohuet, A. Human skin volatiles: a review. *J. Chem. Ecol.* **39**, 569–578 (2013).

135. Dormont, L., Bessière, J.-M., McKey, D. & Cohuet, A. New methods for field collection of human skin volatiles and perspectives for their application in the chemical ecology of human–pathogen–vector interactions. *J. Exp. Biol.* **216**, 2783–2788 (2013).

136. Grabowska-Polanowska, B. *et al.* Development of sampling method and chromatographic analysis of volatile organic compounds emitted from human skin. *Bioanalysis* **9**, 1465–1475 (2017).

137. Jiang, R., Cudjoe, E., Bojko, B., Abaffy, T. & Pawliszyn, J. A non-invasive method for in vivo skin volatile compounds sampling. *Anal. Chim. Acta* **804**, 111–119 (2013).

138. Duffy, E., Guzman, K. D., Wallace, R., Murphy, R. & Morrin, A. Non-Invasive Assessment of Skin Barrier Properties: Investigating Emerging Tools for In Vitro and In Vivo Applications. *Cosmetics* **4**, 44 (2017).

139. Duffy, E., Jacobs, M. R., Kirby, B. & Morrin, A. Probing skin physiology through the volatile footprint: Discriminating volatile emissions before and after acute barrier disruption. *Exp. Dermatol.* **26**, 919–925 (2017).

140. Duffy, E., Albero, G. & Morrin, A. Headspace Solid-Phase Microextraction Gas Chromatography-Mass Spectrometry Analysis of Scent Profiles from Human Skin. *Cosmetics* **5**, 62 (2018).

141. Schmidt, K. & Podmore, I. Current Challenges in Volatile Organic Compounds Analysis as Potential Biomarkers of Cancer. *J. Biomark.* **2015**, (2015).

142. Mochalski, P. *et al.* Monitoring of selected skin- and breath-borne volatile organic compounds emitted from the human body using gas chromatography ion mobility spectrometry (GC-IMS). *J. Chromatogr. B* **1076**, 29–34 (2018).

143. Reynolds, J. C. *et al.* Detection of volatile organic compounds in breath using thermal desorption electrospray ionization-ion mobility-mass spectrometry. *Anal. Chem.* **82**, 2139–2144 (2010).

144. Nazemi, H., Joseph, A., Park, J. & Emadi, A. Advanced Micro- and Nano-Gas Sensor Technology: A Review. *Sensors* **19**, (2019).

145. Núñez Carmona, E. *et al.* Detection of food and skin pathogen microbiota by means of an electronic nose based on metal oxide chemiresistors. *Sens. Actuators B Chem.* **238**, 1224–1230 (2017).

146. Güntner, A. T. *et al.* Sniffing Entrapped Humans with Sensor Arrays. *Anal. Chem.* **90**, 4940–4945 (2018).

147. Lawson, B. *et al.* Skin alcohol perspiration measurements using MOX sensors. *Sens. Actuators B Chem.* **280**, 306–312 (2019).

148. Dormont, L., Bessière, J.-M. & Cohuet, A. Human Skin Volatiles: A Review. *J. Chem. Ecol.* **39**, 569–578 (2013).

149. Stevens, D. *et al.* Spatial variations in the microbial community structure and diversity of the human foot is associated with the production of odorous volatiles. *FEMS Microbiol. Ecol.* (2015) doi:10.1093/femsec/fiu018.

150. Verhulst, N. O., Weldegergis, B. T., Menger, D. & Takken, W. Attractiveness of volatiles from different body parts to the malaria mosquito Anopheles coluzzii is affected by deodorant compounds. *Sci. Rep.* **6**, 27141 (2016).

151. Penn, D. J. *et al.* Individual and gender fingerprints in human body odour. *J. R. Soc. Interface* **4**, 331–340 (2007).

152. Elias, P. M. Primary role of barrier dysfunction in the pathogenesis of atopic dermatitis. *Exp. Dermatol.* **27**, 847–851 (2018).

153. Rippke, F., Schreiner, V., Doering, T. & Maibach, H. I. Stratum corneum pH in atopic dermatitis: impact on skin barrier function and colonization with Staphylococcus Aureus. *Am. J. Clin. Dermatol.* **5**, 217–223 (2004).

154. Piérard-Franchimont, C., Quatresooz, P. & Piérard, G. E. Sebum Production. in *Textbook of Aging Skin* (eds. Farage, M. A., Miller, K. W. & Maibach, H. I.) 343–352 (Springer, 2010). doi:10.1007/978-3-540-89656-2_33.

155. Bernier, U. R., Kline, D. L., Barnard, D. R., Schreck, C. E. & Yost, R. A. Analysis of human skin emanations by gas chromatography/mass spectrometry. 2. Identification of volatile compounds that are candidate attractants for the yellow fever mosquito (Aedes aegypti). *Anal. Chem.* **72**, 747–756 (2000).

156. Gallagher, M. *et al.* Analyses of volatile organic compounds from human skin. *Br. J. Dermatol.* **159**, 780–791 (2008).

157. Curran, A. M., Prada, P. A. & Furton, K. G. The differentiation of the volatile organic signatures of individuals through SPME-GC/MS of characteristic human scent compounds. *J. Forensic Sci.* **55**, 50–57 (2010).

158. Prada-Tiedemann, P. & Furton, K. Human Scent Detection: A Review of its Developments and Forensic Applications. *Rev. Cienc. Forenses* **1**, 81–87 (2008).

159. Bommannan, D., Potts, R. O. & Guy, R. H. Examination of the effect of ethanol on human stratum corneum in vivo using infrared spectroscopy. *J. Controlled Release* **16**, 299–304 (1991).

160. Gupta, R., Badhe, Y., Rai, B. & Mitragotri, S. Molecular mechanism of the skin permeation enhancing effect of ethanol: a molecular dynamics study. *RSC Adv.* **10**, 12234–12248 (2020).

161. Horita, D. *et al.* Molecular mechanisms of action of different concentrations of ethanol in water on ordered structures of intercellular lipids and soft keratin in the stratum corneum. *Biochim. Biophys. Acta BBA - Biomembr.* **1848**, 1196–1202 (2015).

162. Cartner, T. *et al.* Effect of different alcohols on stratum corneum kallikrein 5 and phospholipase A2 together with epidermal keratinocytes and skin irritation. *Int. J. Cosmet. Sci.* **39**, 188–196 (2017).

163. Filipiak, W. *et al.* A Compendium of Volatile Organic Compounds (VOCs) Released By Human Cell Lines. *Curr. Med. Chem.* **23**, 2112–2131 (2016).

164. James, A., Casey, J., Hyliands, D. & Mycock, G. Fatty acid metabolism by cutaneous bacteria and its role in axillary malodour. *World J. Microbiol. Biotechnol.* **20**, 787–793 (2004).

165. Kleesz, P., Darlenski, R. & Fluhr, J. W. Full-Body Skin Mapping for Six Biophysical Parameters: Baseline Values at 16 Anatomical Sites in 125 Human Subjects. *Skin Pharmacol. Physiol.* **25**, 25–33 (2012).

166. Farage, M. A., Hood, W., Berardesca, E. & Maibach, H. Intrinsic and Extrinsic Factors Affecting Skin Surface pH. *PH Skin Issues Chall.* **54**, 33–47 (2018).

167. Man, M. Q. *et al.* Variation of Skin Surface pH, Sebum Content and Stratum Corneum Hydration with Age and Gender in a Large Chinese Population. *Skin Pharmacol. Physiol.* **22**, 190–199 (2009).

168. Choi, S.-J. *et al.* Comparison of transepidermal water loss, capacitance and pH values in the skin between intrinsic and extrinsic atopic dermatitis patients. *J. Korean Med. Sci.* **18**, 93–96 (2003).

169. Jacobi, U., Gautier, J., Sterry, W. & Lademann, J. Gender-related differences in the physiology of the stratum corneum. *Dermatol. Basel Switz.* **211**, 312–317 (2005).

170. Lambers, H., Piessens, S., Bloem, A., Pronk, H. & Finkel, P. Natural skin surface pH is on average below 5, which is beneficial for its resident flora. *Int. J. Cosmet. Sci.* **28**, 359–370 (2006).

171. Bicchi, C., Cordero, C., Liberto, E., Sgorbini, B. & Rubiolo, P. Reliability of fibres in solid-phase microextraction for routine analysis of the headspace of aromatic and medicinal plants. *J. Chromatogr. A* **1152**, 138–149 (2007).

172. Spietelun, A., Pilarczyk, M., Kloskowski, A. & Namieśnik, J. Current trends in solid-phase microextraction (SPME) fibre coatings. *Chem. Soc. Rev.* **39**, 4524–4537 (2010).

173. Jiang, J. *et al.* Volatile fatty acids production from food waste: effects of pH, temperature, and organic loading rate. *Bioresour. Technol.* **143**, 525–530 (2013).

174. Lukitawesa, null, Patinvoh, R. J., Millati, R., Sárvári-Horváth, I. & Taherzadeh, M. J. Factors influencing volatile fatty acids production from food wastes via anaerobic digestion. *Bioengineered* **11**, 39–52 (2020).

175. Münch, E. v. & Greenfield, P. F. Estimating VFA concentrations in prefermenters by measuring pH. *Water Res.* **32**, 2431–2441 (1998).

176. Tang, Z., Yang, J., Yu, J. & Cui, B. A colorimetric sensor for qualitative discrimination and quantitative detection of volatile amines. *Sensors* **10**, 6463–6476 (2010).

177. Mazumder, S., Ahamed, R. A., McGahee, E., Wang, L. & Seyler, T. H. A New Automated Method for the Analysis of Aromatic Amines in Human Urine by GC–MS/MS. *J. Anal. Toxicol.* **43**, 25–35 (2019).

178. Ng, T. W., Chan, P. Y., Chan, T. T., Wu, H. & Lai, K. M. Skin squames contribute to ammonia and volatile fatty acid production from bacteria colonizing in air-cooling units with odor complaints. *Indoor Air* **28**, 258–265 (2018).

179. Visciano, P., Schirone, M. & Paparella, A. An Overview of Histamine and Other Biogenic Amines in Fish and Fish Products. *Foods Basel Switz.* **9**, (2020).

180. Doeun, D., Davaatseren, M. & Chung, M.-S. Biogenic amines in foods. *Food Sci. Biotechnol.* **26**, 1463–1474 (2017).

181. Lucaire, V., Schwartz, J.-J., Delhomme, O., Ocampo-Torres, R. & Millet, M. A sensitive method using SPME pre-concentration for the quantification of aromatic amines in indoor air. *Anal. Bioanal. Chem.* **410**, 1955–1963 (2018).

182. Sandlers, Y. Amino Acids Profiling for the Diagnosis of Metabolic Disorders. *Biochem. Test. - Clin. Correl. Diagn.* (2019) doi:10.5772/intechopen.84672.

183. Claes, L., Janssen, M. & De Vos, D. E. Organocatalytic Decarboxylation of Amino Acids as a Route to Bio-based Amines and Amides. *ChemCatChem* **11**, 4297–4306 (2019).

184. Thorn, R. M. S. & Greenman, J. Microbial volatile compounds in health and disease conditions. *J. Breath Res.* **6**, (2012).

185. Mohiuddin, S. S. & Khattar, D. Biochemistry, Ammonia. in *StatPearls* (StatPearls Publishing, 2021).

186. Li, M. *et al.* Human Ammonia Emission Rates under Various Indoor Environmental Conditions. *Environ. Sci. Technol.* **54**, 5419–5428 (2020).

187. Smallegange, R. C., Verhulst, N. O. & Takken, W. Sweaty skin: an invitation to bite? *Trends Parasitol.* **27**, 143–148 (2011).

188. Keller, R. W., Bailey, J. L., Wang, Y., Klein, J. D. & Sands, J. M. Urea transporters and sweat response to uremia. *Physiol. Rep.* **4**, (2016).

189. Nose, K. *et al.* Identification of Ammonia in Gas Emanated from Human Skin and Its Correlation with That in Blood. *Anal. Sci. Int. J. Jpn. Soc. Anal. Chem.* **21**, 1471–4 (2006).

190. Ferrer, F. M., Hobart, K. & Bailey, J. V. Detection of urease and carbonic anhydrase activity using a rapid and economical field test to assess microbially-induced carbonate precipitation. *bioRxiv* 2020.01.10.902379 (2020) doi:10.1101/2020.01.10.902379.

191. Neofotistos, A.-D. G., Tsagkaris, A. S. & Proestos, G. P. D. and C. Emerging Trends in Biogenic Amines Analysis. *Biog. Amines* (2019) doi:10.5772/intechopen.81274.

192. Jamalabadi, H., Mani-Varnosfaderani, A. & Alizadeh, N. PPy-Metal Oxide Hybrid Nanocomposite Sensor Array for Simultaneous Determination of Volatile Organic Amines in High Humid Atmosphere. *IEEE Sens. J.* **17**, 8282–8289 (2017).

193. Xiao-wei, H., Xiao-bo, Z., Ji-yong, S., Zhi-hua, L. & Jie-wen, Z. Colorimetric sensor arrays based on chemo-responsive dyes for food odor visualization. *Trends Food Sci. Technol.* **81**, 90–107 (2018).

194. Rakow, N. A., Sen, A., Janzen, M. C., Ponder, J. B. & Suslick, K. S. Molecular Recognition and Discrimination of Amines with a Colorimetric Array. *Angew. Chem. Int. Ed.* **44**, 4528–4532 (2005).

195. Oh, H. J. *et al.* Washable Colorimetric Nanofiber Nonwoven for Ammonia Gas Detection. *Polymers* **12**, 1585 (2020).

196. Helmy, S. *et al.* Photoswitching Using Visible Light: A New Class of Organic Photochromic Molecules. *J. Am. Chem. Soc.* **136**, 8169–8172 (2014).

197. Helmy, S., Oh, S., Leibfarth, F. A., Hawker, C. J. & Read de Alaniz, J. Design and Synthesis of Donor–Acceptor Stenhouse Adducts: A Visible Light Photoswitch Derived from Furfural. *J. Org. Chem.* **79**, 11316–11329 (2014).

198. Diaz, Y. J. *et al.* A Versatile and Highly Selective Colorimetric Sensor for the Detection of Amines. *Chem. – Eur. J.* **23**, 3562–3566 (2017).

199. Schmidt, F. M. *et al.* Ammonia in breath and emitted from skin. *J. Breath Res.* **7**, 017109 (2013).

200. Martínez-Lozano, P. Mass spectrometric study of cutaneous volatiles by secondary electrospray ionization. *Int. J. Mass Spectrom.* **282**, 128–132 (2009).

201. Furukawa, S. *et al.* Simultaneous and multi-point measurement of ammonia emanating from human skin surface for the estimation of whole body dermal emission rate. *J. Chromatogr. B Analyt. Technol. Biomed. Life. Sci.* **1053**, 60–64 (2017).

202. Bigi, F. *et al.* Clean synthesis in water. Part 2: Uncatalysed condensation reaction of Meldrum's acid and aldehydes. *Tetrahedron Lett.* **42**, 5203–5205 (2001).

203. Palmer, L. I. & Alaniz, J. R. de. Lewis Acid Catalyzed Rearrangement of Furylcarbinols: The Aza- and Oxa-Piancatelli Cascade Reaction. *Synlett* **25**, 08–11 (2014).

204. Piutti, C. & Quartieri, F. The Piancatelli Rearrangement: New Applications for an Intriguing Reaction. *Molecules* **18**, 12290–12312 (2013).

205. Šafář, P. *et al.* Dichotomy in the Ring Opening Reaction of 5-[(2-Furyl)methylidene]-2,2-dimethyl-1,3-dioxane-4,6-dione with Cyclic Secondary Amines. *Collect. Czechoslov. Chem. Commun.* **65**, 1911–1938 (2000).

206. Sidman, J. W. Electronic Transitions Due To Nonbonding Electrons Carbonyl, Aza-Aromatic, And Other Compounds. https://pubs.acs.org/doi/pdf/10.1021/cr50022a004 (2002) doi:10.1021/cr50022a004.

207. Bailey, D. C. Not Normal: the uncertainties of scientific measurements. *R. Soc. Open Sci.* **4**, (2017).

208. Sahu, P. K. & Lee, S.-L. Hydrogen-bond interaction in 1:1 complexes of tetrahydrofuran with water, hydrogen fluoride, and ammonia: A theoretical study. *J. Chem. Phys.* **123**, 044308 (2005).

209. Lam, T. H. *et al.* Understanding the microbial basis of body odor in pre-pubescent children and teenagers. *Microbiome* **6**, (2018).

210. Dekaboruah, E., Suryavanshi, M. V., Chettri, D. & Verma, A. K. Human microbiome: an academic update on human body site specific surveillance and its possible role. *Arch. Microbiol.* **202**, 2147–2167 (2020).

211. Luqman, A. *et al.* Trace amines produced by skin bacteria accelerate wound healing in mice. *Commun. Biol.* **3**, 1–10 (2020).

212. Luqman, A., Nega, M., Nguyen, M.-T., Ebner, P. & Götz, F. SadA-Expressing Staphylococci in the Human Gut Show Increased Cell Adherence and Internalization. *Cell Rep.* **22**, 535–545 (2018).

213. Shetewi, T. *et al.* Investigation of the relationship between skin-emitted volatile fatty acids and skin surface acidity in healthy participants - a pilot study. *J. Breath Res.* (2021) doi:10.1088/1752-7163/abf20a.

214. Lang, W., Blöck, T. M. & Zander, R. Solubility of NH3 and apparent pK of NH4+ in human plasma, isotonic salt solutions and water at 37 degrees C. *Clin. Chim. Acta Int. J. Clin. Chem.* **273**, 43–58 (1998).

# Chapter 4

# Conclusion and Future work

As reviewed in chapter one, the skin is a complex organ that potentially offers a great in-site into an individual physiological state. Exploiting waste products (sweat and volatile organic compounds…etc) expelled by the body via the skin has been getting great attention lately. Non-invasive methods capable of assessing such compound are being investigated and developed into wearable epidermal sensors that are used for monitoring skin properties. Due to the complex composition of skin excreted media development of epidermal sensors that are analyte specific has proven to be challenging. On-going research towards selective material will open up more opportunities for potential use of such sensors for health monitoring and disease diagnosis.

This thesis contributes to the understanding of skin volatile emissions, their composition and influence on skin surface pH. Gender and site variolations in volatiles emitted from the skin were also investigated. Furthermore, the synthesis of a novel dye and its integration into a wearable skin sensors for selective detection of amines is described.

The main conclusions of each chapter have been outlined in bullet points below:

Chapter 2: skin acidic volatile emissions and skin surface pH values are linked. An increase in acidic volatiles emitted from the skin results in decrease in the skin surface pH in both males and females. Several saturated medium- and long-chain fatty acids were identified as being present in participant samples, irrespective of gender and site. However, the abundances of the VFAs differed across groups and attributed to differing sebaceous gland densities and hence sebum secretions and metabolic activity.

Chapter 3: Meldrum's activated pyrrole (MAP) dye can be synthesised via a simple one step condensation reaction between Meldrum's acid and pyrrole-2-carboxaldehyde. The dye showed selectivity towards amines in the solid state. Integration of the dye into a wearable skin sensors showed response towards skin volatiles. With further improvements, the proposed MAP sensor could find application as a wearable colorimetric sensors for amine emissions which can be linked to kidney dysfunction and other disease characterised by a change in amine levels in the body.

The following section highlights area of the research where there is potential for improvement. Firstly, due to Covid rules and regulation set in place by the university, sample population was

limited, increasing sample population to cover a range of ages, genders and ethnic backgrounds will leave less room for speculation for whether results obtained are true or not.

Furthermore, ideally sampling time should be quick (5-10 min). Further work to improve reactivity of the dye through the introduction of amine sensitive moiety to the dye scaffold can be investigated. However since the main focus of the work presented here is analytical rather than synthetic, no changes were applied to the initial structure of the dye. To prevent leaching of dye it would be worthy to investigate possibility of using inkjet printing to manufacture the sensors. Investigate the effect of dye loading (concentration of the dye solution) on the reactivity of the dye towards amines would help understanding properties of the dye. Long term studies would prove useful for to investigating the stability of the dye when dissolved in solution and as a solid. This can be done using $H^1$MNR. A mixture of common amines emitted from the skin can be used to generate the calibration curve rather than just looking at a single amine (ammonia). Since the MAP dye is selective towards amines, this calibration curve would be more accurate to use for extrapolating the amine emission rates for sensor applied to the skin. Skin microbiome can be sampled at each of the studied sites to investigate if a certain microbial genera contribute to the volatile amine emission from skin.